

Power Transformer Magnetization Under GIC/GMD

by

Shu Lu

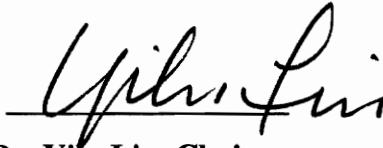
**Dissertation submitted to the Faculty of
Virginia Polytechnic Institute and State University
in partial fulfillment of the requirements for the degree of**

DOCTOR OF PHILOSOPHY

in

Electrical Engineering

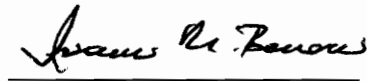
APPROVED:



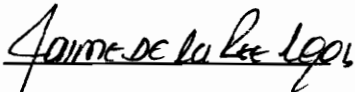
Dr. Yifu Liu, Chairperson



Dr. Arun G. Phadke



Dr. Ioannis M. Besieris



Dr. Jaime De La Ree Lopez



Dr. Lee W. Johnson

March, 1994

Blacksburg, Virginia

C.2

LD
5655
V856
1994
L8
C.2

POWER TRANSFORMER MAGNETIZATION UNDER GIC

by

Shu Lu

Committee Chairperson: Yilu Liu

Electrical Engineering

(Abstract)

Geomagnetically induced currents (GIC) could saturate a transformer core. Two significant effects are the abnormal stray flux in transformers and extremely large harmonic contents in excitation currents, which can lead to serious equipment damage and power system misoperation. Such incidents have occurred during the March 1989 K-9 solar magnetic disturbance.

This dissertation starts with a systematically study of transformer magnetization under GIC. It reviews both dc and ac saturation patterns of five transformer core designs. Magnetic fields along various traverses for dc excitation are presented. Impedance matrix entries of a single phase transformer are compared for normal and dc operations. New observations have been formed based on the simulation results. The study helps to reveal the fundamental transformer magnetization mechanism under GIC in order to assess potential stray flux heating possibilities of geologically vulnerable transformer units.

Based on the finite element analysis, an improved method of modeling transformer excitation under dc bias using equivalent magnetic circuit is developed. There are two unique points in this approach: first, information of 3D finite element magnetic flux distribution analysis is used to construct and verify the circuit model; second, the effect of the transformer tank is included. The model is capable of simulating transformer

excitation currents under different levels of dc bias with good accuracy. As a consequence, the complete variations of excitation current harmonics with respect to an extended range of dc bias are revealed. The sensitivity of transformer winding impedances and core loss on the excitation characteristics are examined. The saturated transformer under no-load and various loading conditions is simulated. A laboratory test is performed on a small scale transformer and compared with the model results. Excitation harmonics generated from dc biased three phase transformer banks with different types of equivalent loads are also simulated. The effect of both unbalanced dc excitations and unbalanced loads are investigated. The results of this study contribute in understanding transformers as harmonic sources and the impact on power systems during a geomagnetic disturbance.

Dedication

This dissertation is dedicated to my parents

Mr. Mengyang Lu and Mrs. Bizhen Guan

for their endless love, unconditional support and their values in education

ACKNOWLEDGMENTS

I owe a debt of thanks to many who have been instrumental in whatever success I have achieved to this point.

My first thanks goes to Dr. Yilu Liu, my major professor. Her unending enthusiasm, encouragement, and guidance have been an immeasurable asset to me. I thank her for her fresh thinking and challenging questions that have kept me working.

I also would like to thank Dr. A. G. Phadke, Dr. I. M. Besieris, Dr. J. De La Ree, Dr. L. W. Johnson, for their time and efforts in serving the advisory committee, and for many of their valuable suggestions.

I wish to thank all my relatives and friends for their love and support. Special thanks are extended to my parents, my parents-in-law, my grandmothers, my brother, my cousins, Mr. Kok Wai Wu, and my friends Mr. and Mrs. Worley, Dr. Li Li, Ms. Xiaohui Huang and her lovely little boy John, and Ms. Xu Lin.

My husband, Jianqing He, and my daughter, Victoria, deserve well over one half of the credit for all the good I have achieved. They have given me so much joy in my life. My husband always has the kind of faith and confidence in me that challenge me to try my best. I could not have found a better husband.

No thanks would be complete without my acknowledging God who gave me whatever talents I have. I wish his continuous blessing for the rest of my life.

Table of Contents

Chapter	Title	Page
1	Introduction	1
	1.1 A Solar Magnetic Disturbance Strike	1
	1.2 Problem Statements	2
	1.3 Literature Review	4
	1.4 The Approach to The Problem	7
	1.5 The Significance of This Study	9
2	Transformer Fundamentals	10
	2.1 Electromagnetic Induction and Magnetic Materials	10
	2.1.1 Electromagnetic induction	10
	2.1.2 Magnetic materials	11
	2.2 Basic Concept of Transformer	12
	2.3 Major Parts of a Power Transformer	13
	2.3.1 Transformer cores	13
	2.3.2 Transformer windings	15
	2.3.3 Transformer tanks	15
	2.3.4 Transformer cooling	16
	2.3.5 Transformer protection	16
	2.4 Transformer Equivalent Circuit for Normal Operations	16
	2.4.1 Inductance	16
	2.4.2 Magnetic coupling of electric circuits	18
	2.4.3 Simplified equivalent circuit	19
	2.4.4 A more completed equivalent circuit	21
3	FEM Analysis Study	32
	3.1 Introduction	32
	3.2 2D DC Magnetizing Flux Simulation	32
	3.2.1 Fundamental dc excitation analysis of	

	a single phase transformer design	33
	3.2.2 H fields along transverses of a single phase transformer	37
	3.2.3 DC effects of three phase core configurations	37
	3.2.4 Effect of unbalanced dc bias on three phase core form transformer	39
	3.2.5 H field profiles of three phase transformers	39
	3.3 2D AC Excitation Under DC Bias	41
	3.3.1 Leakage flux distribution	41
	3.3.2 AC excitation flux distribution	42
	3.3.3 Leakage flux patterns for different winding structures ..	43
	3.3.4 Transformer impedance matrix and circuit model	43
	3.4 3D DC Bias Magnetizing Flux Simulation	46
	3.5 Conclusions	48
4	DC Saturated Transformer Magnetic Circuit Model	74
	4.1 Introduction	74
	4.2 Magnetic Circuit Model Development	75
	4.2.1 Introduction	75
	4.2.2 Model configuration	76
	4.2.3 Computer programming	77
	4.2.4 Circuit parameter adjustment	79
	4.3 An Example	81
	4.4 Excitation Current Harmonics	81
	4.4.1 Typical waveforms of excitation currents vs. dc bias ..	81
	4.4.2 Excitation current harmonics vs. dc bias	83
	4.4.3 RMS excitation current vs. dc bias	85
	4.4.4 Total harmonic distortion vs. dc bias	86
	4.4.5 Reactive power vs. dc bias	86
	4.4.6 The effect of voltage reduction	87

	4.4.7 The total equivalent reluctance vs. dc bias	88
	4.5 The Effect of Transformer Tank	88
	4.6 Discussions	89
5	No-Load and Loaded Transformer Simulation	105
	5.1 Introduction	105
	5.2 Nonlinear Tee Circuit Model	105
	5.2.1 The transformer equivalent Tee circuit	105
	5.2.2 Nonlinear magnetizing inductance L_m	106
	5.2.3 Leakage inductances	106
	5.2.4 Losses	107
	5.2.5 Graphical illustration	107
	5.3 A Complete Circuit for Computation	108
	5.3.1 Connection with the external network	108
	5.3.2 Computation of the nonlinear circuit	109
	5.4 No-load Excitation Current Simulation	111
	5.4.1 No-load dc excitation	111
	5.4.2 The effect of dc levels	113
	5.4.3 The effect of varying L_p and R_p	113
	5.4.4 The effect of varying R_c	114
	5.5 Effect of DC on a Loaded Transformer	115
	5.5.1 Loaded transformer model	115
	5.5.2 The effect of load on excitation current	115
	5.5.3 The effect of dc on the load	116
	5.5.4 Current waveforms	116
	5.6 Conclusions	117
6	Small Scale Transformer DC Excitation Test	128
	6.1 Laboratory Experiments	128
	6.1.1 Experimental setup	128
	6.1.2 Experimental procedures	129

6.2	Test Results	129
7	Harmonics in Three Phase Transformer Banks	137
7.1	Introduction	137
7.2	Three Phase Circuit Analysis	137
7.2.1	Three phase circuit models	137
7.2.2	Harmonic balance method	138
7.3	Three Phase Harmonics	141
7.3.1	Phase relations among the harmonics	141
7.3.2	Balanced Y-Y connection	144
7.3.3	Balanced Y- Δ connection	146
7.3.4	Unbalanced Conditions	146
7.4	Conclusions	147
8	Conclusions and Future Study	158
8.1	A Summary of the Present Work	158
8.2	Conclusions from the FEM Analyses	158
8.3	Modeling and the Results	159
8.4	Significance and Future Study	163
Appendix	Electromagnetic Solver	165
a.1	Numerical Approaches	165
a.1.1	Maxwell's equations	165
a.1.2	Numerical approach	166
a.2	Finite Element Method	167
a.2.1	Introduction to finite element method	167
a.2.2	The original boundary value problem	167
a.2.3	Solving Poisson's equation using FEM	170
a.3	FEM Solver	174
Bibliography	176
VITAE	181

List of Illustrations

Figure	Title	Page
2.1	Typical B-H relationship of magnetic material	26
2.2	A two winding transformer	27
2.3	Simplified transformer equivalent circuit	28
2.4	More completed transformer equivalent circuit	29
2.5	Hysteresis loop	30
2.6	A portion of the lamination slab	31
3.1	Single phase transformer core configuration and its dc flux distribution under heavy saturation	49
3.2	A lumped magnetic equivalent circuit of the single phase core	50
3.3	Single phase transformer's bias levels for each core segment under the same low dc excitation	51
3.4	H profiles along traverses of a single phase transformer	52
3.5	Three phase three leg core form transformer configuration and flux distribution under balanced dc excitation	53
3.6	Bias points of different three phase core designs under the same balanced dc excitation currents	54
3.7	Three phase five leg transformer configuration and flux distribution under balanced dc excitation	55
3.8	Three phase seven leg transformer configuration and flux distribution under balanced dc excitation	56
3.9	Three phase conventional transformer configuration and flux distribution under balanced dc excitation	57
3.10	Three phase core form transformer flux distribution under unbalanced dc excitation	58
3.11	H profiles along the traverses of the three phase core form transformer..	59
3.12	H profiles along the traverses of the three phase five leg transformer.....	60
3.13	H profiles along the traverses of the three phase seven leg transformer...	61

3.14	H profiles along the traverses of the three phase conventional transformer	62
3.15	Leakage flux distributions of a single phase core form transformer	63
3.16	H profiles along two traverses of the single phase core form transformer	64
3.17	Three phase conventional transformer ac excitation flux distribution ...	65
3.18	Average magnetic field intensity H along traverses of a three phase conventional transformer during heavy saturation	66
3.19	Three phase five leg transformer ac excitation flux distribution	67
3.20	Average magnetic field intensity H along traverses of a three phase five leg transformer during heavy saturation	68
3.21	Leakage flux distribution of a single phase transformer with pancake winding	69
3.22	Single phase transformer with FEM mesh	70
3.23	A piece-wise core model of a single phase transformer under saturation..	71
3.24	3D configuration of a three phase three leg transformer and its 2D top view	72
3.25	H profile along line A~D of figure 3.24	73
4.1	A 3D layout of a single phase transformer and its flux distribution during saturation	90
4.2	Equivalent magnetic circuit model of the single phase transformer with tank in figure 4.1	91
4.3	B-H characteristics of the core and the tank materials	92
4.4	Program flow chart for solving the magnetic circuit in figure 4.2	93
4.5	Block diagram for calculation of the total flux and flux in each component	94
4.6	Third harmonic component under different dc biases	95
4.7	The B-H characteristics of the core material	96
4.8	Excitation current waveforms	97

4.9	Harmonics in excitation current vs. dc bias for 1 p.u. and 0.7 p.u. ac voltages	98
4.10	Harmonics in excitation current vs. dc bias for 1 p.u. ac voltages	99
4.11	RMS excitation current vs. dc bias at 1 p.u. and 0.7 p.u. ac voltages	100
4.12	THD in excitation current vs. dc bias at 1 p.u. and 0.7 p.u. ac voltages....	101
4.13	Normalized reactive power vs. dc bias at 1 p.u. and 0.7 p.u. ac voltages..	102
4.14	The total equivalent reluctance vs. dc bias	103
4.15	Comparison of 2nd harmonics in excitation currents	104
5.1	Equivalent Tee circuit of a single phase transformer and a simplified external system representation	118
5.2	Nonlinear magnetizing inductance of the example transformer	119
5.3	An illustration of the nonlinear excitation characteristics	120
5.4	Waveforms of excitation current, magnetizing flux and induced voltage under different levels of dc injection	121
5.5	RMS, THD and dc bias of the excitation currents vs. dc levels	122
5.6	RMS, THD and dc bias of the excitation currents vs. L_p	123
5.7	RMS, THD the of excitation currents vs. R_p	124
5.8	RMS, THD of secondary currents vs. dc levels	125
5.9	Efficiency of the transformer vs. dc levels	126
5.10	Waveforms of currents of the primary, secondary, excitation, load, and system	127
6.1	Winding arrangement of the experimental transformer	131
6.2	The experimental setup for excitation current measurement under dc bias	132
6.3	Primary current vs. primary voltage	133
6.4	Excitation current waveform without dc bias	134
6.5	Excitation current waveform under dc bias	135
6.6	Harmonic components vs. dc bias	136
7.1	Equivalent Tee circuit of a single phase transformer	149

7.2	Model of the a) Y-Y bank with on grounded neutral	
	b) Y- Δ bank with grounded neutral	150
7.3	Model circuits separated into nonlinear and linear subsystems	151
7.4	Harmonic distribution of balanced Y-Y with various power factors under 50A/phase dc	152
7.5	Secondary line currents of balanced Y-Y under 50A/phase dc	153
7.6	Waveforms of delta winding and line currents under balanced capacitive loads	154
7.7	Excitation current harmonics of the Y- Δ connection under unbalanced capacitive loads	155
7.8	Excitation, primary, secondary winding and line current waveforms for the Y- Δ connection under unbalanced capacitive load	156
7.9	Excitation, primary, and secondary current waveforms for the Y-Y connection under unbalanced dc	157

CHAPTER I. INTRODUCTION

1.1 A Solar Magnetic Disturbance Strike

On March 13, 1989, a K-9 geomagnetic storm of solar cycle 22 struck the Hydro Quebec system [1]. The Hydro-Quebec system had remote generation sources linked by transmission lines extending more than 1000 km and running above areas of highly resistive igneous rock. Therefore, this system had high susceptibility to the effects of geomagnetic storms. On that day, the geomagnetic-induced currents caused half-cycle saturation of power transformers which created excessive harmonics in the bulk transmission network. The harmonic currents flowed into nearby static voltampere reactive compensators and quickly loaded the capacitors to an extent that the protective systems sensed an overload and took the static VAR compensators off-line to prevent equipment damage. Within a minute of the storm's onset, the seven static VAR compensators tripped. Eight seconds after the loss of the static compensators, one of the five 735 kV lines on the La Grande transmission network tripped. Within one second, this disturbance caused the other four lines from the La Grande complex to trip. Frequency and voltage throughout the rest of the system fell. A series of automatic load reduction measures failed to restore proper balance between available (reduced) generation and load. The capacity lost was too large and the load could not be shed fast enough to restore stability. Six seconds after the La Grande complex was disconnected from the system, power swings tripped the lines that supplied generation from the Churchill Falls generation complex. Within 18 seconds of this second separation, the entire system failed and the Quebec province was blacked out.

While the Hydro-Quebec system was under an outage, many others were also affected. Many utilities across North America felt the disturbance, especially in parts of the eastern United States. Not only the harmonics caused trouble to the system, some transformers

also suffered severe damage due to the stray flux overheating. For example, a generator step-up transformer, owned by the Public Service Electric & Gas Co. of Newark, N.J., had to be replaced at a cost of several million dollars.

Solar activity is at its peak in a cycle of 11 years. The levels of geomagnetic activity can be measured using the K index, which is a 3-hour index of geomagnetic observations. Generally, geomagnetic disturbance (GMD) has to be classed above K-5 or K-6 before noticeable effects appear on electric power systems [2,3].

Solar activities such as the occurrence of sunspots generate a very large amount of charged particles. When these particles (protons and electrons), also called solar wind, move toward the earth and are captured by the earth's magnetic field, currents circulating around the earth's geomagnetic poles are generated. These currents (auroral electrojets) lead to the fluctuation of the earth's magnetic field, known as the GMD. The aurora borealis in the northern hemisphere and the aurora australis in the southern hemisphere are the two visual forms of GMD. GMD induces the earth's surface potential (ESP). As a result, electric currents flow in low resistive paths such as pipelines or power transmission lines. These currents are called GIC. Typically, the frequency of the GIC is in the range of 0.001 ~ 0.1 Hz. The peak values could be as high as 200 A and last from several minutes to hours. In comparison with 60 Hz power frequency, GIC can be considered as quasi-dc injection when it enters a power system [4,5,6,7].

1.2 Problem Statements

A power transformer is designed that, when it operates at its rated voltage and has no dc injection, the maximum flux density is right below the knee region of the magnetizing curve in order to minimize its size and cost. In other words, the transformer operates in the linear region of the B-H curve. Under this normal operation, the iron core provides a

very low reluctance path for the magnetic flux. Only a very small amount of excitation current is needed to maintain the necessary excitation flux. The excitation current is usually about 0.6 ~ 1% of the load current and is symmetric to the origin. The magnetic gradient, H , is in the order of 10 At/inch (or about 400 At/m) along the core lamination [8]. Because the majority of the flux stay in the core, leakage or stray flux is within a tolerant level as far as losses are concerned.

When a dc source is applied to a transformer, it generates a certain level of off-set dc flux. The transformer is biased somewhere off the origin. With an ac source superimposed, part of the operation is pushed into the saturation region where more ampere-turns are required to produce the same amount of flux in order to sustain the sinusoidal voltage level of the system. The waveform of the excitation current is no longer symmetric but has a large peak in half of the cycle. The part having the peculiar shape in the excitation current corresponds to the saturation region of the B-H curve. Therefore, this condition is called half cycle saturation [9].

A series of reactions occur associated with the half cycle saturation of the transformer core. Two of the most profound effects are the harmonic generation and the transformer heating. The greatly increased excitation current is rich in harmonics, which in turn could cause an overall increase in transformer reactive power consumption, capacitor overload, false operations of protective relays, and possible power system collapses. The saturated core becomes a much higher reluctance path due to the reduced core permeability. A large amount of stray flux is pushed out of the core. Stray flux heating could occur in windings, clamping structures, and tank plates. Local hot spots could develop. These hot spots could damage paper insulation and cause gassing and transformer oil combustion [10]. Therefore, dc injection is very undesirable for the power transformer. However, it may exist as a result of many causes. GIC is one of the sources of the undesirable dc injection.

Power systems are susceptible to GIC when they are located in the northern latitudes, which are near the auroral electrojets and in the igneous rock region having high resistivity. The power systems whose neutral ground points span long distances can link large cumulative earth surface potentials. They are also vulnerable to GIC [11,12,13,14].

Although designing a large power transformer that would be immune to GIC is practically unrealistic due to its excessive size and prohibitive cost, it is possible to predict and mitigate the effects during GMD. Much of the research has been done through experiments and theoretical analysis. To prevent GIC from entering a power system, several methods have been suggested, for example, using passive components such as capacitors in the neutral of the power transformers to block GIC, and using an active control circuit to inject a dc current to offset the GIC flux [15]. There are also methods in protecting transformers and power systems from damages due to transformer half cycle saturation. These methods include, for example, placing metallic parts somewhere inside a transformer to direct or diverse the flux [16] and reducing generator loading to provide reserve reactive capacity [12]. The effectiveness of these mitigation methods rely on understanding of the transformer dc saturation mechanism. Therefore, systematic analysis of transformer magnetization and harmonic generation under GIC is highly desired and it constitutes the research presented in this dissertation.

1.3 Literature Review

Since the first transformer was installed for alternating current transmission by electric industries in 1886, power transformers have been studied for more than a century. As a simple, convenient, and reliable device, transformer losses, efficiency and reliability have been well controlled by design engineers under the normal operation. However, during GMD, GIC can enter a power system through the neutral of the grounded wye transformers. These quasi-dc currents bias the transformer core and cause transformer

half cycle saturation. As a result, two significant effects arise. They are the abnormal stray flux and the extremely high excitation currents which can lead to system misoperation and serious damages [2,8,18,19,20,21,22,23].

The effects of GMD on electric power systems have been observed for decades. The first research effort aimed at the comprehensive measurement of GIC and systematic observation of their effects in power systems was conducted from 1969 to 1972 by the University of Minnesota, the General Electric Company, and 30 electric utility companies in the United States. For over 20 years, many aspects of the effects of GIC on power systems have been studied by Albertson, Kappenman, Aspnes, et. al.. GIC effects on power transformers, in particular, were studied by Gattens, Girgis, and Nevins [18], Ringlee and Steward [8], Walling and Khan [24], Bolduc and Aubin [25], McNutt [26], and Xu, Martinich et. al. [27]. To study transformer heating due to GIC, measurements on scale models by Pasco, Norton, Nilsson [28], Tay and Swift [29], Takasu, Oshi, et. al. [30] as well as field tests on actual transformers by Kappenman [31], were performed. Reports on transformer flux analysis using numerical methods were found [18,24,32,34].

In an effort to simulate the excitation currents of dc saturated transformers, different transformer models were proposed. Four typical methods are reviewed and discussed here.

Bolduc and Aubin [25] developed a mathematical model for calculating the magnetizing current. The model was derived based on the classical equivalent circuit of a transformer. The magnetizing curve was approximated with two segments of straight lines. Thus the magnetizing inductance in the equivalent circuit had two different constant values corresponding to the unsaturated or saturated regions. By further simplifying the unsaturated magnetizing inductance as infinity, an analytical solution of the magnetizing current was derived from the circuit equation. The analytical expressions provided a direct and simple way to calculate the magnetizing currents of

different transformer design. However, due to the two straight-line approximation of the magnetizing curve, the model was only acceptable for a certain range of dc injection. A large discrepancy could begin to occur at small values of dc currents because the knee of the magnetizing curve was poorly represented.

Yacamini and Oliveira [35] introduced a simple way to calculate excitation currents. In their method, the simplified two straight lines were also used for describing the excitation characteristic. AC flux was assumed to be sinusoidal so that the excitation current could be expressed as a function of the fundamental flux and dc flux. Then Fourier analysis of the excitation current was performed to obtain the harmonic components in terms of the ac and dc flux. By equating the direct component of the excitation current with the injected dc current, the dc flux level was calculated. Therefore, the rest of the harmonic components could be determined. This method showed the direct relationship between the core flux and the harmonic components of the excitation current. Nevertheless, the primary resistance and leakage inductance were ignored by the sinusoidal flux assumption. As a result, significant error may occur at large dc injections.

Walling and Khan [17] presented a magnetic circuit modeling technique for determining excitation current waveform. The lumped-parameter nonlinear magnetic circuit models were solved for the equilibrium saturation condition by using an iterative approach. In the magnetic circuit models, time domain constant flux sources represented the coil and linear and nonlinear reluctance branches represented the flux path. If the parameters of the lumped elements were well adjusted, and the distorted flux was taken into consideration, the model should be able to simulate the excitation current in good accuracy. However, only the normal flux paths were considered in the models which had a large discrepancy in heavy saturation. Also, the undistorted sinusoidal flux was assumed in the model. This assumption eliminated the impact of winding impedances which can affect the excitation current under a large dc bias.

Fuchs, Masoum and Roesler [32,33] introduced a large signal nonlinear model for anisotropic transformers. A quasi three-dimensional magnetic field solution was obtained by employing the finite difference method. The analysis considered many design details such as the effects of the interlamination, butt-to-butt air gaps, the exchange of flux between any two neighboring anisotropic laminations, and the influences of the end windings. The so called quasi three-dimensional method was that, the magnetic fields in XY, XZ and YZ planes were calculated separately and the solutions were linked through the pre-calculated mixed-core B-H characteristics. This approximation saved the effort in solving the complicated three dimension magnetic field. The core-loss current, as part of the excitation current, was computed from the iron-core losses. Their study showed that the iron-core losses were not only a function of the maximum flux density but also the flux harmonic phase shift with respect to the fundamental. Obviously, this modeling technique was much more accurate than all the previously mentioned methods because the magnetic field was actually solved. However, it involved tremendous work for modeling each new core design even only quasi 3D was used. To determine the phase-factor function for evaluating the harmonic phase shift, measurements of the actual transformer were required. Overall, this technique was not efficient for studies of a variety of transformers in spite of its accuracy.

1.4 The Approach to The Problem

A systematic finite element analysis of transformer dc magnetization is first performed using a finite element computer software package. DC saturation patterns of five simplified generic core configurations are reviewed. Magnetic fields along various traverses are examined for both ac and dc excitations. Unbalanced excitation and different winding structures are also simulated. Impedance matrix entries of a single

phase transformer are calculated for normal and dc operations. Simulation results from both two dimensions (2D) and three dimensions (3D) are compared.

Based on the results of 3D finite element magnetic flux distribution analysis, an improved method of modeling transformer excitation under dc bias using equivalent magnetic circuit is developed. There are two unique points in this approach. First, the structure of a lumped magnetic circuit model of the entire transformer and initial parameters are determined based on the physical configuration and the FEM analysis results. FEM results are used again for justification at different regions of operation. Second, the effects of transformer tank and the complicated flux path within the core during saturation are considered in the model. The equivalent magnetic circuit is able to simulate not only the linear and knee region operations, but also the heavily saturated region and the so called "air core" region. As a result, the impact of dc over a much greater range on transformer harmonic production is characterized. The complete variations of excitation current harmonics as a function of dc bias are revealed.

Next, a modified nonlinear equivalent Tee circuit is presented. The constant magnetizing inductance of the conventional Tee circuit is replaced by the nonlinear magnetizing inductance which is obtained from the equivalent magnetic circuit model. A single phase transformer operation over a wide range of dc levels at no-load and various loading conditions is simulated. The sensitivity of the excitation current to each lumped component in the Tee circuit (leakage inductances, winding resistances, core loss resistance) is examined in detail. Harmonics interaction with the rest of the power system is also studied with a simplified system representation.

Finally, harmonics from dc biased three phase transformer banks are calculated. Harmonic characteristics of the Y-Y (with one grounded neutral) and Y- Δ three phase banks and single phase connections are compared. Information on how excitation current harmonics shared between the primary and secondary of the three phase transformer

banks is provided. The effect of both unbalanced dc excitations and unbalanced loads are investigated.

1.5 The Significance of This Study

The FEM analysis provides new findings regarding GIC susceptibility of different transformer core configurations, both confirmed and modified some early predictions based on analytical approaches. The study helps to reveal and confirm the fundamental transformer stray flux heating mechanism and provide information for predicting future transformer heating possibilities with respect to different designs and core configurations. It is hoped that the classification of the GIC subjected transformers in the igneous rock zone by their potential risk factors may become possible.

Also, the knowledge of harmonics produced by dc biased transformers will be valuable resources in many applications. To name a few, triggers of monitor and alarm devices could make use of the property of the harmonic components as a GIC saturation indicator. Intelligent protective relays could be designed using one or several harmonic components to distinguish between a transformer internal fault, an in-rush current, or a GMD strike. Restraint functions based on the properties of harmonics from a GIC saturated transformer could be implemented on some capacitor protective relays to block unwanted triggering during a GMD [5,19,20]. Ultimately, this study could help to secure our vast power system from the powerful damaging force of mother nature.

CHAPTER II. TRANSFORMER FUNDAMENTALS

2.1 Electromagnetic Induction and Magnetic Materials

2.1.1 Electromagnetic induction

In 1831, Michael Faraday discovered the phenomenon of electromagnetic induction. It states that a time-varying flux linking a coil induces an emf (or voltage) in the coil. Assume a coil with N turns is placed in a magnetic field which varies with time. Each turns is linked with the same amount of magnetic flux ϕ . Then according to Faraday's law, a voltage v is induced in the coil,

$$v = -\frac{d\lambda}{dt} \quad (2.1)$$

where,

$$\lambda = N\phi \quad (2.2)$$

is flux linkage. Let ϕ be a sinusoidally varying flux of amplitude ϕ_m and frequency f ,

$$\phi = \phi_m \cos(2\pi ft) \quad (2.3)$$

then

$$v = 2\pi f N \phi_m \sin(2\pi ft) = \sqrt{2} V \sin(2\pi ft) \quad (2.4)$$

Thus the magnitude of the induced sinusoidal voltage is

$$V = 4.44 f N \phi_m = 4.44 f N B_m A_c \quad (2.5)$$

where B_m is the amplitude of sinusoidal flux density and A_c is the net cross section of the iron core carrying the sinusoidal flux.

2.1.2 Magnetic materials

Assume a magnetic field exists in a medium with magnetic flux density B and magnetic field intensity H , the permeability (apparent permeability) of the medium is defined as

$$\mu = \frac{B}{H} \quad (2.6)$$

For air (or free space) the permeability is a constant μ_0 ($= 4\pi \times 10^{-7}$ H/m). Materials whose permeability is considerably larger than μ_0 are considered as magnetic materials. Often, the permeability of a magnetic material is expressed in terms of relative permeability μ_r :

$$\mu = \mu_r \mu_0 \quad (2.7)$$

The significant characteristic of magnetic materials such as iron and most soft steel is the nonlinear relationship of B to H . A typical B - H relationship for iron used in some magnetic circuits is shown in figure 2.1. By examining the figure it can be seen that, the B - H curve can be divided into two main regions. The curve in region I can be approximated by a straight line, in which case the permeability is considered constant. In region II, a large change in H results in a relatively small change in B , and eventually B approaches a certain value where the material (iron) saturates. Consequently, the B - H curve is also known as the saturation curve or the magnetization curve. Region II is essentially the nonlinear operating region where the permeability can be expressed by the incremental or differential permeability, μ_d , which is defined by

$$\mu_d = \frac{\Delta B}{\Delta H} \quad (2.8)$$

where ΔB and ΔH are small changes in B and H, respectively.

2.2 Basic Concept of a Transformer

A transformer is a device of electric energy transformation. The application range of transformers extends from extremely low-voltage low-power electronic circuits to very high-voltage high-power transmission systems. A transformer is commonly used to perform the following functions:

1. Changing the voltage and current levels in an electrical system.
2. Impedance matching, as in many communication circuits where the load is matched to the line.
3. Electrical isolation, to block dc signals, and to provide safety in electrical appliances.

Transformers are made up of electric circuits interlinked by magnetic circuit. The coupled electric circuit is provided by the windings of the transformer. The magnetic circuit is realized by the core of the transformer. Electric currents flow through electric circuits and magnetic fluxes flow through magnetic circuits. Electric power transformation is completed through the interaction between electric currents and magnetic fluxes.

Figure 2.2 is a two winding transformer. Its electric currents and magnetic fluxes are also illustrated in the figure. Coils with turns N_1 and N_2 are denoted as primary and secondary winding, respectively. The turns ratio n of primary to secondary is

$$n = \frac{N_1}{N_2} \quad (2.9)$$

If an ideal transformer is assumed, that is, a transformer without leakage flux, without losses and magnetic flux without magnetizing current, the following relationships hold for the given transformer.

$$\frac{V_1}{V_2} = n \quad (2.10)$$

and

$$\frac{I_2}{I_1} = n \quad (2.11)$$

Equation (2.11) is derived from the law of ampere-turn balance in the transformer windings. Which is,

$$I_1 N_1 = I_2 N_2 \quad (2.12)$$

A transformer with $n > 1$ is a step-down transformer and that with $n < 1$ is a step-up transformer.

2.3 Major Parts of Power Transformer

2.3.1 Transformer cores

A power transformer core (iron core) is made of laminated silicon steel, a magnetic material universally used in power system. Its important function is to maximize the

magnetic coupling between its windings and to minimize the dispersion of the magnetic field into the surrounding regions of the transformer.

An iron core has very high permeability. The relative permeability of the core steel of a power transformer varies with the magnitude of magnetic flux density in the core and the effect of magnetic hysteresis. This variation is a nonlinear relationship. The high self-inductance due to the high permeability reduces the no-load or exciting current to a reasonably small value, and the high coefficient of coupling results in small voltage regulation under load. An iron core, however, produces core losses which have an important effect on the efficiency and temperature rise of the transformer. The nonlinear magnetization characteristics of iron also causes the waveform of the exciting current to be nonsinusoidal even when the flux varies sinusoidally. Therefore, under specific operation range, an iron core is designed to minimized core losses within the requirements of size, thermal capability and mechanical strength.

Core losses include hysteresis loss and eddy current loss. Hysteresis loss is determined by the characteristics of the magnetic material while eddy current loss depends on the resistivity of the iron core. The use of grain-oriented silicon-iron since the early 1940's has greatly reduced the hysteresis loss. In the meantime, the use of thin steel sheets and adequate insulation materials between the lamination of the core are important to ensure that eddy current losses are kept to minimum. The commonly used insulation materials are paper, mixtures of china clay and flour, and varnishes [36]. The application of some kind of additional phosphate treatment to the coreplates can give a thinner and more heat-resistant coating.

Core losses are also affected by the ways of core construction, such as the joints made between the core legs and the core yokes, and the clamping of a core. Both butt joint and interleaved joint are practiced. The main concern of building a joint is to minimize the

loss due to cross fluxing and the traverses of flux in directions other than parallel to the rolling direction.

2.3.2 Transformer windings

The basic materials used as conductors are copper and aluminum. Depending on the current and voltage requirements, various forms, such as wires, strips, foil and sheet, have been employed. Parallel conductors are transpositioned to keep down the stray loss which is resulted from the time varying leakage flux.

Both concentric and disk coil windings are practiced with taps built for adjusting the voltage ratio. Certain kinds of insulation and cooling duct are essential. The requirements of a winding design are to provide sufficient electric strength, to control temperature rise within an acceptable level, to minimize the load losses which include the copper loss and stray loss, and to withstand electromagnetic forces of considerable magnitude produced on the winding during fault conditions.

2.3.3 Transformer tanks

Transformer tanks are normally constructed in rectangular shape. Occasionally cylindrical shapes are employed for small sizes. They are fabricated in nearly all cases from mild steel plate in thickness of 4 to 6 mm [36]. However, tanks for very large transformers are often constructed from aluminum in order to reduce mass or to avoid excessive tank heating due to induced eddy currents. Transformers with above 50 kVA rating need additional surfaces for cooling purposes. Radiators or cooling tubes can be built to obtain the extra surfaces. Bushings are often employed to bring out the ends of the winding through the transformer tank for connection to the external system.

2.3.4 Transformer cooling

The purpose of cooling is to transport the unavoidable heat generated inside a transformer through a cooling medium to ambient air or to running water. The cooling arrangement has to be designed in a way that the hot spots in the core and in the windings always remain below specified maximum values. Air or gas is the cooling medium in a dry-type transformer. Mineral oil is commonly used in oil-immersed transformers.

2.3.5 Transformer protection

Transformers used in power system or industrial applications need to be installed in such a manner that they are protected against excessively high voltages and dangerous overloads. Over voltages are surges which result from lightning, switching or faults in the power system. The cure are to use lightning arresters which can provide a heavy current carrying path around the transformer and thus harmlessly dissipate the over-voltage energy. Overcurrent arises if a dangerously high winding current is present either from an abnormal overload or as a result of internal failure of the transformer insulation. Automatic disconnection is provided either by fuses or by automatic circuit breakers which open the circuit before the heating effect of the overcurrent becomes serious. A sensor is fitted to read the temperature accurately under all conditions. It is used for forced cooling control, alarm and finally a trip. Notice that high temperature can be caused by ferroresonance, a most unusual case of overheating.

2.4 Transformer Equivalent Circuit for Normal Operation

2.4.1 Inductance

In magnetic circuit, inductance (L) is a measure of magnetic flux linking a coil,

$$L = \frac{\lambda}{I} = \frac{N\phi}{I} \quad (2.13)$$

That is, inductance L is defined as flux linkage per ampere.

If a N -turn coil is wound on a core, the magnetic flux produced by the coil carrying current I is evaluated in terms of its magnetomotive force, or mmf,

$$F = NI \quad (2.14)$$

The unit of mmf is ampere-turn (At). The reluctance of the core is

$$R = \frac{l}{\mu A} \quad (2.15)$$

where l and A stand for the mean length and cross sectional area of the core, respectively.

The flux produced by the mmf is

$$\phi = \frac{F}{R} = \frac{NI}{R} \quad (2.16)$$

therefore, inductance in a magnetic circuit can be expressed in terms of R

$$L = \frac{N^2}{R} \quad (2.17)$$

As a circuit element, inductance manifests itself only in time-varying situations, such as in ac circuit.

Self inductance is determined by virtue of the coil flux linkage as produced by the coil mmf. For example, the self inductance L_{11} of winding N_1 in figure 2.2 is

$$L_{11} = \frac{N_1(\phi_c + \phi_p)}{I_1} \quad (2.18)$$

where ϕ_c and ϕ_p are the mutual flux and the leakage flux of the primary winding, respectively. Leakage flux is the magnetic flux mostly channeled outside the core due to the unavoidable magnetic reluctance. It may also be described as stray flux. The magnitude of leakage flux is proportional to the current in the windings

2.4.2 Magnetic coupling of electric circuits

Refer to figure 2.2, it is seen that the leakage flux links with one of the coils only. However, the mutual flux ϕ_c links with both coils. In other words, coils N_1 and N_2 are mutually coupled through the mutual flux. The effectiveness of ϕ_c is measured by the mutual inductance between N_1 and N_2 . The mutual inductance L_{12} is defined as

$$L_{12} = \frac{N_2\phi_c}{I_1} \quad (2.19)$$

If ϕ_c is expressed as a fraction of the total flux ϕ , such that

$$\phi_c = k\phi \quad (2.20)$$

where k is a constant less than 1. If R is the reluctance as seen by the mmf N_1I_1 , then

$$\phi = \frac{N_1I_1}{R} \quad (2.21)$$

Combining (2.19) and (2.21) yields

$$L_{12} = \frac{kN_1N_2}{R} \quad (2.22)$$

If L_{21} is defined as

$$L_{21} = \frac{N_1 \phi_c}{I_2} \quad (2.23)$$

then it may be readily verified that

$$L_{12} = L_{21} \quad (2.24)$$

For simplification, the symbol M is used to denote the mutual inductance between two coils.

The factor k is known as the coupling coefficient and can be written

$$k = \frac{M}{\sqrt{L_{11}L_{22}}} \quad (2.25)$$

where k is between 0 and 1.

2.4.3 Simplified equivalent circuits

Representing a transformer by an equivalent circuit comprising some lumped components such as resistance and inductance is useful in analysis. Equivalent circuits often aid in visualizing the relations expressed in the fundamental theory. Neglected the effects of magnetic nonlinearity, loss, and the distributed capacitances of the windings, the coupled-circuit voltage equations for a transformer in terms of self inductance L_{11} , L_{22} and mutual inductance M are

$$v_1 = L_{11} \frac{di_1}{dt} + M \frac{di_2}{dt} \quad (2.26)$$

$$v_2 = L_{22} \frac{di_2}{dt} + M \frac{di_1}{dt} \quad (2.27)$$

where v_1 , v_2 are the instantaneous terminal voltages of the two windings and i_1 , i_2 are the instantaneous currents. Inspection of these equations shows that they apply not only to the transformer but also to the circuit of figure 2.3, which therefore is equivalent to the transformer to the extent that its electrical characteristics are specified by equation (2.26) and (2.27).

For further discussion, assume that the currents and voltages vary sinusoidally so that the voltage equations can be written in vector form as

$$V_1 = jX_{11}I_1 + jX_m I_2 \quad (2.28)$$

$$V_2 = jX_{22}I_2 + jX_m I_1 \quad (2.29)$$

where X_{11} , X_{22} are the self reactance of the primary and secondary, respectively. X_m is the mutual reactance. If equation (2.29) is multiplied by an arbitrarily chosen number A and the secondary current I_2 is divided by A , the voltage equations can be written as

$$V_1 = jX_{11}I_1 + jAX_m \frac{I_2}{A} \quad (2.30)$$

$$AV_2 = jA^2 X_{22} \frac{I_2}{A} + jAX_m I_1 \quad (2.31)$$

Since A may have any arbitrarily chosen value, there is an infinite number of these equivalent circuits, each corresponding to a particular value of A . Notice that the leakage inductance X_p and X_s can be given as

$$X_p = X_{11} - (N_1/N_2)X_m \quad (2.32)$$

$$X_s = X_{22} - (N_2/N_1)X_m \quad (2.33)$$

Therefore when A equals the turns ratio, the equivalent circuit of figure 2.3 becomes figure 2.4, an equivalent circuit involving leakage inductances and with all the parameters referred to the primary. Here L_m is the magnetizing inductance which is equal to

$$L_m = \frac{N_1 X_m}{N_2 \omega} = \frac{N_1}{N_2} M \quad (2.34)$$

2.4.4 A more completed equivalent circuit

Although an "equivalent" circuit can not be equivalent to the actual transformer in all respects, including losses in the equivalent circuit is desirable. Transformer losses are the electric power, supplied by the source, that is converted to thermal power in the transformer and which has to be dissipated. A distinction is made between the no-load loss, arises in the core from the effects of magnetic hysteresis and of eddy currents, and the load loss which results from the load current carried in the windings. The two losses are considered separately, as shown in figure 2.4. The no-load loss, also called core loss, is represented by R_c which is in parallel with the shunt magnetizing inductance. R_p and R_s correspond to the load losses arise from the current carried in the primary and secondary windings respectively. They are in series with the leakage inductance of the corresponding windings. All the losses are discussed in the following sections.

1. Core loss (no-load loss)

Hysteresis loss

Hysteresis loss is the energy dissipation causes by magnetic hysteresis, a tendency of the material to retain magnetism or to oppose a change in magnetism. Its occurrence has an

important effect on the efficiency, the temperature rise, and hence the rating of many electromagnetic devices. It is measured by a loop involved in the B-H characteristic of the material when the material is subjected to a cyclic magnetizing force. Typical loop is illustrated in figure 2.5. It is the energy converted into heat as a result of work done on the material when it responds to the magnetization. Thus the energy dissipated in the core per unit volume per cycle because of hysteresis can be calculated as

$$w_h = \frac{1}{4\pi} \left(\int_{-B_{\max}}^{B_{\max}} H_1(B) dB + \int_{B_{\max}}^{-B_{\max}} H_2(B) dB \right) = \frac{A_{loop}}{4\pi} \quad (2.35)$$

where $H_1(B)$ is the curve when B increases from $-B_{\max}$ to B_{\max} and $H_2(B)$ is the curve when B decreases from B_{\max} to $-B_{\max}$. A_{loop} is the area of the hysteresis loop. Thus the hysteresis power loss is

$$P_h = \frac{Vf}{4\pi} \times A_{loop} \quad (2.36)$$

where V is the volume of the material in which the flux density is uniform everywhere. f is the flux variation frequency. Since the loss varies as a function of B_{\max} , it can be determined accurately through repeating the calculation for hysteresis loops having various values of B_{\max} . If symmetrical hysteresis loop, in which B ranges between equal positive and negative values, and no reentrant loop, the expression for the energy loss per unit volume per cycle can be empirically given as

$$w_h = \eta B_{\max}^m \quad (2.37)$$

where m and η have values that depend on the material. m may range between 1.5 to 2.5 and may not be a constant for a given material, depending on the range of B_{\max} . If the corresponding value of the coefficient η is used, the total hysteresis loss can then be expressed empirically as

$$P_h = \eta V f B_{\max}^m \quad (2.38)$$

Eddy current loss

Whenever the magnetic flux in a medium is changing, an electric field appears within the medium as a result of the time variation of the flux. This expression can be given by the Faraday induction law as

$$\oint_{abcd} \vec{E} \cdot d\vec{l} = -\frac{d}{dt} \int \vec{B} \cdot \vec{n} ds \quad (2.39)$$

where abcd is the circuital path bounding the area crossed by the flux ϕ . Eddy current is the current set up around this path by the induced electromotive force e resulting from the line integral of the electric field. Eddy current loss which is proportional to i^2R results in the material. The calculation of the eddy current loss can be illustrated through the following example.

Figure 2.6 shows a portion of the lamination slab which has unit height, unit width, and thickness τ and is symmetrical about the OY axis which passes through the center of the slab. The direction of the flux is normal to the surface abcd. Neglecting skin effect, uniform magnetic field distribution is assumed. Because of the great height as compared with the thickness, the voltage gradient is practically uniform along the vertical current paths except near the top and bottom of the slab. Therefore, any horizontal slice of unit height not too near the top or the bottom has practically the same configuration of voltage gradients and current densities as any other horizontal slice. If the conducting material has a volume resistivity ρ , the current density J_x along bc or da can be calculated by combining equation (2.38). It is

$$J_x = \frac{E_x}{\rho} = -\frac{1}{\rho} \frac{d}{dt}(Bx) = \left(-\frac{x}{\rho}\right) \frac{dB}{dt} \quad (2.40)$$

where E_x is the vertical voltage gradient at a horizontal distance x from the YZ plane. Integral equation (2.39) over the thickness τ , the instantaneous eddy current loss per unit cube of laminated material with perfect insulation between the slabs so that no current exists across the lamination is

$$\frac{2}{\tau} \int_0^{\tau/2} J_x^2 \rho dx = \frac{\tau^2}{12\rho} \left(\frac{dB}{dt} \right)^2 \quad (2.41)$$

Substituted equation (2.1) into (2.40), the instantaneous power $p(t)$ can be expressed in terms of induced voltage $e(t)$

$$p(t) = \frac{\tau^2}{12N^2A^2\rho} e(t)^2 \quad (2.42)$$

where $e(t)$ can be written as a Fourier series of harmonic components

$$e(t) = V_{dc} + \sum_n \sqrt{2} V_n \cos(n\omega t + \alpha_n) \quad (2.43)$$

and the average value of $e(t)$ over a cycle is equal to the rms value E , it is

$$E = \sqrt{\frac{1}{T} \int_0^T [e(t)]^2 dt} \quad (2.44)$$

Thus the average eddy current power loss per unit volume is

$$p_e = \frac{\tau^2 E^2}{12N^2A^2\rho} \quad (2.45)$$

If flux density is varying sinusoidally at a frequency f , p_e can be expressed in terms of B_{\max}

$$p_e = \frac{\pi^2 f^2 \tau^2 B_{\max}^2}{6\rho} \quad (2.46)$$

Taken skin effect into account, a more accurate expression can be given as

$$p_e = \frac{fB_{\max}^2}{12\mu}(\alpha d)^2 \left[1 - \frac{6}{945}(\alpha d)^4 \dots \right] \quad (2.47)$$

where αd is given by

$$\alpha d = \pi \tau \sqrt{\frac{2\mu f}{\rho}} \quad (2.48)$$

The above analysis shows that the eddy current loss increases quickly when the thickness of the slab increases. Therefore, to keep the eddy currents produced of a low value, the steel laminations should be thin and electrically insulated from one another.

2. Load loss

All the losses associated with the windings are called load loss or copper loss. They can further divided into two categories: the first one is the I^2R loss resulted from the resistance of the windings; the second one is the eddy current loss due to the leakage flux which traverses through any metallic parts other than the core. This kind of eddy current loss is also called stray loss. Stray loss can exists in windings, in clamps and in tanks. Sometimes clamps and tanks can cause further loss and excessive local heating by the fact that the most common material for the structural parts of the transformer is mild steel, which magnetic properties result in a concentration of flux in it. Therefore, although the loss due to winding resistance forms the major part of the load loss, stray loss can become quite significant and should be considered carefully.

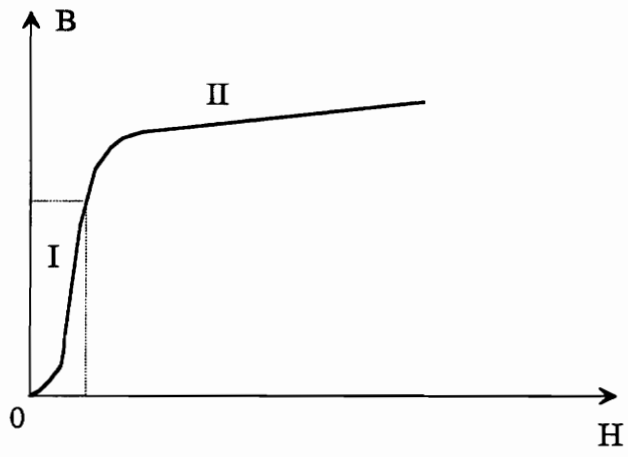


Figure 2.1 Typical B-H relationship of magnetic material

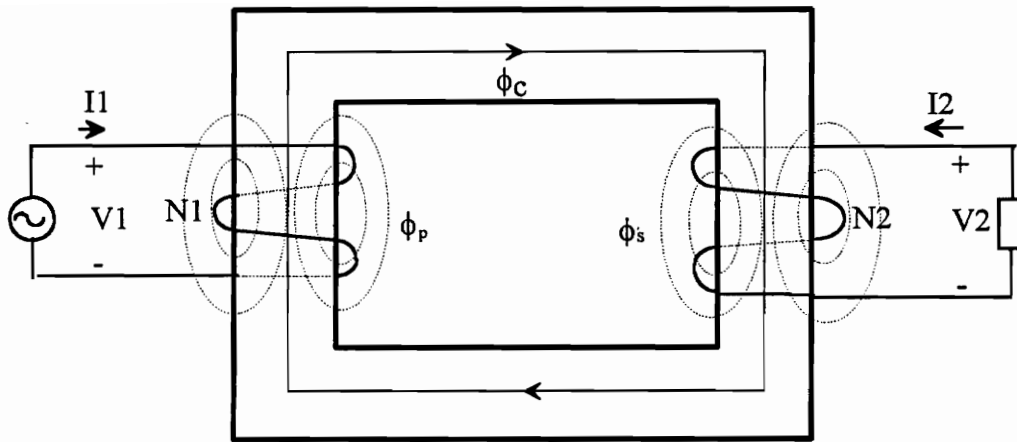


Figure 2.2 A two winding transformer

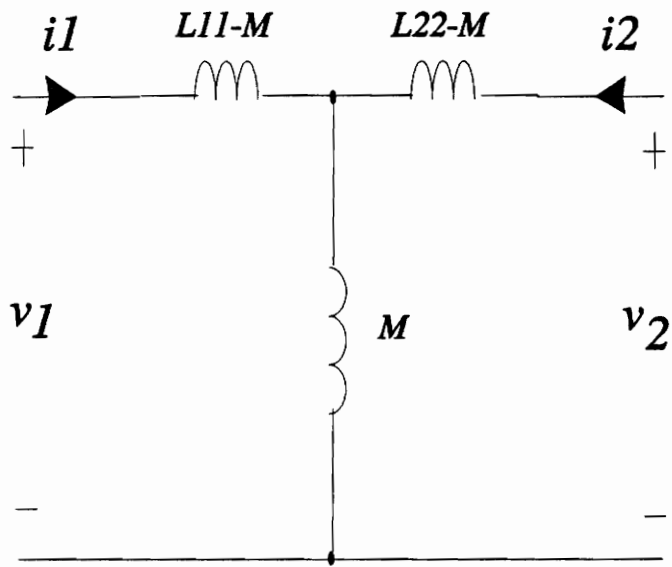


Figure 2.3 Simplified transformer equivalent circuit

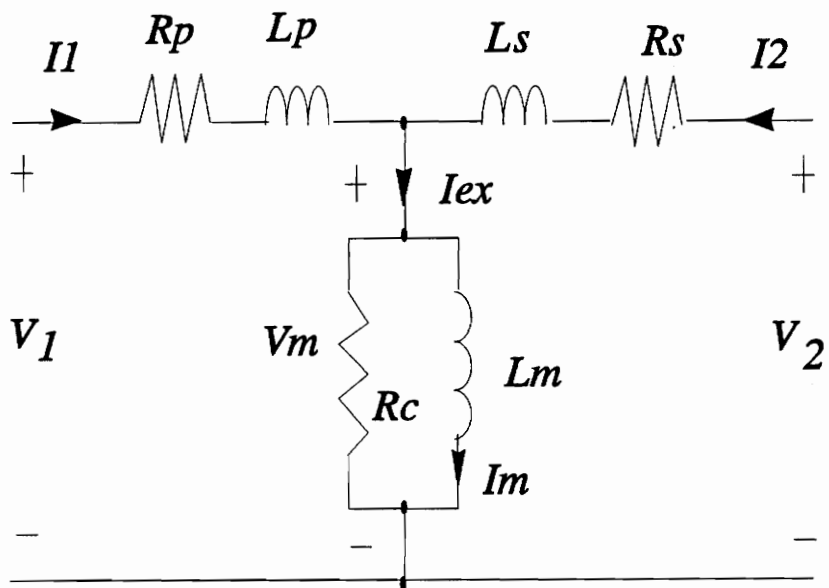


Figure 2.4 More completed transformer equivalent circuit

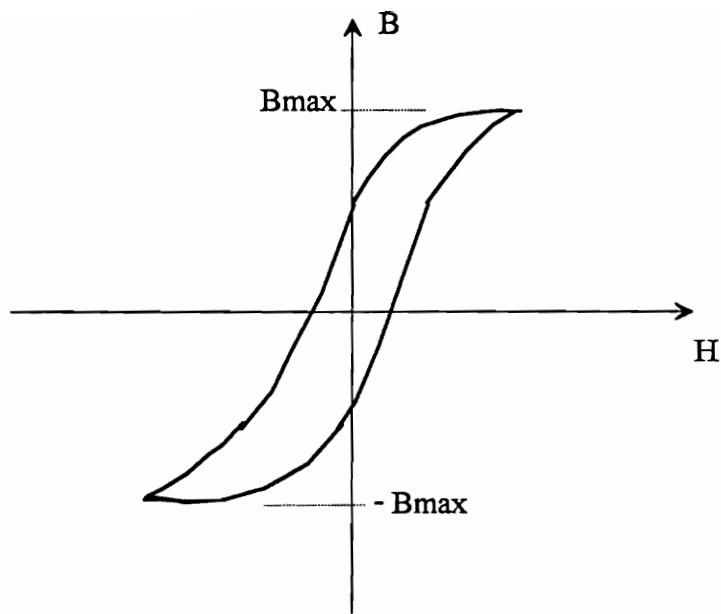


Figure 2.5 Hysteresis loop

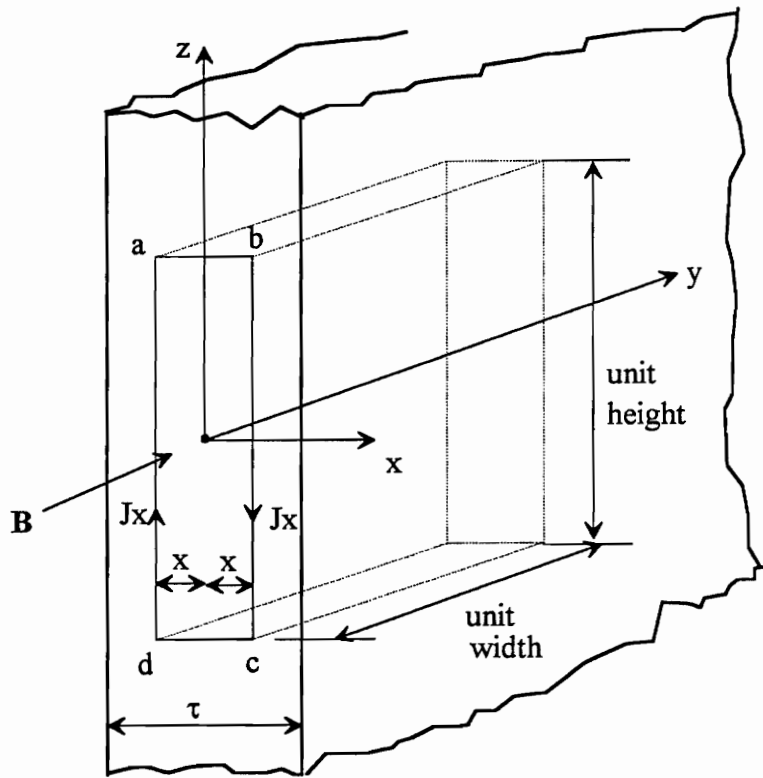


Figure 2.6 A portion of the lamination slab

CHAPTER III. FEM ANALYSIS STUDY

3.1 Introduction

Many aspects of the effect of geomagnetically induced currents on power systems have been studied for more than two decades. However, very few reports on transformer flux analysis using finite elements method are found and they often focused on one particular design. Overall, a complete FEM analysis covering most of the transformer designs is not available.

In this chapter, a systematic finite element analysis of transformer dc magnetization is presented. Analysis of transformer dc magnetization of five simplified generic core configurations is performed. The studies include the analysis of profiles of magnetic field intensity (H) and transformer impedance matrix (Z) parameters. The objective of this initial study is to understand the trends of dc and ac flux distribution under different levels of core saturation for various transformer designs and core configurations.

Each design is a unique case. Although completely general laws are not practical based on the generic cases analyzed at the present time, typical cases can be used to infer similar designs.

3.2 2D DC Bias Magnetizing Flux Simulation

DC flux distributions of simplified core geometries, winding and tank structures are studied first. The objective is to study the dc effect on core saturation for various transformer designs and core configurations. This study also considers the effect of extreme dc levels that may have not been observed in the past, and cases which would be

difficult to achieve in full scale tests due to either limitations of adequate dc test sources or the risk of damaging a healthy transformer. The following transformer core configurations are included in this study.

- 1) Single phase transformer core
- 2) Three phase three leg transformer core
- 3) Three phase five leg transformer core
- 4) Three phase seven leg transformer core
- 5) Three phase conventional transformer core

3.2.1 Fundamental dc excitation analysis of a single phase transformer design

The single phase designs including both shell form and core form can always provide a return path for zero sequence magnetic flux. Flux distribution is well confined inside the core during normal operation. Under dc excitation, the dc current will bias the core at different saturation regions depending on the magnitude of the current. As a result, part of the flux is being pushed out of the saturated core, causing leakage flux, or stray flux, surrounding the core. Flux distribution of a single phase transformer under heavy saturation is shown in figure 3.1. Because of its tendency to seek a low reluctance path, the stray flux is going to concentrate in regions where magnetic materials exist. Therefore, heating problem due to eddy loss is likely to occur in these regions under ac operation.

When a transformer saturates, the whole core usually does not saturate on the same level. That is, part of the core may saturate more than other parts, while some part may not saturate at all. The core saturation patterns vary with, not only core configurations, but also the core leg dimensions.

Figure 3.1 shows a single phase transformer. Since only dc excitation current is applied for the simulation, only the primary winding is drawn on the figure. The following paragraphs describe the impact of changing side leg cross section on overall core saturation. During normal operation without dc, assuming no leakage flux leaving the core, the operating point lies in the linear region of the B-H curve and the core possesses a somewhat uniform permeability μ_r . If the cross sectional area of the side legs and yokes is half of that of the main leg, the relationship between the main leg flux, ϕ_c , and the side leg flux, ϕ_r , as shown in figure 3.1, is given by,

$$\phi_c = 2\phi_r \quad (3.1)$$

Because the reluctance for each segment of the core is expressed by equation (2.15), the core can be modeled by a lumped magnetic equivalent circuit shown in figure 3.2. Since the cross sectional area of the side legs and the yokes is half of that of the main leg, the dimensions of the transformer core are,

$$A_r = 1/2 A_c, \quad L_r = 5 \text{ ft}, \quad L_y = 4.5 \text{ ft}$$

where L_r and L_y are the effective length of the side legs and the yokes respectively. The reluctance values of the elements in the equivalent circuit are calculated as,

$$R_r = 2 R_c, \quad R_y = (9/5) R_c$$

The mmf is,

$$F = \phi_c \left(R_c + \frac{2R_y + R_r}{2} \right) = 3.8\phi_c R_c \quad (3.2)$$

Thus,

$$B_c = \frac{\phi_c}{A_c} = \frac{1}{3.8} \frac{F}{R_c A_c} \quad (3.3)$$

$$B_r = \frac{\phi_c/2}{A_r} = \frac{1}{3.8} \frac{F}{R_c A_c} \quad (3.4)$$

where R_c , R_r and R_y are the reluctances of the main leg, side leg, and the yoke. F is the magnetomotive force (mmf). ϕ_c , B_c , and A_c are the flux, flux density and the cross sectional area of the main leg, respectively. B_r is the flux density of each side leg or yoke.

Based on the equivalent circuit, two additional cases with respect to figure 3.1 are examined. First, the side leg cross sectional area is increased such that it is equal to A_c . Then,

$$A_{r1} = A_c, \quad L_{r1} = 6 \text{ ft}, \quad L_{y1} = 5 \text{ ft}$$

Hence the flux density can be calculated,

$$B_{c1} = \frac{1}{2.8} \frac{F}{R_c A_c} \quad (3.5)$$

$$B_{r1} = \frac{1}{5.6} \frac{F}{R_c A_c} \quad (3.6)$$

Second, the side leg cross sectional area is decreased such that it is equal to a quarter of A_c . Then,

$$A_{r2} = 1/4 A_c, \quad L_{r2} = 4.5 \text{ ft}, \quad L_{y2} = 4.25 \text{ ft}$$

The flux density is calculated as,

$$B_c = \frac{1}{6.1} \frac{F}{R_c A_c} \quad (3.7)$$

$$B_r = \frac{1}{3.05} \frac{F}{R_c A_c} \quad (3.8)$$

It can be seen from the flux density results that for the same dc excitation level, the larger cross sectional area of the side leg A_r results in the lower dc flux density in the side leg while higher dc flux density in the main leg. Therefore, one can conclude that:

- a) Comparing the main leg saturation level of the three cases, the one with the largest side leg will saturate first.
- b) Comparing the side leg saturation level of the three cases, the one with the smallest side leg will saturate first.
- c) For the case shown in figure 3.1 that the side leg cross sectional area is half of that of the main leg, the entire core will reach saturation at the same time.

Resulted from finite element solution, the bias levels for each core segment under low saturation dc excitation are shown in figure 3.3. Notice that once the core reaches saturation, calculations based on the above equivalent circuit are no longer valid because the permeability μ_r is not uniform. Also, equation (3.1) does not hold due to the existence of stray flux.

The results obtained from the above analysis can be applied to different transformer core configurations. The core saturation patterns for a particular transformer can be used to roughly predict the patterns for those having the same core configuration but different core leg dimensions.

3.2.2 H fields along traverses of a single phase transformer

Examining the field intensity H outside the core regions can help understand potential stray flux heating effect in those regions. Since flux density B is proportional to H , knowing the magnitude of the field intensity H in the air region can lead to rough prediction of eddy losses if conducting material exists. Areas having higher H are likely to be more sensitive to heating problem, although H will be redistributed in the presence of magnetic materials. It is important to point out that ac and dc flux patterns may not be the same depending on core configurations.

H profiles along A and B lines (figure 3.1) under heavy saturation is shown in figure 3.4. It is found that the inside corner regions have the highest H if at least one leg adjacent to the corner is saturated. The stray flux shows more concentration in those regions. Also, two peaks are seen at the edges of the windings.

3.2.3 DC effects of three phase core configurations

Under balanced dc excitations in the three phases, it seems logical that the following magnetic designs are more susceptible to half cycle saturation since they allow a flux path for zero sequence excitation mmf. Those include three phase conventional core as well as three phase five leg and seven leg core designs.

Other designs where a closed path through the iron core for zero sequence mmf is not possible are expected to be much less susceptible to GIC. The three phase three leg core form is an example. Its configuration including tank is illustrated in figure 3.5. When the three phases are biased under balanced dc excitation currents, there exists no return path for the dc flux. DC flux tends to leave the core. Since the air exhibits a very high reluctance path for the magnetic flux, the dc flux bias is low. Consequently, the three phase three leg core type is less susceptible to GIC if the dc excitation is balanced. This

is illustrated by showing its operating points in the linear region under very high excitation currents in figure 3.6.a.

It is very important to notice that a three phase three leg core form transformer will eventually reach saturation if the dc bias is increased further. In this simulation, when the dc excitation current is doubled, the core will operate at the knee of the saturation curve, as shown by the cross markers in figure 3.6.a.

The same dc bias as that used in the three leg core form transformer is applied to a three phase five leg and a seven leg transformer. Saturation occurs as expected in both cases. A comparison of the saturation magnetizing flux between these two cases is illustrated by figure 3.7 and figure 3.8. The results indicate that part of the seven leg core has higher saturation level than the five leg core. Their bias points are shown in figure 3.6.b and 3.6.c.

A three phase conventional core design is shown in figure 3.9. As we increase the dc excitation, it is apparent that region 1 and 2 will saturate first since they provide paths for two branches of flux. The same dc bias as that used in the three phase core form is applied. Region 1 and 2 are now under heavy saturation.

Based on the simulation with the specified three phase core dimensions shown from the figures, an order of increasing susceptibility to GIC damage can be given as following:

- The three phase five leg core design
- The three phase seven leg core design
- The three phase conventional core design

This order may change if the proportion of the dc flux return area (or side leg dimensions) varies. Because a transformer saturation level depends on both the core

configuration and the core dimension, there is no absolute susceptibility order for three phase transformers.

3.2.4 Effect of unbalanced dc bias on three phase core form transformer

How neutral GIC current divides among transformer windings is determined by the dc resistances along the three phases as well as the system resistances. Usually it is assumed that the three phase windings have approximately the same resistance and the rest of the power system has less effect due to smaller resistances. Experiments on actual transformers tend to suggest that the GIC may not be evenly distributed among the three phases. Some degree of flux cancellation may result due to this unbalanced situation.

Flux distribution of the three phase three leg core form transformer under unbalanced dc excitations was examined for two setups. First, the unbalanced excitation is obtained by decreasing the dc excitation current in one of the three phases. For example, current in winding a is decreased. Second, the unbalanced excitation is obtained by increasing winding a current. The resultant flux distribution for the second setup is shown in figure 3.10. A return path is provided for the net magnetic flux due to the unbalanced flux in the three phases. As a result, part of the core will saturate, as illustrated by the flux density in figure 3.10.

3.2.5 H field profiles of three phase transformers

1. H profiles along traverses outside the core

Considering the three leg core form and the five leg and seven leg designs mentioned above, the magnitude of the field intensity H along lines A ~ F (shown in figure 3.5, 3.7 and 3.8) are plotted in figures 3.11, 3.12 and 3.13, respectively. It can be seen that the H

values along lines C and E outside the core are similar in these configurations. Since high H is found outside the cores, high dc flux density near the tanks is expected.

H outside the three phase conventional core is also examined. An interesting phenomenon occurs that H along line C and line E, as shown in figure 3.14, is much lower compared with those in the previously described three phase configurations. Flux density inside the tank is therefore very low.

2. H profiles along traverses outside the tank

H along lines D and F for all configurations decreases uniformly towards the direction leaving the tank, except at the corners where there are small peak values, as shown in figures 3.11, 3.12 and 3.13.

3. H profiles along traverses across the main leg

H values along lines A and B in figure 3.11 are low in the corners since the dc bias inside all the main leg cores are low. They peak in the air outside of the corners and in regions between windings a and b, b and c. In figure 3.12, the H value along line A has almost the same shape as that in figure 3.11, while the H along line B shows two peaks in the side leg corners due to the side leg saturation. For the conventional configuration, since yokes 1 and 2 are under heavy saturation, it is understandable that H near these two yokes is very high.

The three phase seven leg transformer has similar H profiles as the five leg configuration except that along line B there is a minimum appearing between winding b and c as well as winding a and b. This is resulted from the extra core legs between the two adjacent windings.

3.3 2D AC Excitation Under DC Bias

3.3.1 Leakage flux distribution

When a transformer core is saturated, large amount of flux is pushed out of the core. Figure 3.15.a and figure 3.15.b illustrate the ac leakage flux distributions of a single phase transformer under normal excitation ($\mu_r = 2000$) and heavy dc saturation ($\mu_r = 2$). It is understood that the ac leakage flux portion increases within the total ac flux during saturation. However, the absolute value of the ac leakage flux decreases since the total ac flux decreases drastically due to saturation. In other words, the average permeability in the core goes down and reaches a value close to air core permeability, so does the total ac flux ($\text{total}_{ac} = \text{mutual}_{ac} + \text{leakage}_{ac}$). Thus the increased proportion in leakage may not be able to offset the effect of total ac flux decrease. H profiles along two transverses under normal excitation and heavy dc saturation are given in figure 3.16.a and figure 3.16.b, respectively. It is seen that majority of the leakage flux concentrates between windings. When μ_r decreases 1000 times, the field intensity H between windings only changes 6%. Although H values near the tank show noticeable change, they are still negligible comparing to the very high H between windings.

This can also be seen from the change in transformer impedance (Z) matrix parameters discussed in the next section. The difference of leakage inductance before and after saturation is minimum. This indicates that, during GIC bias, the possible danger caused by leakage flux heating is as much as it was under normal excitation. The potential contributor of stray flux heating probably comes from the excitation flux which forms loops inside as well as outside the magnetic core. As the core saturates, flux may have to seek paths in metallic structural parts and the tank as well.

3.3.2 AC excitation flux distribution

Since leakage flux is unlikely to cause additional heating under dc operation, the magnetizing flux under dc was investigated subsequently. Two three phase transformers, the three phase conventional transformer and the three phase five leg transformer, were excited with a three phase ac source under normal and heavy dc saturation. An average relative permeability of 2000 was used for normal excitation. For heavy saturation the relative permeability was assumed to be 2. The tank was also included in the simulation. Heavy saturation ac excitation flux distributions were examined along six traverses for each transformer design. Higher harmonic components in the ac excitation current were not included. The effective magnitude of ac excitation current was chosen to be 10 times the normal excitation current to simulate the saturated condition (During the GIC bias half cycle, excitation current of 50 times the normal ac excitation has been observed). Due to the mesh size constraint which has to be less than half of the skin depth, the dimension of the generic finite element models was set in the millimeter range. However, the model should produce qualitatively valid results in spite of reduced dimension.

Figure 3.17.a and 3.17.b show the three phase conventional transformer ac flux distribution at t_0 when phase a current is at its maximum and at t_1 when phase a current is minimum. Its average magnetic field intensity H along traverses A ~ F is plotted in figure 3.18 for heavy saturation condition. Figure 3.19.a and figure 3.19.b show the three phase five leg transformer ac flux distribution at t_2 when phase b current is at its maximum and at t_3 when phase c current is at its maximum. Figure 3.20 shows the average magnetic field intensity H along traverses A ~ F for a three phase five leg transformer under heavy saturation condition.

3.3.3 Leakage flux patterns for different winding structures

Transformer winding is also a very important part of a transformer design. The two common winding structures are cylindrical winding and pancake winding. While the excitation flux patterns are identical for transformers having the same core configuration, their leakage flux patterns are greatly different. The leakage flux distribution of a single phase transformer core with pancake winding is illustrated in figure 3.21, It is obvious to distinguish this leakage flux pattern from the one with cylindrical winding as it is given in figure 3.15. However, since the leakage flux contributes little on the potential heating during dc saturation, only cylindrical winding is used throughout the study.

3.3.4 Transformer impedance matrix and circuit model

It is usually convenient to model magnetic circuits using their electric analogies. A typical transformer model for low frequency is the equivalent Tee circuit (figure 2.4). It consists of leakage inductances L_p and L_s , magnetizing inductance L_m , and ac winding resistances, R_p and R_s . The shunt resistance R_c is used to represent core losses. Transformer two port network impedance matrix is defined as:

$$Z = \begin{bmatrix} Z_{11} & Z_{12} \\ Z_{21} & Z_{22} \end{bmatrix} = \begin{bmatrix} (R_{11}, L_{11}) & (R_{12}, L_{12}) \\ (R_{21}, L_{21}) & (R_{22}, L_{22}) \end{bmatrix} \quad (3.9)$$

$$= \begin{bmatrix} \left(R_p + \frac{R_c \omega^2 L_m^2}{R_c^2 + \omega^2 L_m^2}, L_p + \frac{R_c^2 L_m}{R_c^2 + \omega^2 L_m^2} \right) & \left(\frac{R_c \omega^2 L_m^2}{R_c^2 + \omega^2 L_m^2}, \frac{R_c^2 L_m}{R_c^2 + \omega^2 L_m^2} \right) \\ \left(\frac{R_c \omega^2 L_m^2}{R_c^2 + \omega^2 L_m^2}, \frac{R_c^2 L_m}{R_c^2 + \omega^2 L_m^2} \right) & \left(R_s + \frac{R_c \omega^2 L_m^2}{R_c^2 + \omega^2 L_m^2}, L_s + \frac{R_c^2 L_m}{R_c^2 + \omega^2 L_m^2} \right) \end{bmatrix}$$

The impedance matrix of a single phase transformer without including tank is calculated using the finite element method. Figure 3.22 shows the single phase transformer 2D model with finite element meshes. Both primary and secondary windings are included in the model. In this example, the core conductivity is set at $1e+6$ m/S. The winding

conductivity is $5.8e+7$ m/S (copper). Since the impedance matrix calculation involves ac operation, the periodically varying flux inside any conducting materials tends to be crowded toward the surface. This phenomenon is known as skin effect. The numerical calculation requires that the largest mesh size of any conducting material must be smaller than half of its skin depth. In order to meet this requirement without drastically increasing the computation time, the model has been scaled down to millimeter range and a frequency of 10 Hz is used. Modeling of core lamination becomes less critical with the smaller core size. Three cases are used to simulate the different dc bias levels.

Case 1 simulates the normal operation assuming an average relative permeability of 50,000 for the core material. The parameters as defined in equation (3.9) is given by Z_1 . Case 2 is under saturation. Since the relative permeability μ_r is no longer uniform in the core as discussed earlier, piece-wise μ_r is assigned for different parts of the core, as shown in figure 3.23. Z_2 gives parameters for this case. Case 3 simulates the extreme case by assuming an air core ($\mu_r = 1$). Its parameters are given by Z_3 .

All units in the impedance matrixes are in MKS. Note that the Z matrix entries are for an conceptual transformer design. Only the changes of those parameters are used to illustrate the change due to dc bias:

$$Z_1 = \begin{bmatrix} (2.0303e-1, 3.6205e-3) & (1.8771e-1, 3.6202e-3) \\ (1.8771e-1, 3.6202e-3) & (2.0304e-1, 3.6206e-3) \end{bmatrix}$$

$$Z_2 = \begin{bmatrix} (1.5326e-2, 2.5730e-5) & (6.2434e-6, 2.5650e-5) \\ (6.2434e-6, 2.5650e-5) & (1.5326e-2, 2.6240e-5) \end{bmatrix}$$

$$Z_3 = \begin{bmatrix} (1.5326e-2, 6.1629e-7) & (4.3721e-9, 4.6033e-7) \\ (4.3721e-9, 4.6033e-7) & (1.5326e-2, 1.0060e-6) \end{bmatrix}$$

The following changes can be observed:

Mutual Coupling

The tight coupling introduced by the iron core is less effective at saturation. The coupling coefficient k is used to indicate the coupling efficiency which is given by equation (2.25).

FEM analysis of the above single phase transformer shows that coupling coefficients decrease when the saturation level increases. Here, the coupling coefficient is 0.9999 under the normal operation and 0.9872 during core saturation. The air core coupling coefficient is 0.6521.

Mutual inductance between the primary and secondary winding decrease from $L_{12} = 3.620e-3$ MKS to $L_{12} = 4.603e-7$ MKS corresponding to a change of average μ_r from 50,000 to 1, respectively. The simulation indicates that the mutual inductance L_{12} (or L_{21}) is nearly in proportion to the core permeability, which is true when R_c is much greater than ωL_m .

Leakage Inductances

The leakage inductance L_p of the primary winding for this particular design can be found from the difference between L_{11} and L_{12} .

Normal operation:

$$L_p = L_{11} - L_{12} = 3.6205e-3 - 3.6202e-3 = 2.6e-7 \text{ MKS}$$

Under core saturation:

$$L_p = L_{11} - L_{12} = 2.5730e-5 - 2.5650e-5 = 0.80e-7 \text{ MKS}$$

Air core case:

$$L_p = L_{11} - L_{12} = 6.1629e-7 - 4.6033e-7 = 1.56e-7 \text{ MKS}$$

These numbers show that leakage inductance varies a little under dc bias. This indicates that net change of the leakage flux introduced by the load current is almost negligible. The major leakage flux under saturation is resulted from the drastically increased magnetizing current.

Resistances

The difference between R_{11} and R_{21} in the Z matrix is the winding loss R_p in the equivalent circuit. Here R_p represents copper loss as well as stray loss in the primary winding. R_c represents the core loss which is also reflected in the expressions of all the Z matrix entries.

Based on the above discussion, if the basic parameters in the transformer equivalent circuit are to be preserved, they will have to be modified accordingly. This merits further study since saturation occurs only during part of each half cycle and the model needs to reflect the dynamic nature of the transformer operation under GIC.

3.4 3D DC Bias Magnetizing Flux Simulation

2D simulation can only provide information on the symmetric plane while 3D simulation can provide information everywhere around the whole object. 3D approach is closer to the real world physical condition. However, 3D simulation demands much more computer memory and computational time due to the complexity of a 3D object, thus limiting its application. The following section presents the dc transformer 3D simulation

results. The purpose of this study is to verify the 2D results and determine the discrepancies when the interested regions are away from the symmetric plane.

The 3D configuration of a three phase three leg transformer and its 2D top view are shown in figure 3.24. All the materials and dc input current are the same as those used in the 2D simulation as illustrated in figure 3.5. The symmetric plane has the same dimensions as the corresponding 2D configuration. The magnitude of the field intensity H along line A (shown in figure 3.24), which corresponds to line B in figure 3.11, is given in figure 3.25.a. The trend of this plot shows good agreement with the 2D result except some differences in magnitude in certain sections.

When line A moves away from symmetric plane along the X direction while it still goes through the core legs, the observed H profiles along these moving lines are all similar. The H profile along line B is illustrated in figure 3.25.b. The only noticeable changes are between the winding area because the winding location on the line is changing when line A moves. The magnitude of H in these area is actually increasing. Once line A leaves the core, for example, as shown in line C, some sections which were across the core legs are now exposed in the air. The magnitude of H in these air sections are about the same as those around the winding area in the symmetric plane due to the cylindrical design of the windings. The H profile of line C is plotted in figure 3.25.c.

When line C moves towards the X direction, the magnitude of H between the winding area continues to increase slowly. It reaches its maximum value at a certain point. Then the magnitude of the whole curve starts to decrease gradually as line C continues to move towards the X direction. The H profile along line D is given in figure 3.25.d.

The above study shows that the 2D simulation can produce acceptable results on the transformer symmetric plane. The approximate patterns along different directions of the

transformer can be estimated according to the results from the symmetric plane. Therefore, 2D simulation is practically useful for qualitative study.

3.5 Conclusions

The FEM analysis results here have confirmed most of the previous conclusions based on analytical studies regarding the GIC susceptibility of different transformer core configurations. All single phase and three phase designs are susceptible to GIC. This study further points out that the three phase three leg core form could also be susceptible if unbalanced GIC currents in the three phases become significant.

Under dc bias the leakage flux distribution in a single phase transformer changes very little. It is unlikely to introduce additional heating loss from what was normally there before saturation. The major source of possible stray flux heating is very likely from the magnetizing current. It contains higher harmonics and has an increased effective value under saturation.

Including the transformer tank in the simulation proved to be necessary. The results show that the magnetic field intensity outside the core with tank is much higher than without the tank. Winding location and winding configuration also affects the magnetic field distribution during saturation. The area close to the winding is likely to have higher H. Under normal conditions, when the flux is confined inside the core, the effect is less significant. Whenever a transformer saturates, the area having high field intensity H is most likely to introduce heating problems when conductive material exists.

2D simulations have been compared with 3D simulations. On the symmetric planes, 2D and 3D simulations show good agreement. This proves that 2D simulation can also provide useful information.

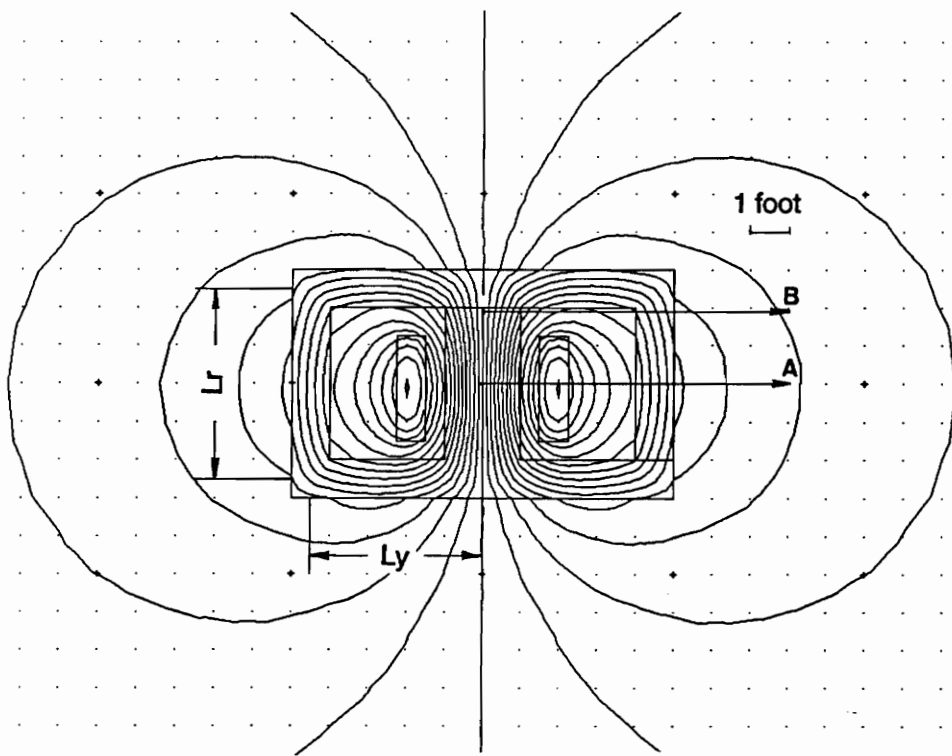


Figure 3.1 Single phase transformer core configuration and its dc flux distribution under heavy saturation

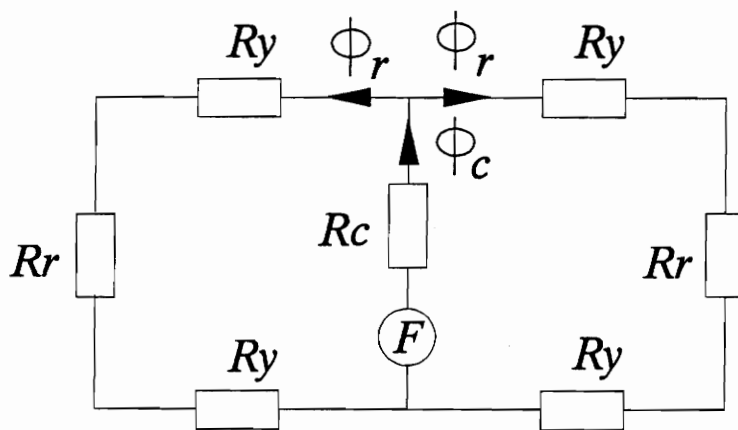
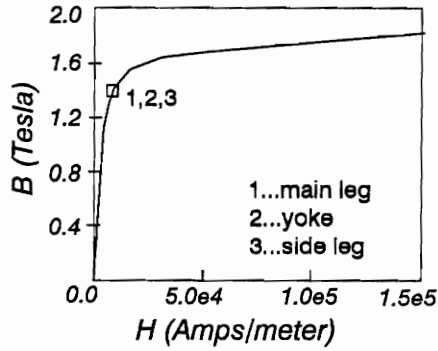
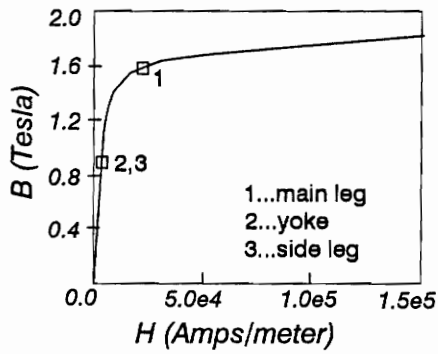


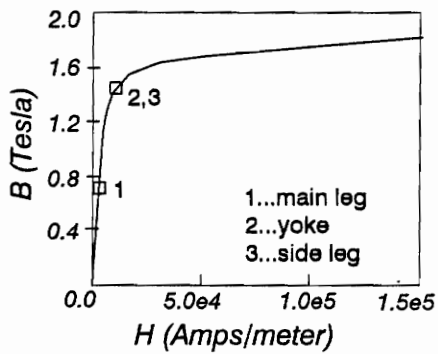
Figure 3.2 A lumped magnetic equivalent circuit of the single phase core



a) side leg area is equal to the main leg area



b) side leg area is twice of the main leg area



c) side leg area is a quarter of the main leg area

Figure 3.3 Single phase transformer's bias levels for each core segment under the same low dc excitation

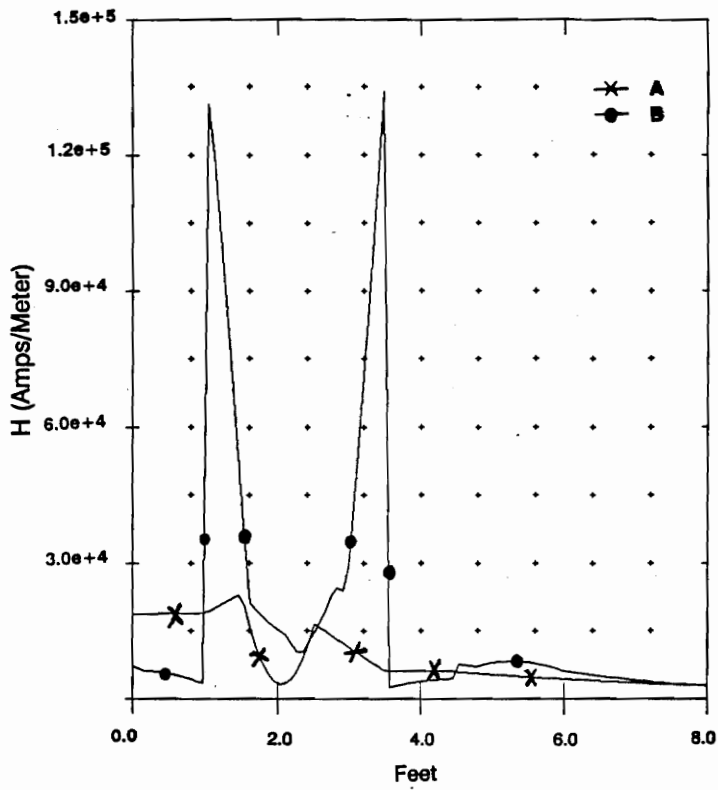


Figure 3.4 H profiles along traverses of a single phase transformer

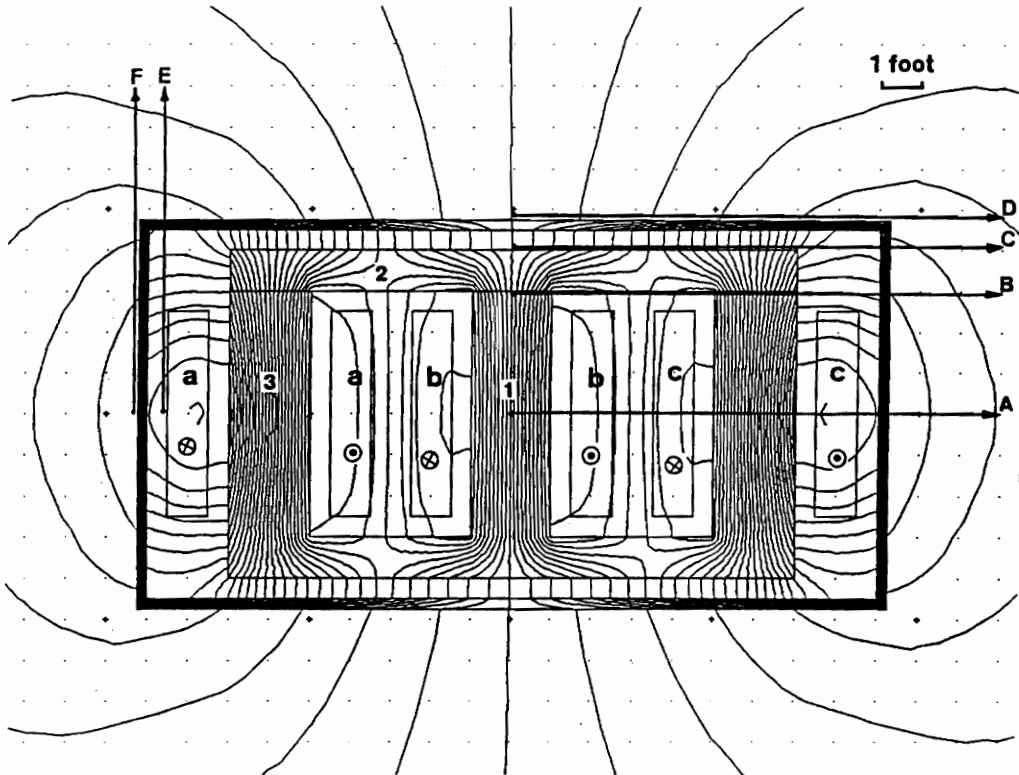
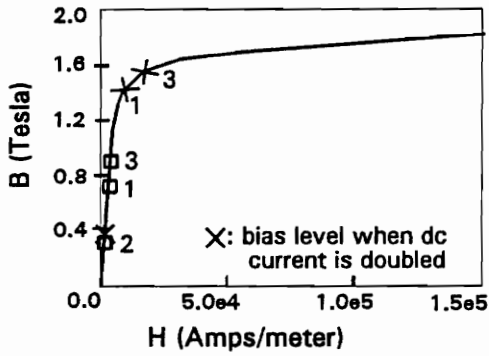
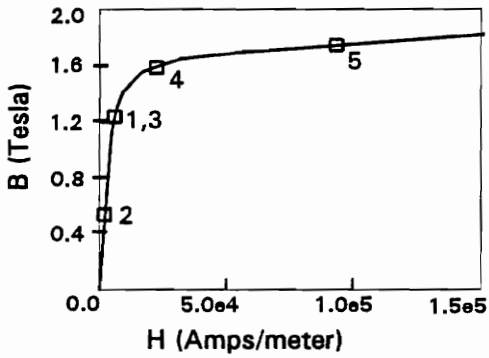


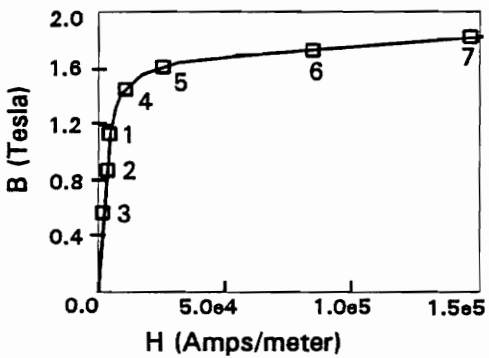
Figure 3.5 Three phase three leg core form transformer configuration and flux distribution under balanced dc excitation



a) three phase three leg core



b) three phase five leg core



c) three phase seven leg core

Figure 3.6 Bias points of different three phase core designs under the same balanced dc excitation currents (shown by the square markers)

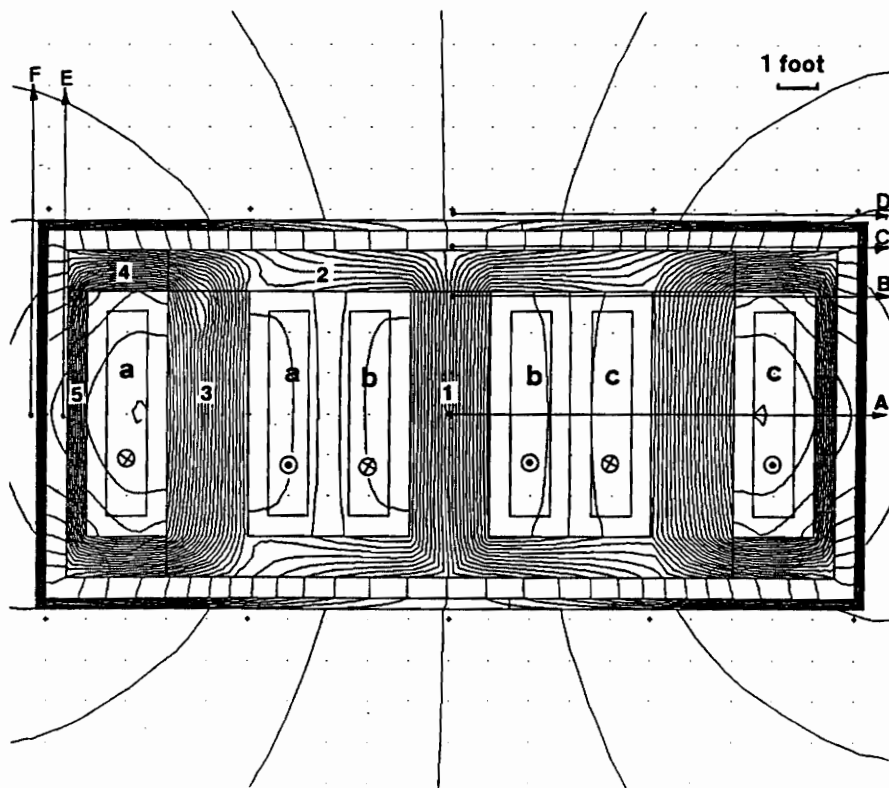


Figure 3.7 Three phase five leg transformer configuration and flux distribution under balanced dc excitation

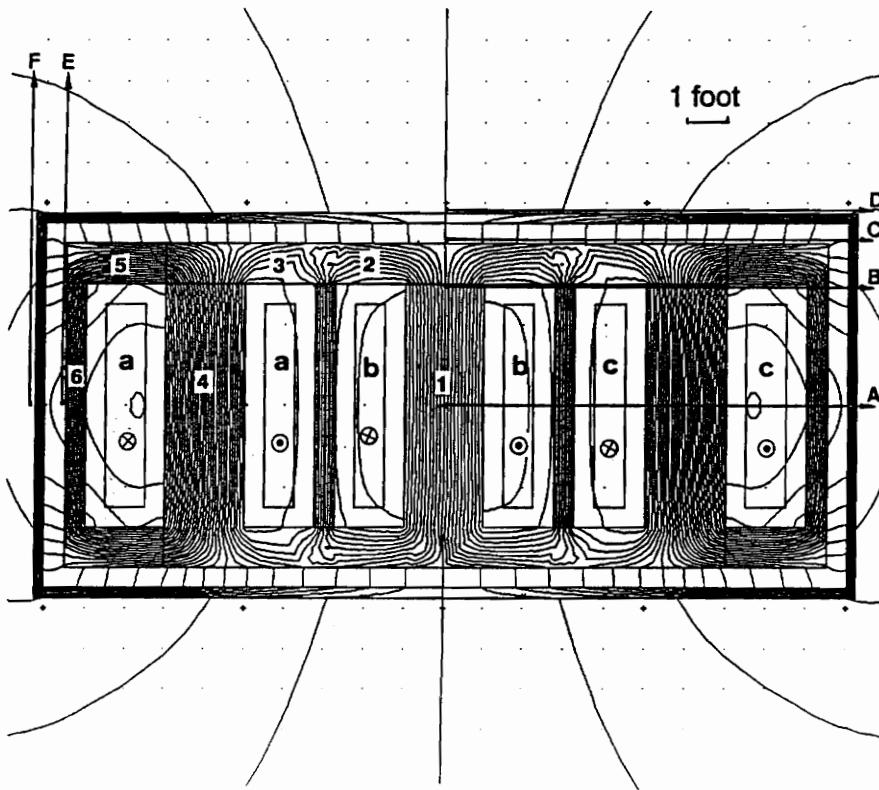


Figure 3.8 Three phase seven leg transformer configuration and flux distribution under balanced dc excitation

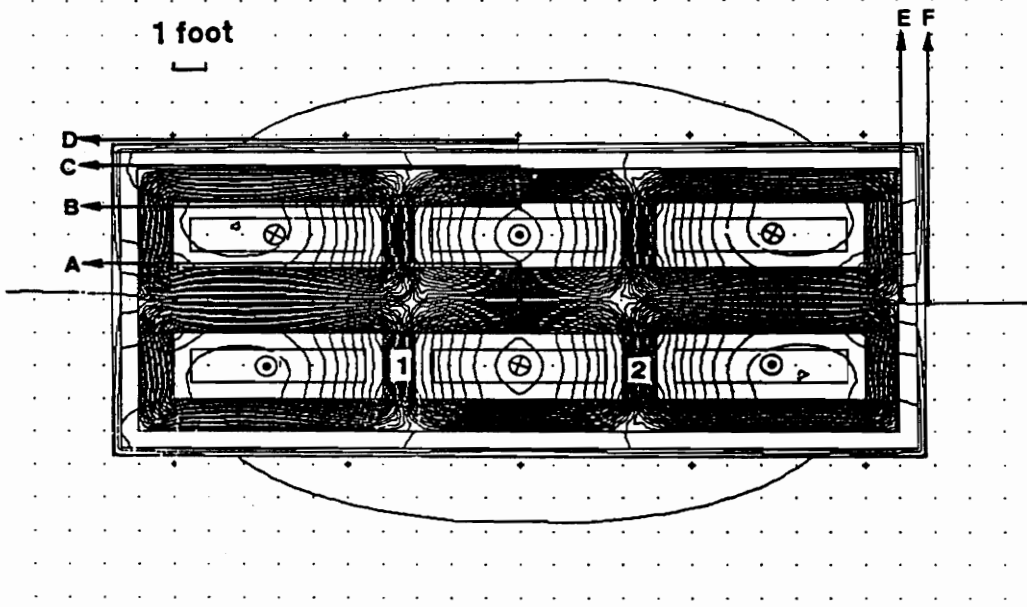


Figure 3.9 Three phase conventional transformer configuration and flux distribution under balanced dc excitation

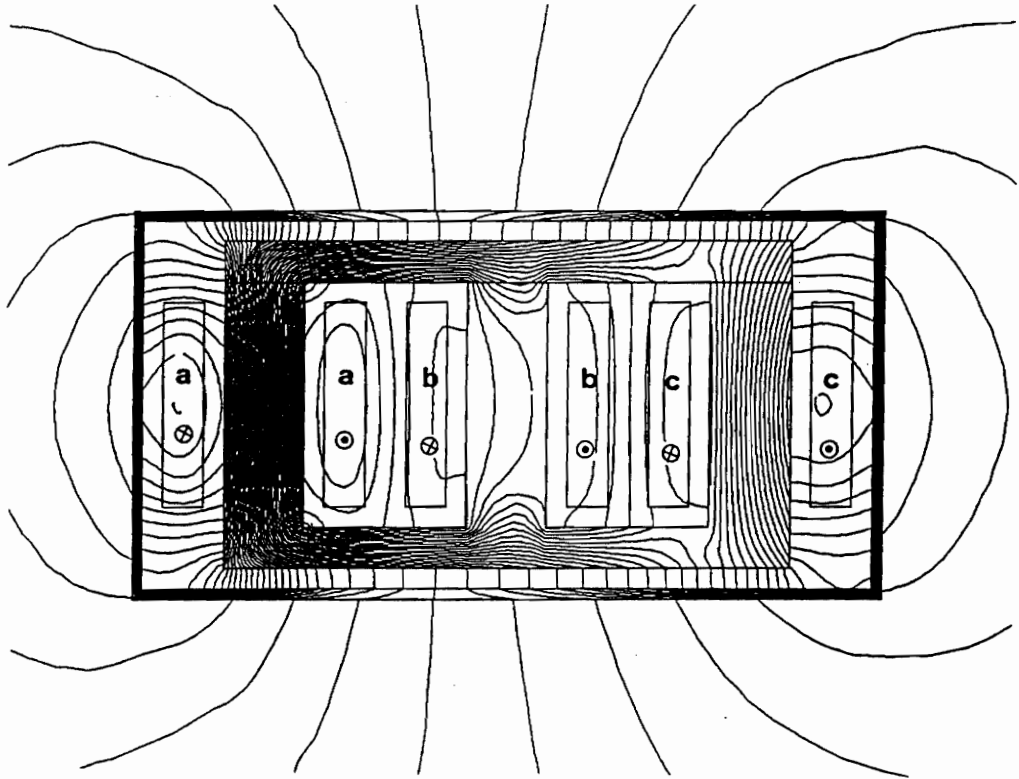


Figure 3.10 Three phase core form transformer flux distribution under unbalanced dc excitation

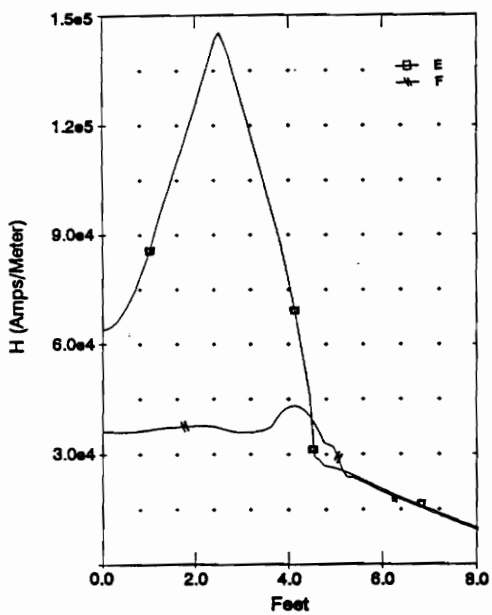
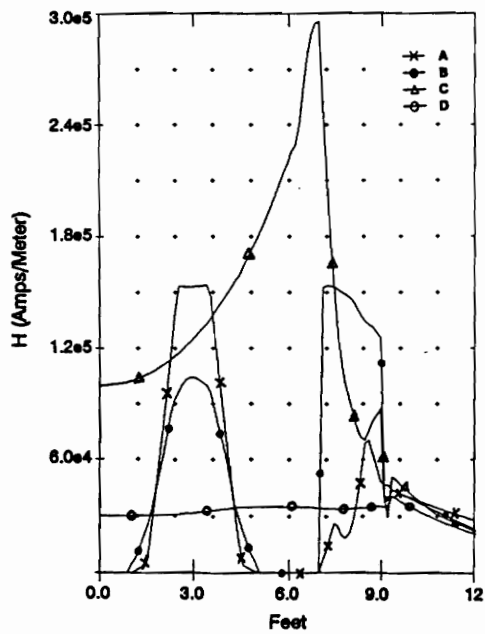


Figure 3.11 H profiles along the traverses of the three phase core form transformer

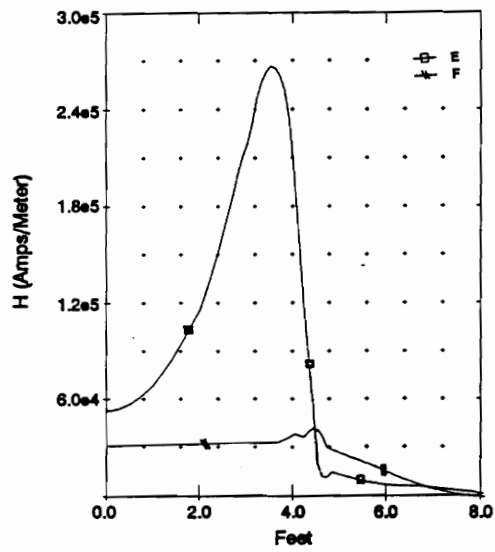
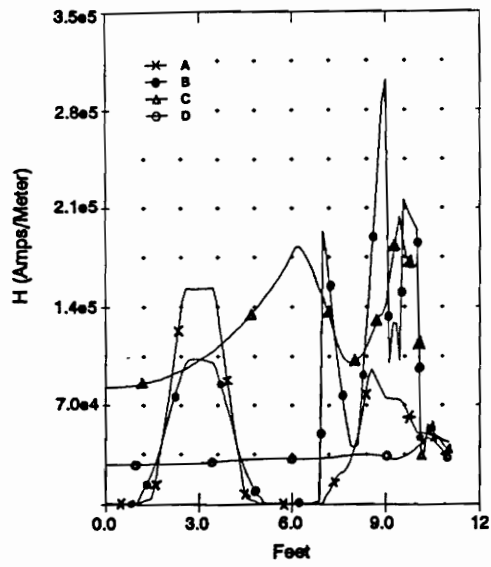


Figure 3.12 H profiles along the traverses of the three phase five leg transformer

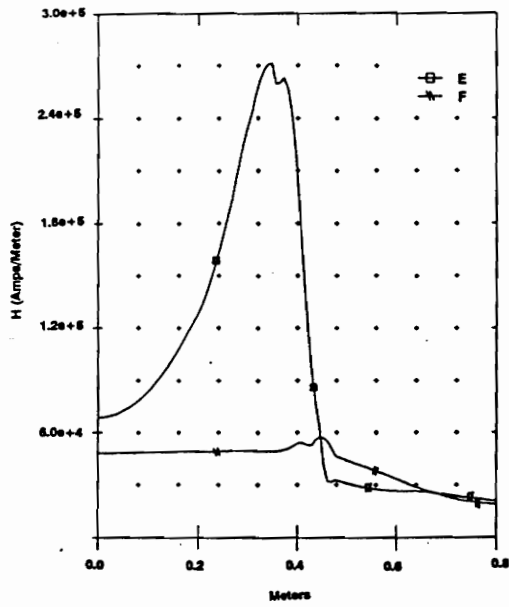
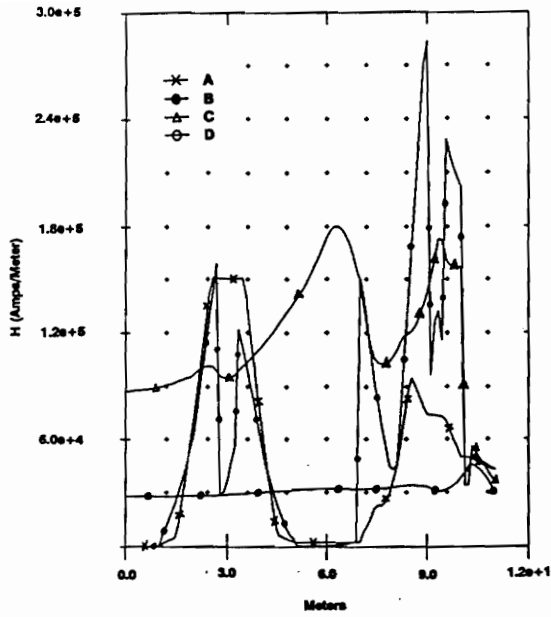


Figure 3.13 H profiles along the traverses of the three phase seven leg transformer

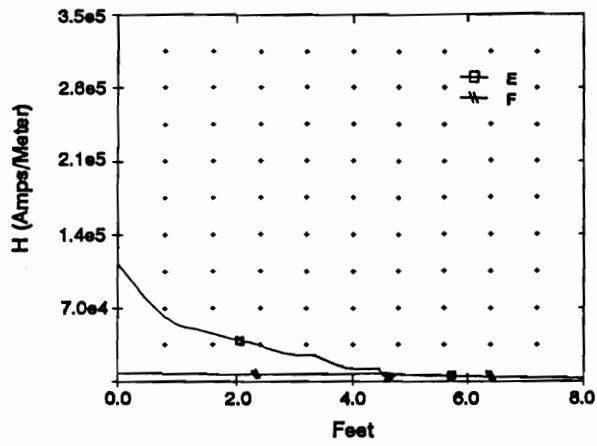
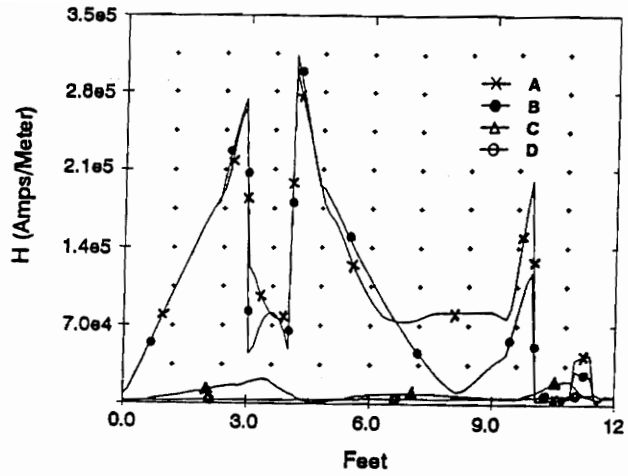
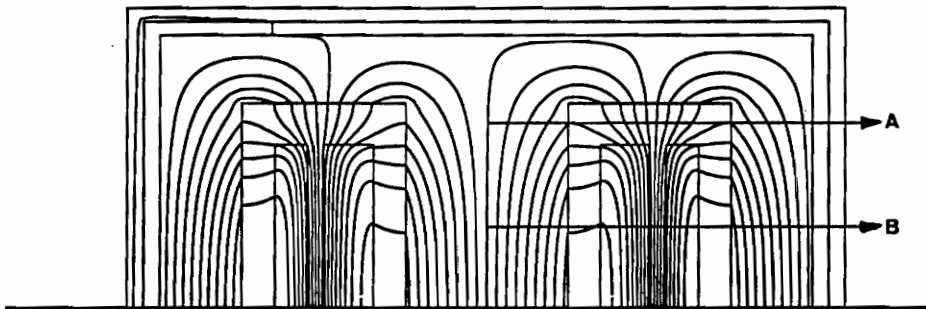
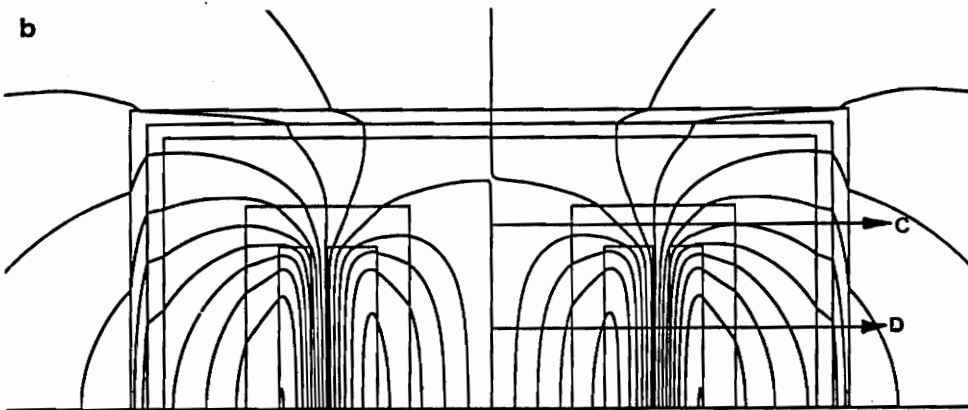


Figure 3.14 H profiles along traverses of the three phase conventional transformer

a



b



a) Normal operation

b) Saturation operation

Figure 3.15 Leakage flux distributions of a single phase core form transformer

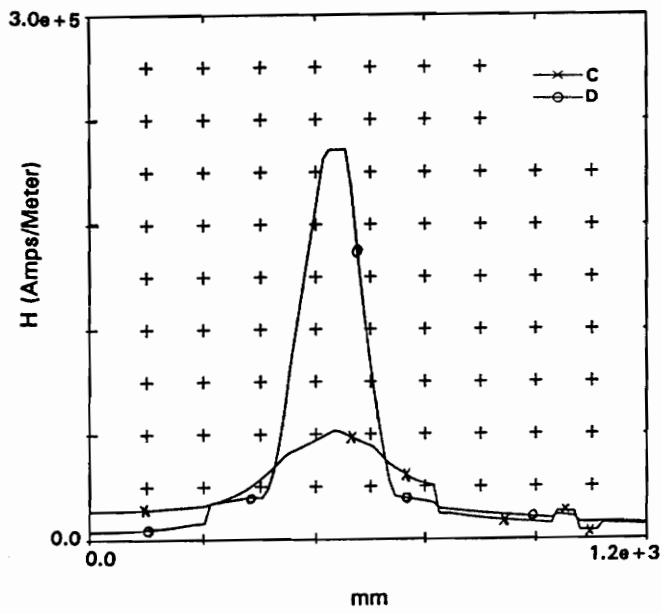
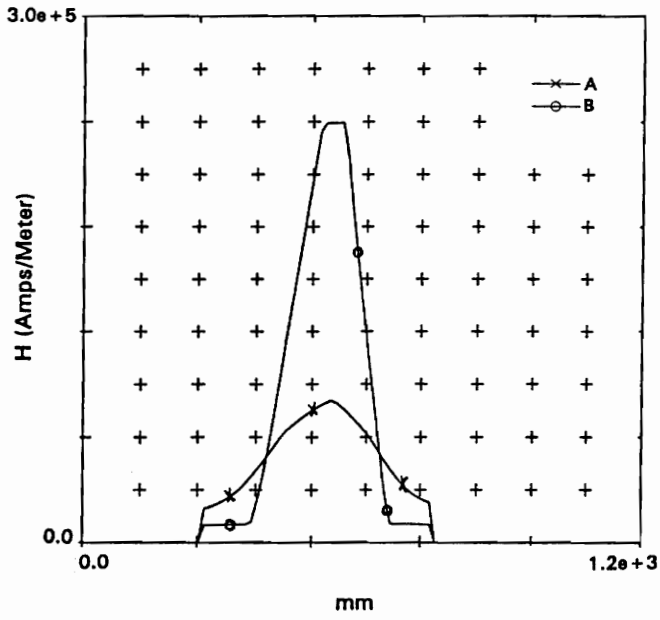
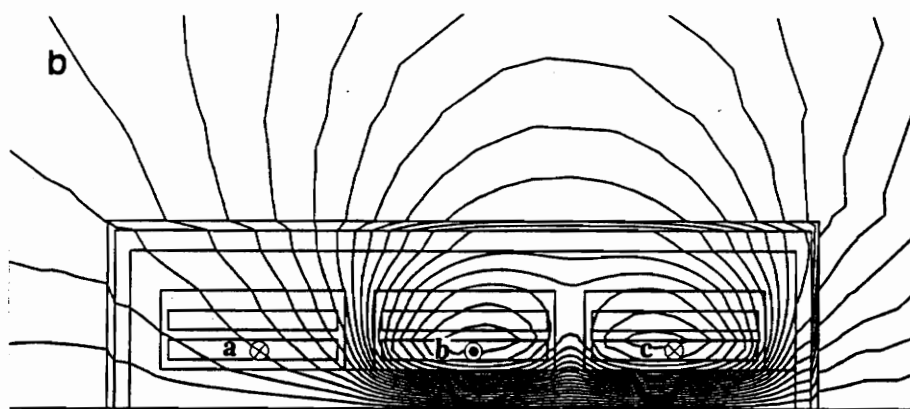
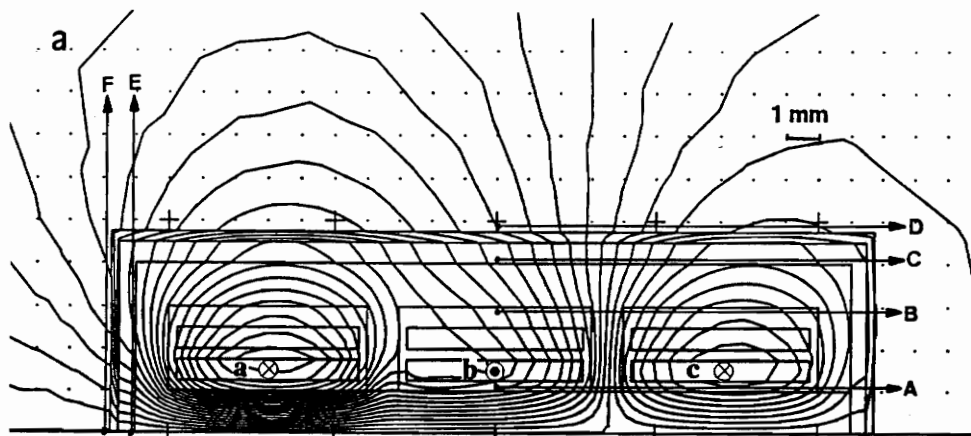


Figure 3.16 H profiles along two traverses of the single phase core form transformer



(a) at t_0 when phase a current is at its maximum

(b) at t_1 when phase a current is at its minimum

Figure 3.17 Three phase conventional transformer ac excitation flux distribution

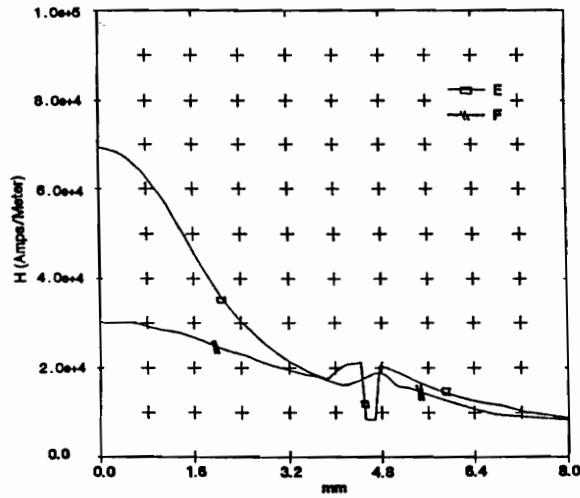
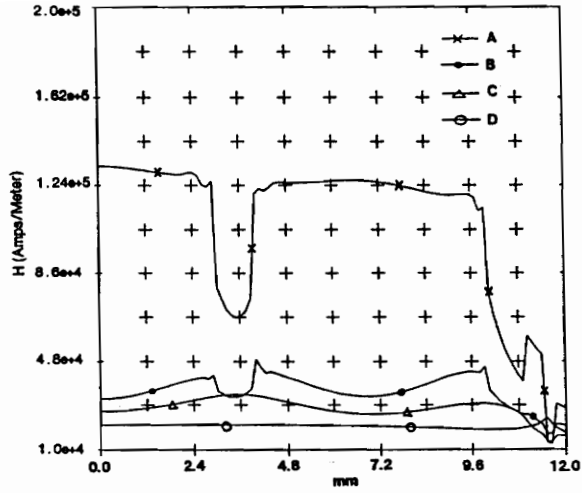
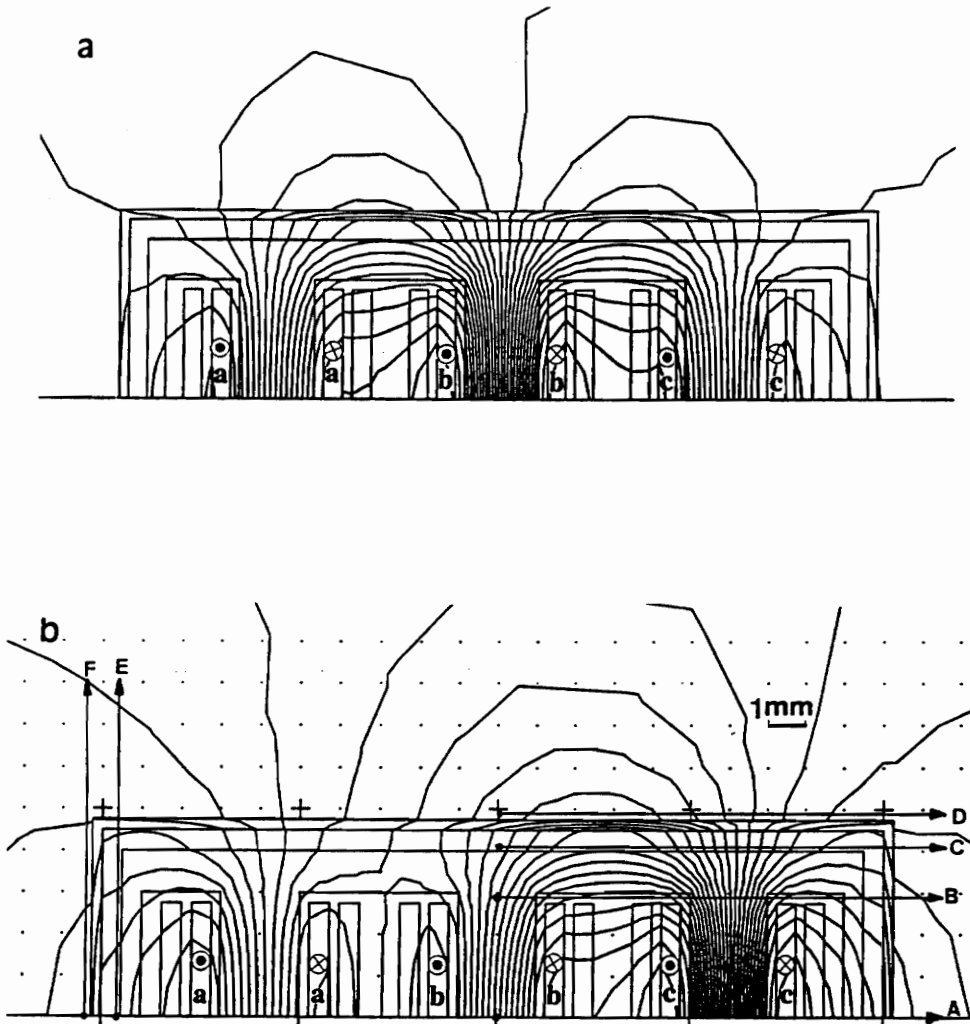


Figure 3.18 Average magnetic field intensity H along traverses (A~F) of a three phase conventional transformer during heavy saturation



- (a) at t_2 when phase b current is at its maximum
- (b) at t_3 when phase c current is at its maximum

Figure 3.19 Three phase five leg transformer ac excitation flux distribution

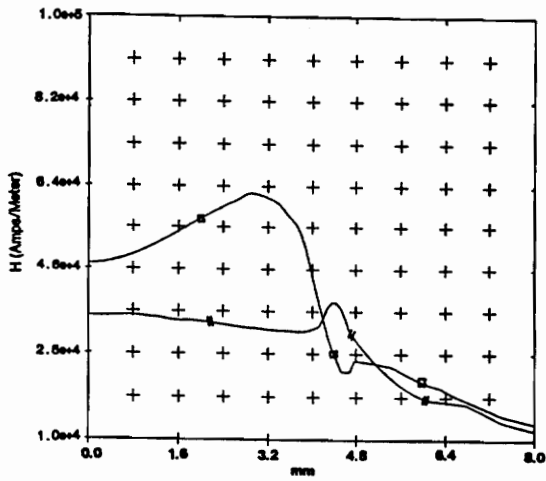
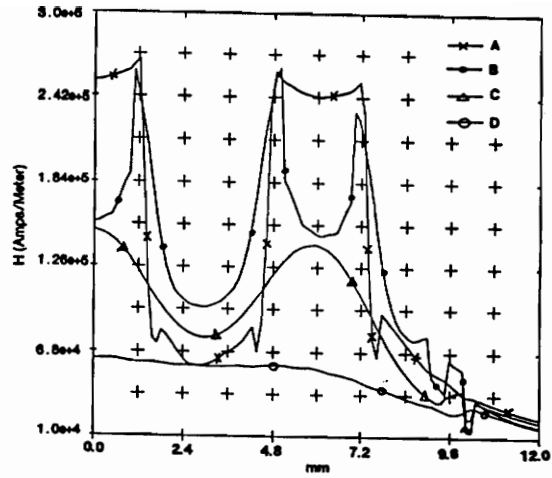


Figure 3.20 Average magnetic field intensity H along traverses (A~F) of a three phase five leg Transformer during heavy saturation

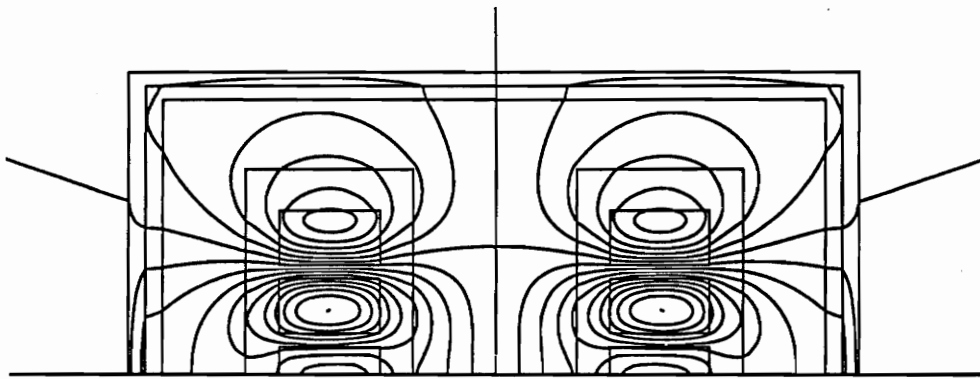


Figure 3.21 Leakage flux distribution of a single phase transformer with pancake winding.

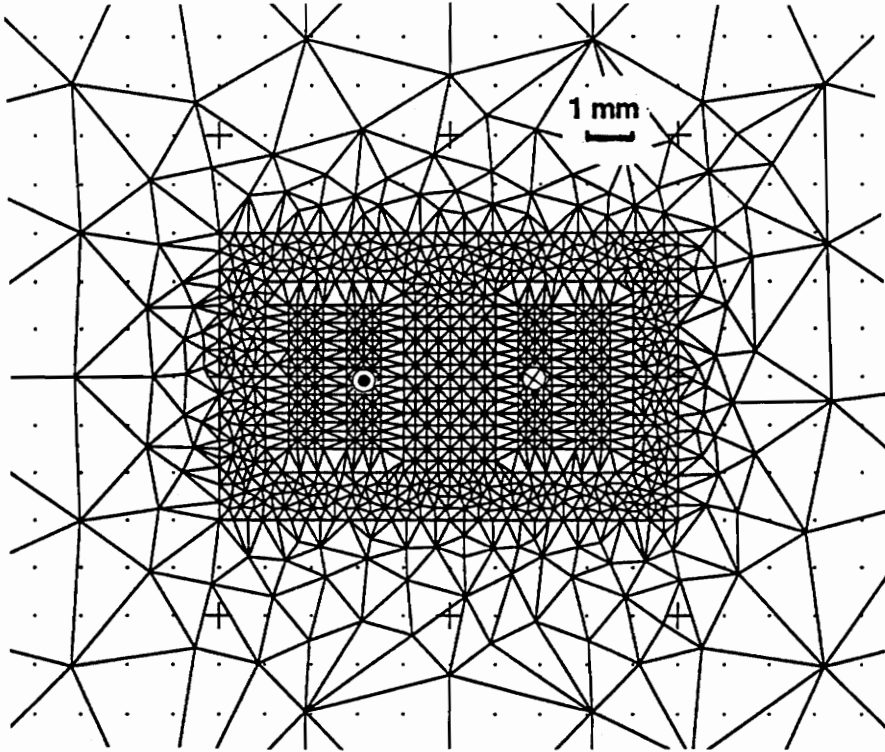


Figure 3.22 Single phase transformer with FEM mesh

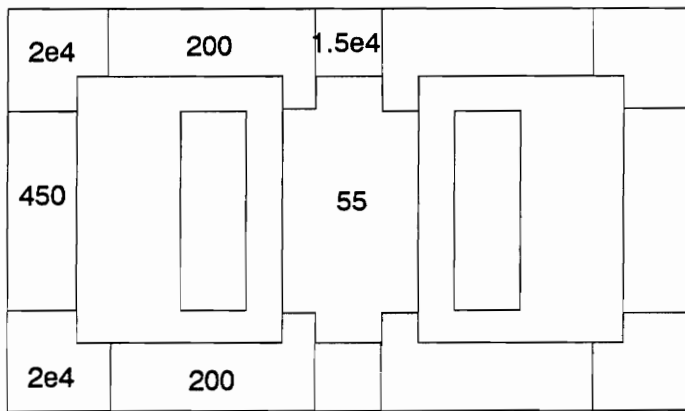


Figure 3.23 A piece-wise core model of a single phase transformer under saturation, the numbers indicate values of μ_r in each region

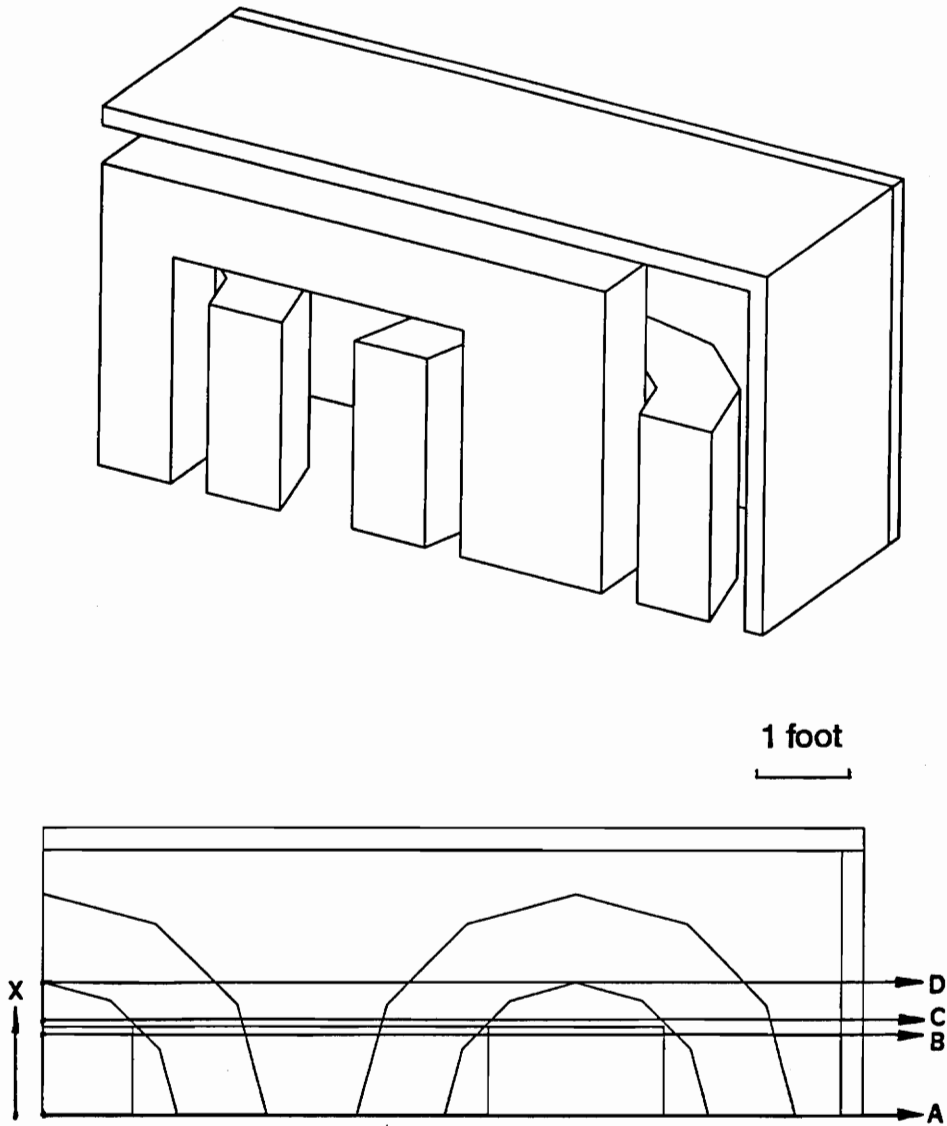


Figure 3.24 3D configuration of a three phase three leg transformer and its 2D top view

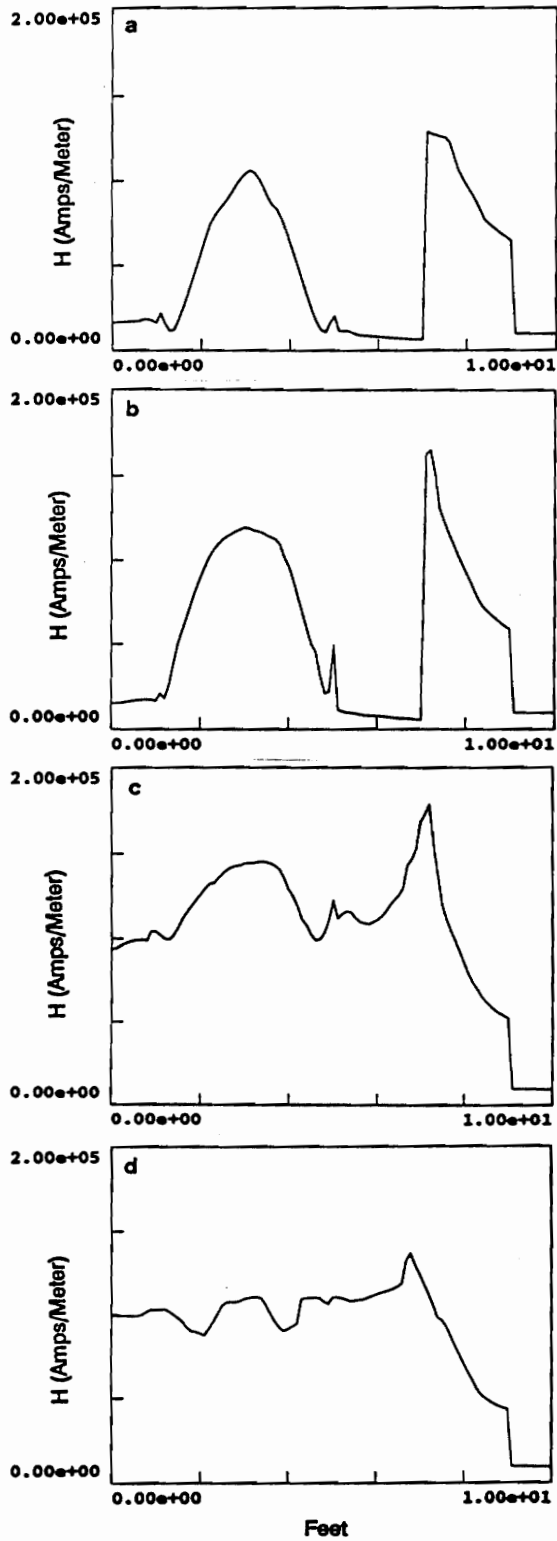


Figure 3.25 H profile along line A ~ D of figure 3.24

CHAPTER IV. DC SATURATED TRANSFORMER MAGNETIC CIRCUIT MODEL

4.1 Introduction

It is essential to know the harmonic currents generated from GIC biased transformers in order to calculate the amount of harmonics injected into a power system and to analyze the power system responses to SMD. Direct measurement during SMD and staged dc injection tests have been performed to obtain this information [28,29,31]. On the other hand, to be able to calculate transformer excitation currents based on an adequate equivalent circuit model is as desirable in order to provide information for a large group and variety of transformers, under different levels of dc bias. Several calculation methods have been reported [24,25,27,32,33,34,37,38].

However, early efforts have relied on models developed for normal or low saturation operations. Under dc bias, the conditions have changed adversely. FEM analysis results show that the total flux could differ by over 100% at different parts of the same core leg during saturation. More model details are necessary. Also, reports of the 1989 K-9 solar magnetic disturbance [5,8,18] and the FEM studies have shown that transformer tank begins to play an important role during saturation. It was not included in earlier models. In summary, more appropriate GIC transformer model ought to consider the complicated flux paths and the effect of the tank. Using FEM analysis information to validate the model is also desirable.

This study describes an improved approach of modeling transformer excitation under dc based on the results of 3D finite element magnetic flux distribution analysis. First, flux distribution is analyzed using 3D FEM. Based on the physical configuration and the FEM analysis results, the structure of a lumped magnetic circuit model of the entire

transformer and initial parameters are determined. FEM results are used again for verifications at different regions of operation. The effect of transformer tank is considered. Detailed procedures are illustrated through an example of a single phase transformer. The model is capable of not only the linear and knee region operations, but also the heavily saturated region and the so called "air core" region. As a result, the impact of dc over a much greater range on transformer harmonic production is characterized. The complete variations of excitation current harmonics as a function of dc bias are revealed, and many new observations are made for the example transformer used in this study.

4.2 Magnetic Circuit Model Development

4.2.1 Introduction

The requirements are that the model should be able to simulate not only the linear region operation, but also give accurate results in the knee and heavy saturation region. Three major steps are involved in the magnetic circuit model development:

1. The field distribution is first analyzed using 3D FEM. Based on the physical configuration and the FEM analysis results, the structure of the lumped magnetic circuit model of the entire transformer (including the tank) and initial parameters (dimensions of the lumped reluctance elements) are determined.
2. After the lumped magnetic circuit is established, the reluctances of the initial linear air and nonlinear magnetic materials are found. The circuit is then solved using an iterative computer program. At any given dc mmf (dc) bias and ac voltage, the program calculates magnetic field density (or total flux) in each circuit branch and the magnetizing current at any time instant of a 60 Hz cycle.

3. FEM results are used again for verifications at different regions of operation. Model parameters (dimensions) will be modified based on FEM analysis results.

4.2.2 Model configuration

According to the analogy between magnetic and electric circuits, a transformer core can be modeled by a network of reluctance components, as shown in figure 3.2. Each reluctance represents different segments of the core with corresponding dimensions. Reluctance R of a given segment can be calculated by equation (2.15). Since μ varies along the B-H curve of the magnetic core, reluctances representing the magnetic core segments are nonlinear variables.

When a transformer is working in the linear region, flux is well confined inside the core. Thus the model shown in figure 3.2 is adequate. Under dc saturation, the core presents high reluctance paths. As a result, part of the flux is pushed out of the core. Therefore, the core model in figure 3.2 is no longer able to represent transformer performance under dc operation. More components should be added for a complete model.

Consider a single phase transformer with tank included, where the air region and the tank can also provide flux paths. Figure 4.1 shows its flux distribution obtained from the FEM analysis. Its lumped element model considering several major flux paths is constructed and shown in figure 4.2. In the figure, subscript "c", "a", and "t" stand for core, air and tank, respectively. Subscript "1", "2", and "3" describe different major branches of the flux paths. Branch 1 corresponds to the flux all within the excitation windings. The flux of branch 1 is also considered as total excitation flux. Branch 2 represents the flux path in the yoke segment while branch 3 is the sum of the flux in the side leg and the amount of flux leaving the core from the side leg. Branch 4 models the flux being pushed out of the core from the yoke region. This branch of flux forms a loop with branch 1 and has no contribution to branch 3. DC input is accommodated in the circuit by a dc mmf

source. AC voltage in the form of ac flux is in series with the dc mmf source. The ac voltage (thus, ac flux) is assumed to be sinusoidal in this model.

The increase of model complexity is necessary because the saturation levels will be different at different core segments when heavy saturation is reached. Figure 4.3 gives the FEM analysis results showing different dc bias levels at three core regions under heavy saturation.

Also, considering the tank in the model is very important since the tank wall can provide a relatively low reluctance path for the amount of flux being pushed out from the core. Notice that the reluctances representing different tank segments are also nonlinear variables because the tank is made of magnetic material (mild steel). The air components ($R'a_4$ and Ra_3) in series with the tank components (Rt_3 , Rt_4) represent the flux paths that use air gaps and the tank. Air components are dominant factors in the series branches 3 and 4 before the tank reaches saturation.

The dimensions of the reluctance elements are estimated by taking into account the physical structure of a transformer and the nonuniformly distributed flux. These reluctance values will be modified later with the help of the FEM analysis. In this model, winding resistance is not considered. Since the core loss component is not included in the model, exciting current is equal to magnetizing current as another approximation.

4.2.3 Computer programming

A computer program using iteration methods is developed to solve the nonlinear circuitry shown in figure 4.2. For a fixed dc bias, the permeability of each nonlinear component is found by iteration at each instantaneous ac flux level. Once the permeability of all nonlinear components is known, the total reluctance (R_T) with respect to the source can

be found. Thus the instantaneous excitation current (I_{ex}) can be obtained from equation (2.16). In the program, B-H curves are considered to be piece-wise linear and their slopes should be monotonically increasing. The solution flow chart is shown in figure 4.4. The iteration process to calculate either the dc bias of each nonlinear component or R_T involves determination of the flux in each element and the total flux Φ . Figure 4.5 gives the block diagram of the iteration process. Subroutines to solve the flux in each branch are needed in the iteration process. The subroutine for branch 1 can be summarized as follows,

- (i) Set the flux in component Rc1 (Φ_{Rc1}).
- (ii) Find the permeability μ_{Rc1} in Rc1 from the B-H curve.
- (iii) Calculate the value of Rc1 according to equation (2.15).
- (iv) Set the mmf of Rc1 equals to that of Ra1, that is

$$F_{Ra1} = \Phi_{Ra1}Ra1 = F_{Rc1} = \Phi_{Rc1}Rc1 \quad (4.1)$$

- (v) Calculate the flux Φ_{Ra1} in Ra1 from equation (4.1).
- (vi) Therefore, the total flux in branch 1 is,

$$\Phi_1 = \Phi_{Rc1} + \Phi_{Ra1} \quad (4.2)$$

The subroutine for branch 3 and branch 4 involves more complicated process. However, the basic principle is similar to that of branch 1.

The program input includes: B-H curves of the tank and core materials, dimensions of the reluctance elements, dc current (GIC) and ac voltage; the program output includes: B (or Φ) in each branch, the excitation current waveform and its harmonic contents.

At normal operation, $\mu_c \gg \mu_0$, which implies $Rc \ll Ra$. Most of the flux is confined in the core. When $\mu_c \approx \mu_0$, that is, Rc and Ra are close in magnitude, flux will distribute into

all the components. This is similar to the case of saturation. Therefore, this lumped equivalent magnetic circuit shows an advantage. That is, with the dimensions of the elements fixed, a wide range of operation levels can be simulated.

4.2.4 Circuit parameter adjustment

Since flux is not uniformly distributed in a transformer, determining the effective (or equivalent) dimensions of each element in the model becomes an important issue. The dimensions of the reluctance elements are modified with the help of FEM analysis. (The following discussion will consider dc excitation only). Different cross sectional areas based on the direction of the flux are chosen and flux densities are integrated over these areas in order to calculate the total flux in different branches. Then, the element dimensions are adjusted until the flux distribution in different components matches the FEM analysis results.

Many linear and nonlinear components are involved in the circuit model. In order to model a wide range of nonlinear operations, it is impossible to determine all of the dimensions based on a single set of FEM simulation data. Thus, different bias currents are injected to simulate different operation levels along the nonlinear B-H curve so that the component values in the circuit model can be adjusted one group at a time. The following sections describe each simulation step in detail.

Linear region operation. In the linear operation region, the majority of flux is well confined in the core. It can be assumed that there is only one branch of flux and this branch is inside the core. At this time, the reluctances representing the core segments (R_{c1} , R_{c2} , R_{c3}) are much smaller than the rest of the components. Core components are playing the most important role in the circuit model. These components can be adjusted according to the FEM simulation results in the linear region operation.

Knee region operation. In this region, the core reaches some degree of saturation and the flux starts to branch out of the core. Since the tank is still operating in the linear region, the reluctances representing the tank wall are small. In other words, the air gap reluctances which are in series with the tank reluctances are dominant in these branches. Therefore, the amount of flux entering the air and the tank is determined by the air gap reluctances (R_{a3} , R_{a4} , R'_{a4}). The dimensions of these air elements can be adjusted so that the air flux numbers match the FEM results.

Very heavy saturation region. More and more flux leaves the core and enters the tank through the air gap when the core reaches very heavy saturation. The tank wall starts to saturate and exhibits high reluctance. As a result, the reluctances representing the tank wall are no longer negligible. Therefore, the flux differences between the FEM analysis and the magnetic circuit calculation can be minimized by adjusting the dimensions of the tank components (R_{t3} , R_{t4}).

After fitting the three operation regions and making comparisons with the FEM results, all parameters in the equivalent magnetic circuit will be fixed. Varying the input dc current and ac voltage, the model will be able to simulate a wide range of operation. In summary, the parameter determination steps are listed below,

- 1) core reluctances are determined during linear region simulation.
- 2) air reluctances are determined during knee region simulation.
- 3) tank reluctances are determined during very heavy saturation simulation.

Each step may also involve adjusting other kinds of components depending on the matching requirement. As shown in the example given below, matching the knee region with the FEM result is more important.

4.3 An Example

Figure 4.1 shows a single phase transformer with detailed dimensions. Its equivalent magnetic circuit is the same as the one shown in figure 4.2. The B-H curves used for the core and the tank materials are given in figure 4.3. The ac voltage is adjusted so that the transformer operates close to the knee of the B-H curve without dc bias. In this study, Ampere-turn (At) is used instead of Ampere for the excitation current, its harmonics, and the dc excitation (GIC). This is done to avoid using the actual number of turns in the excitation winding, and to preserve generality.

The dimensions of all the reluctance components are optimized to fit the FEM results. Comparisons of the major flux paths in the three different operation regions are given in table 4.1. The differences between the FEM analysis and the magnetic circuit model for all the flux branches are close to 1% over a wide range of operation. Some mismatch could go up to 8% in very few segments of the core for dc bias at the knee region.

The excitation current simulation shows that, when dc current is biased at the knee region of the B-H curve, the third harmonic component reaches its maximum value, see figure 4.6. Both linear region operation and heavy saturation where the operations are right above the knee region produce fewer harmonic components. Thus, when adjusting component values, fitting the knee region with the FEM result is more important.

4.4 Excitation Current Harmonics

4.4.1 Typical waveforms of excitation currents vs. dc bias

The B-H characteristics of the transformer core is redrawn in figure 4.7. The excitation

Table 4.1 Comparison of dc flux between FEM and model calculations for three operation regions

DC bias	20 A-t		500 A-t		1e5 A-t	
Methods	FEM	Model	FEM	Model	FEM	Model
Φ_t (Wb)	0.03795	0.03803	0.4322	0.4308	0.5736	0.5703
Φ_{c1} (Wb)	0.03793	0.03802	0.4125	0.4306	0.4948	0.4925
Φ_{c2} (Wb)	0.01903	0.01887	0.2076	0.2121	0.2376	0.2373
Φ_{c3} (Wb)	0.01884	0.01886	0.2156	0.2120	0.2374	0.2364

Φ_t : total flux linking the excitation winding
 Φ_{c1} : main leg flux excluding air

Φ_{c2} : yoke flux
 Φ_{c3} : side leg flux

current waveforms shown in figures 4.8 is found by applying different dc bias as indicated in figure 4.7 in regions 1 through 6 on the B-H curve. The excitation current waveforms are plotted to show the change of patterns at different levels of saturation. They can be used to identify to what extent dc bias have saturated the transformer.

Figure 4.8.a and figure 4.8.f show either pure or dc biased sine waves reflecting the linear v-i relationship in these two regions. Between the two linear regions, the excitation current waveforms show different degree of distortions.

In the example transformer, 200 At is used for normal excitation corresponding to a 1 p.u. ac voltage with an excitation current of 0.3 A peak value, for instance. Thus, a 20,000 At dc bias will be equivalent to 30 A GIC (assume dc and ac excitations follow approximately the same B-H curve). As will be shown later in figure 4.8, all higher order harmonics will die out at around 200,000 At dc bias, which has the equivalent GIC of 300 A. At this level of dc bias, the core is completely saturated and the B-H curve is linear with $\mu_c \approx \mu_0$.

4.4.2 Excitation current harmonics vs dc bias

In figure 4.9 and 4.10, starting from dc component up to the 10th harmonic current are plotted against the same dc bias scale.

The on-set dc bias levels for all harmonic components are around 150 At. Each harmonic will follow a certain pattern as the dc bias increases. All harmonics except the dc and the fundamental components will disappear eventually with the increase of dc bias. This phenomenon may or may not be observed during a geomagnetic disturbance if GIC fail to reach a very high level. These final points roughly correspond to a dc bias of 1000 times the normal excitation current.

The dc component I_{dc} of the excitation current, figure 4.9.a, increases monotonically with respect to the increase in dc bias level I_b . It has the fastest rate of increase when the core is biased in the knee region of the B-H curve (region "2" in figure 4.7). This dc component, which is also the total GIC in the winding can be decomposed into two parts,

$$I_{dc}(\text{GIC}) = I_b + I_0 \quad (4.3)$$

I_b equals to the applied dc bias, and I_0 is a dc component caused by the change in the total equivalent reluctance (R_T), in other words, the nonlinearity of the B-H curve.

The fundamental component in figure 4.9.b increases monotonically and reaches its maximum when the core is saturated and begins to act like an "air core". It stays at this peak magnitude which is affected only by the ac excitation voltage.

In figure 4.9.c, the second harmonic picks up when dc bias is around the knee region. It holds steady for a very wide range of dc bias, showing one flat region as the dc bias level increases. The peak amplitude tends to decrease if voltage reduction (or under excitation) is implemented.

In figure 4.9.d, the third harmonic shows two peaks with the increase of dc bias. The two peaks correspond to two of the distorted excitation current wave shapes shown in figure 4.9.c and figure 4.9.e. Voltage reduction lowers the peak amplitude and moves the peaks closer towards each other.

The fourth harmonic also shows a clear pattern with two sharp peaks and one rather flat region in the middle as shown in figure 4.9.e. The lowered ac voltage moves the two sharp peaks closer and shortens the flat middle region, all with lower magnitudes.

The even and odd harmonics follow two general patterns. This can be seen by comparing figures 4.9.c.e and 4.10.g.i.k with figures 4.9.d and 4.10.f.h.j. The number of peaks in each harmonic is somewhat in proportion to the harmonic order, not necessarily following a one-to-one correspondence. Between two maximums, there will be a change of polarity through a 90 degree phase-shift. As the harmonic order increases, the phase-shift becomes more frequent, thus the patterns of higher order harmonics become more complicated. For the same reason, the higher harmonics tend to reach their maximums earlier. The change of ac operating voltage, from 1 p.u. to 0.7 p.u., has some effect on the lower order harmonics in terms of wave shapes and magnitudes. The effects are more pronounced for higher order harmonics (not shown).

4.4.3 RMS excitation current vs. dc bias

RMS value is the effective value of a periodically varying signal $g(t)$. It is defined as,

$$G_{rms} = \sqrt{\frac{1}{T} \int_0^T [g(t)]^2 dt} \quad (4.4)$$

where T is the period of $g(t)$. If the signal is expressed as a Fourier series of harmonic components, its rms value can be expressed as,

$$G_{rms} = \sqrt{G_0^2 + \sum_n G_n^2} \quad (4.5)$$

where G_0 is the direct component and G_n is the rms value of the n th-harmonic component.

The rms value of the excitation current is calculated from its Fourier series of harmonic components. The result shows that the rms excitation current also increases monotonically with the rise of dc bias level. Figure 4.11 shows the rms excitation

currents at 1 p.u. and 0.7 p.u. ac system voltage levels. Next to the dc component, the fundamental is the dominant component compared with all higher order harmonics, as also will be illustrated in next section.

4.4.4 Total harmonic distortion vs. dc bias

The total harmonic distortion (THD) is used to describe the total harmonic components in proportion to the fundamental component. THD is given by:

$$\text{THD} = \frac{(I_2^2 + I_3^2 + I_4^2 + I_5^2 + \dots)^{1/2}}{I_1} \quad (4.6)$$

where I_i is the i -th order harmonic current.

Figure 4.12 shows changes of THD with respect to dc bias for 1 p.u. and 0.7 p.u. ac excitations. The total harmonic distortion reaches maximum once and goes to zero eventually. The sharp rise of THD happens when the dc bias is at around the knee region of the B-H curve and drops quickly thereafter. The sharp peak may have been caused by the relatively low fundamental component at the on-set of saturation. THD reaches a maximum of 1.4 in this example. Over most of the region THD is below 0.5. The general trends for the two ac excitations are similar with some degree of reduced THD at 0.7 p.u. system voltage.

4.4.5 Reactive power vs dc bias

Reactive power is believed to be a good indicator of transformer saturation. It is predicted that the demand of large reactive power may result from simultaneous half cycle saturation of a large number of transformers [5].

Several definitions for reactive power under nonsinusoidal conditions have been suggested [39,40,41]. In this study, the product of the fundamental component of excitation current and the ac system voltage is used, which is physically meaningful in a power system. That is,

$$Q_1 = V_{\text{rms}} \times I_{\text{rms}} \quad (4.7)$$

Here current lags voltage by 90 degrees. Figure 4.13 shows reactive power as a function of dc bias. The values given in the figure are normalized using the reactive power at zero dc and 1 p.u. ac voltage as the common base. As can be seen in figure 4.13, reactive power increases suddenly at around 150 At dc bias. This could correspond to a very low GIC level.

4.4.6 The effect of voltage reduction

Voltage reduction scheme has been used in some situations to shed load without terminating power supply. During a geomagnetic disturbance, can the impact of GIC be reduced by lowering the system voltage? The 0.7 p.u. system voltage is used to see the effectiveness of this method. Comparison of harmonics (figure 4.9.a to 4.9.e), rms excitation currents (figure 4.11), THD (figure 4.12), and reactive powers (figure 4.13) are given at the two ac voltage levels. The general trends for the two cases are similar with some degree of reduced harmonic magnitudes and delayed responses for the 0.7 p.u. system voltage. This is because that when ac voltage is reduced, less operation region will be spanned by each voltage cycle. In this example, the amount of change made by voltage reduction may not be significant enough to justify its use during a geomagnetic disturbance.

4.4.7 The total equivalent reluctance vs. dc bias

The reluctance of each core segment is inversely proportional to the permeability of the nonlinear magnetic material used. Saturation will force the flux to seek paths in the air and the tank as well. The combined effect will produce an equivalent total reluctance R_T (with respect to the mmf sources, see figure 4.14) representing the core, the tank, and the air. Figure 4.14 shows this total reluctance as a function of dc bias. R_T has a smoother changing rate compared with the core B-H curve. This is due to the contributions from the linear air reluctance elements and the fact that not all core segments reach saturation at the same time.

4.5 The Effect of Transformer Tank

Previous FEM analysis results show that flux could decrease as much as 14% in the center leg if the tank is not considered during saturation. For comparison, simulation of the same transformer but without considering its tank is also performed. Figure 4.15 shows the difference in second harmonic with and without the tank. At lower dc bias, the tank practically does not participate in the major flux paths. However, as dc level increases, and the core reaches saturation, the tank becomes an indispensable flux path, its significance begins to show at around 200 At dc bias when the core starts to saturate. Since this is very likely the region where actual GIC magnitude could reach, it is necessary to include the tank in the magnetic circuit model.

Furthermore, calculation of THD at 1×10^5 At dc bias shows that, the equivalent circuit with tank gives 0.1779 THD in the calculated excitation current while the one without tank gives 0.2673 THD. The difference in THD is as high as 50%. This result also proves that including the effect of the tank in the model is necessary.

4.6 Discussions

The reactive power consumption increases with respect to dc bias, and the trend follows exactly the fundamental component of excitation current since voltage is considered constant.

Several simplifications are made in this study. The winding loss and core loss as well as voltage drop across the leakage inductances are not included in the excitation current calculations. All these approximations are considered to be of lower order affect. They will not influence the general trend which is the focus of this study.

In actual construction, the top tank wall may be further away from the core compared with the simplified model used in this example. This difference can be corrected by adjusting the value of the air reluctance $R'a4$.

The transient characteristics of transformer GIC responses is not within the scope of this study. Instead, steady state dc (or GIC) is assumed due to the fact that GIC varies slowly with a frequency close to dc.

Since the study is done on a specific transformer design, there are limits in generality. For example, three phase transformers may have different characteristics which merit future investigation.

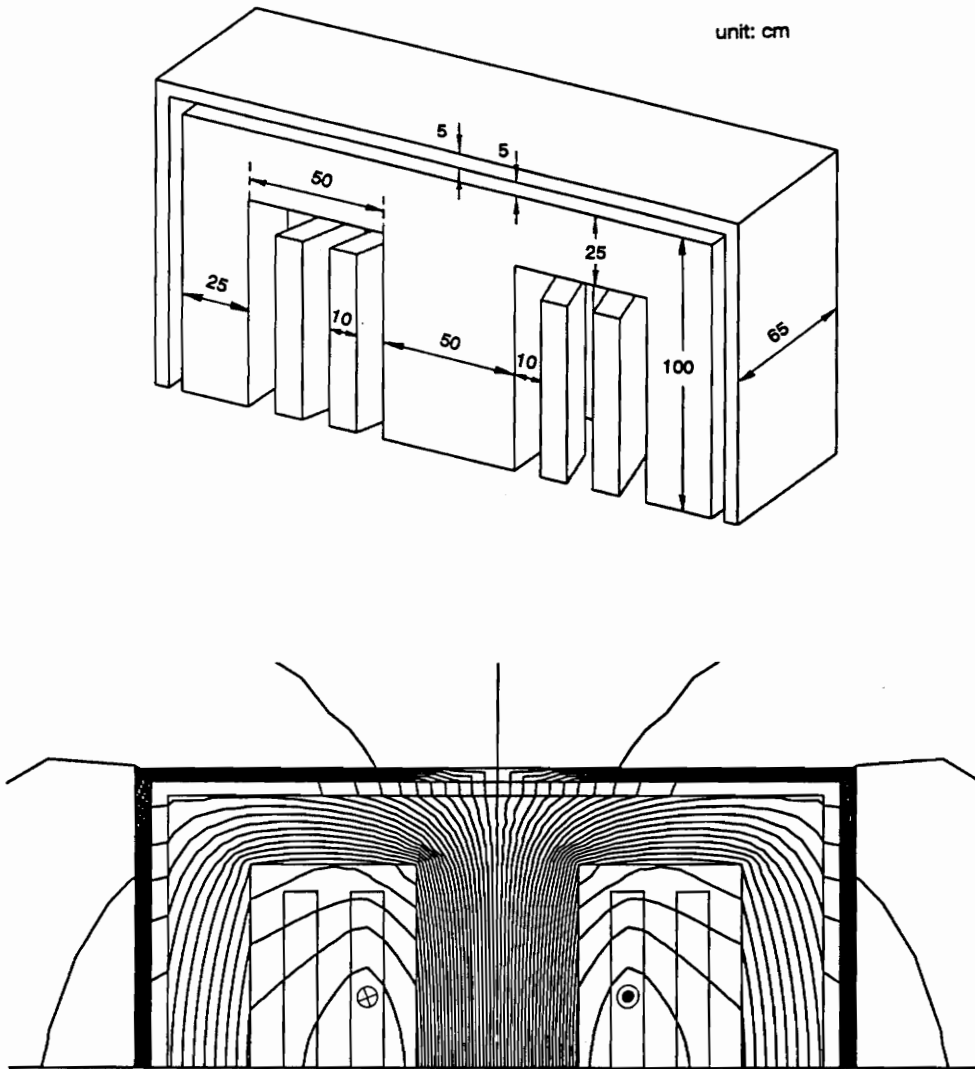


Figure 4.1 A 3D layout of a single phase transformer and its flux distribution during saturation

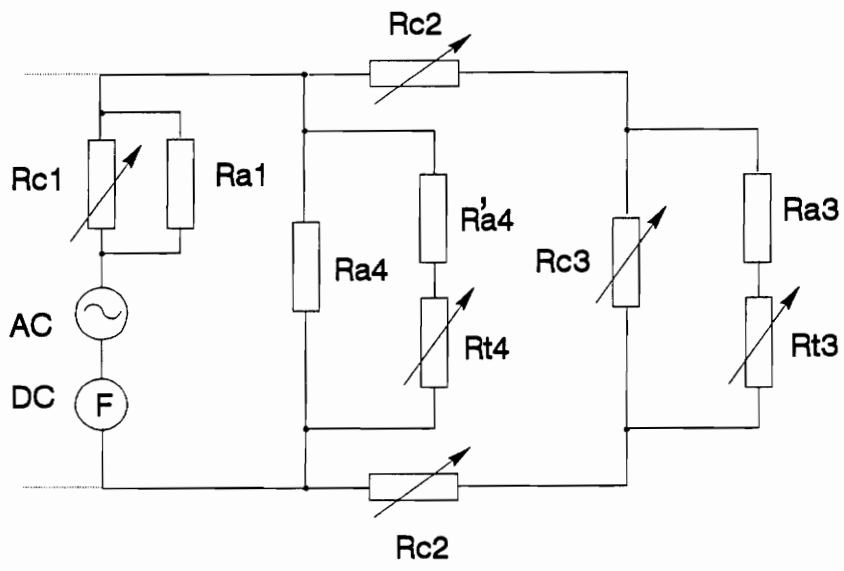


Figure 4.2 Equivalent magnetic circuit model of the single phase transformer with tank in figure 4.1

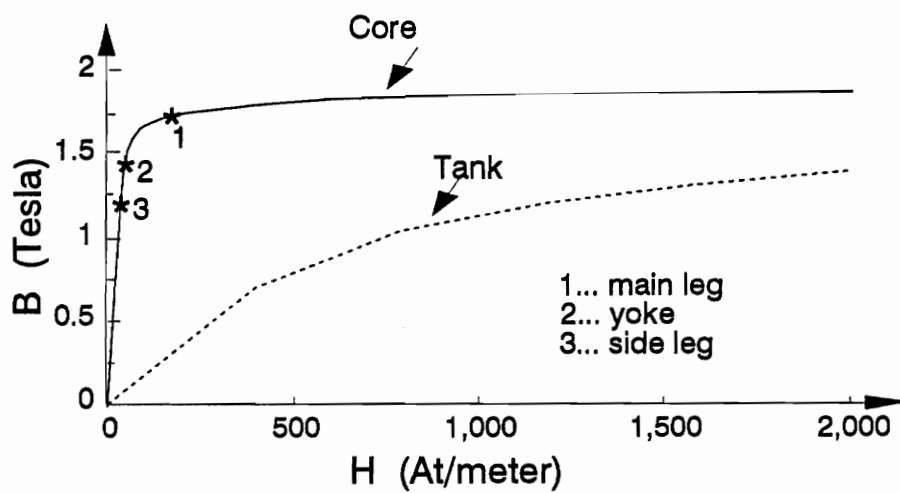


Figure 4.3 B-H characteristics of the core and the tank materials (source: ABB, [42])

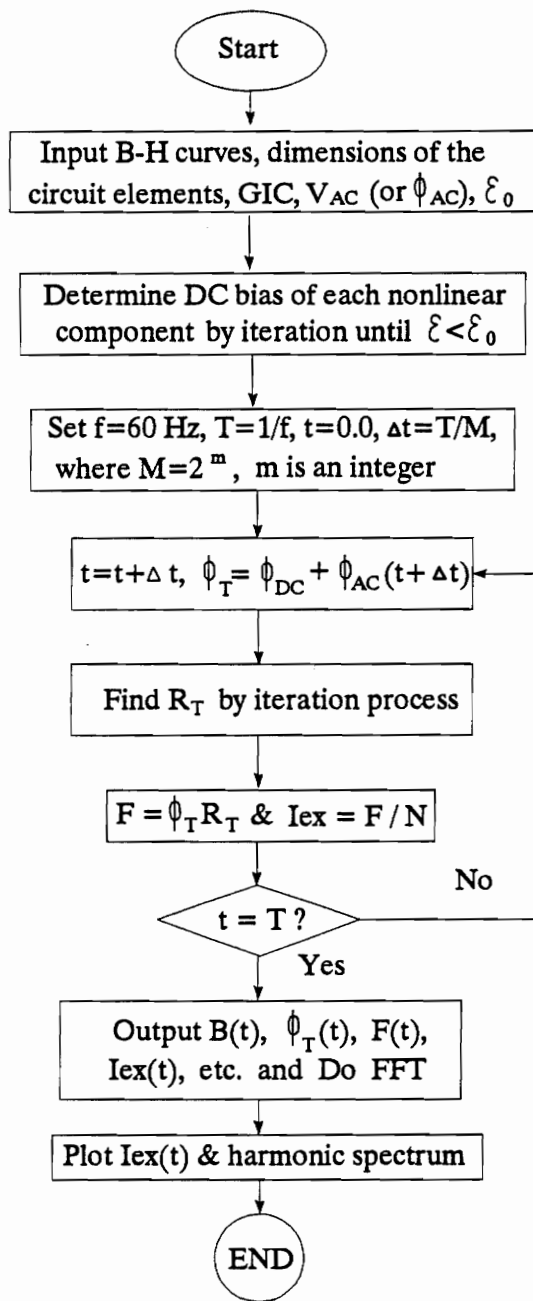


Figure 4.4 Program flow chart for solving the magnetic circuit in figure 4.2

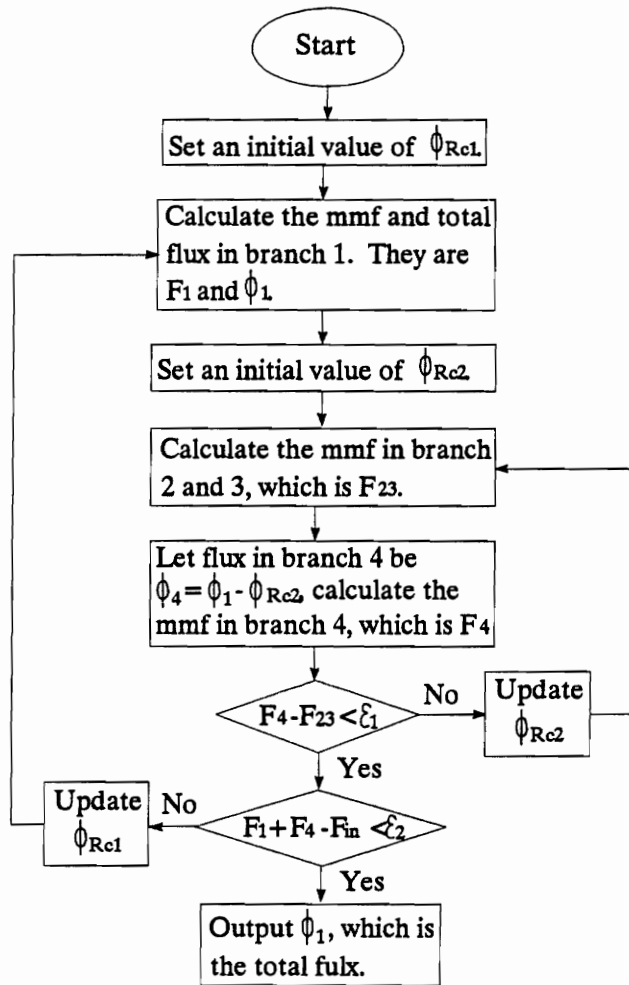


Figure 4.5 Block diagram for calculation of the total flux and flux in each component

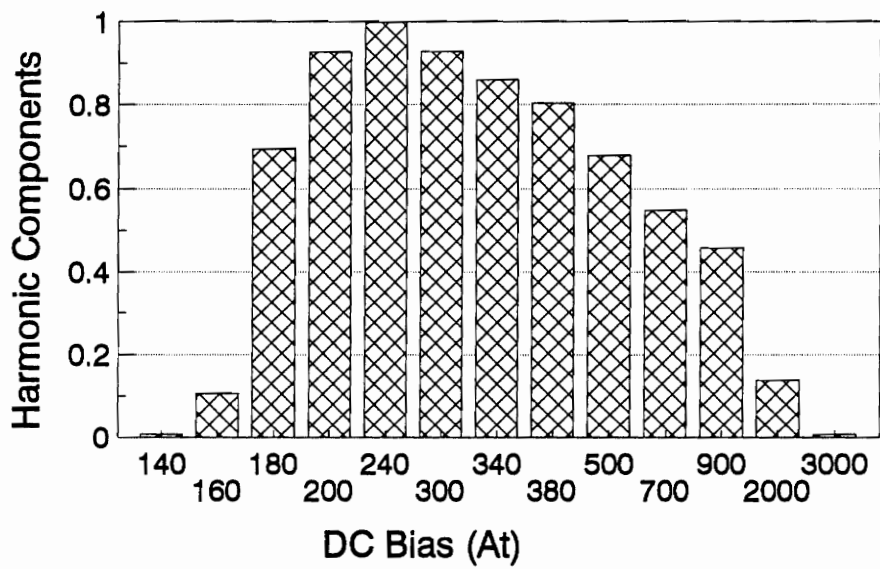


Figure 4.6 Third harmonic component under different dc biases (normalized to I_{3max})

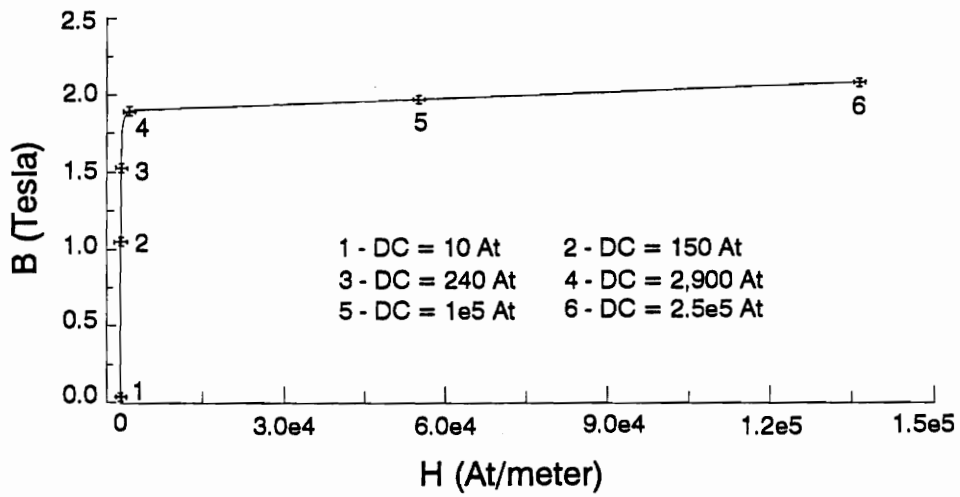


Figure 4.7 The B-H characteristics of the core material.

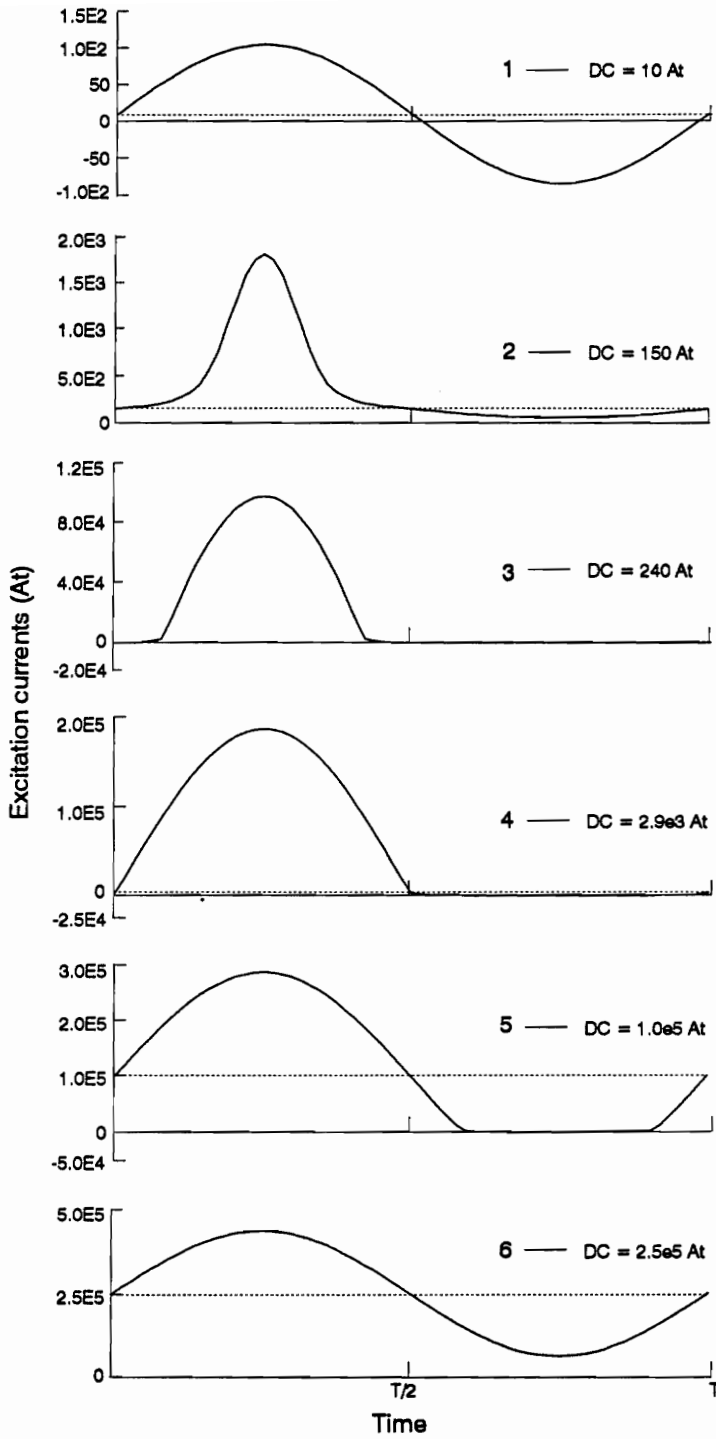


Figure 4.8 Excitation current (I_{ex}) waveforms.

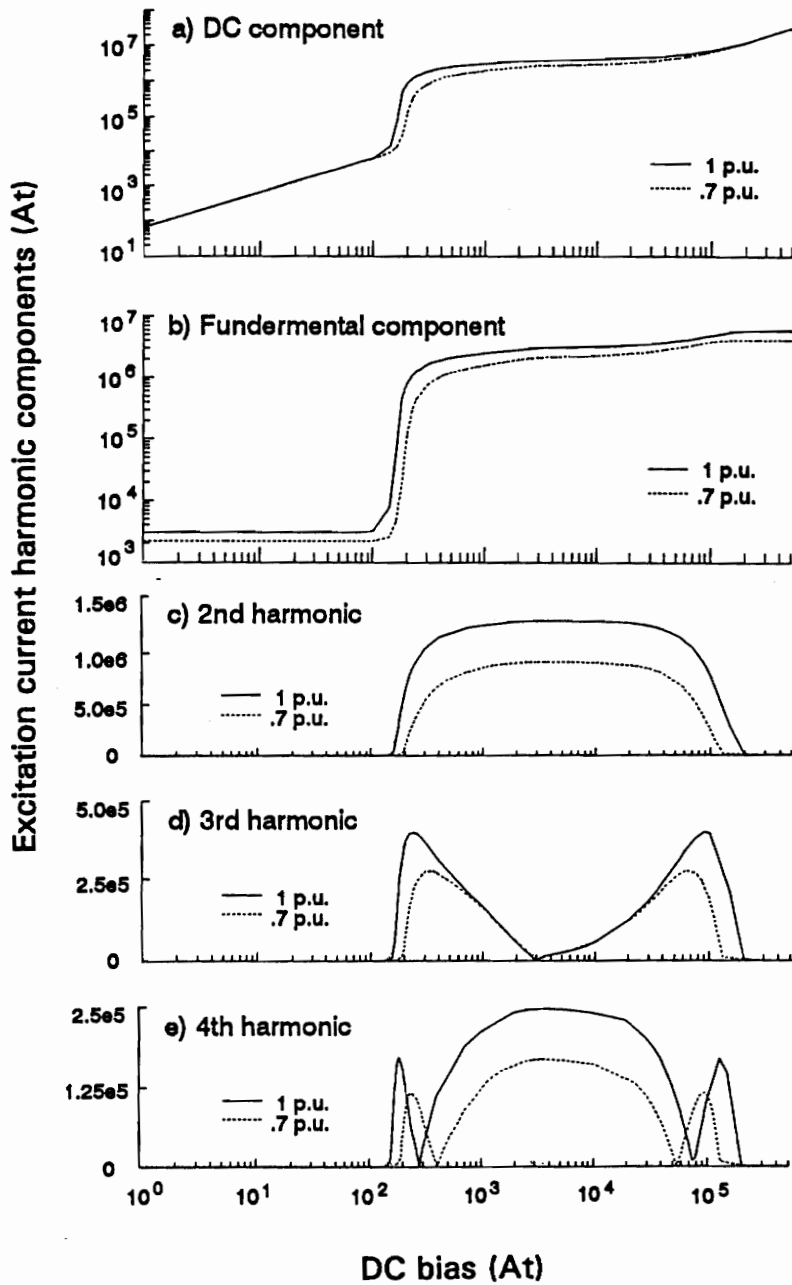


Figure 4.9 Harmonics in excitation current vs. dc bias for 1 p.u. and 0.7 p.u. ac voltage

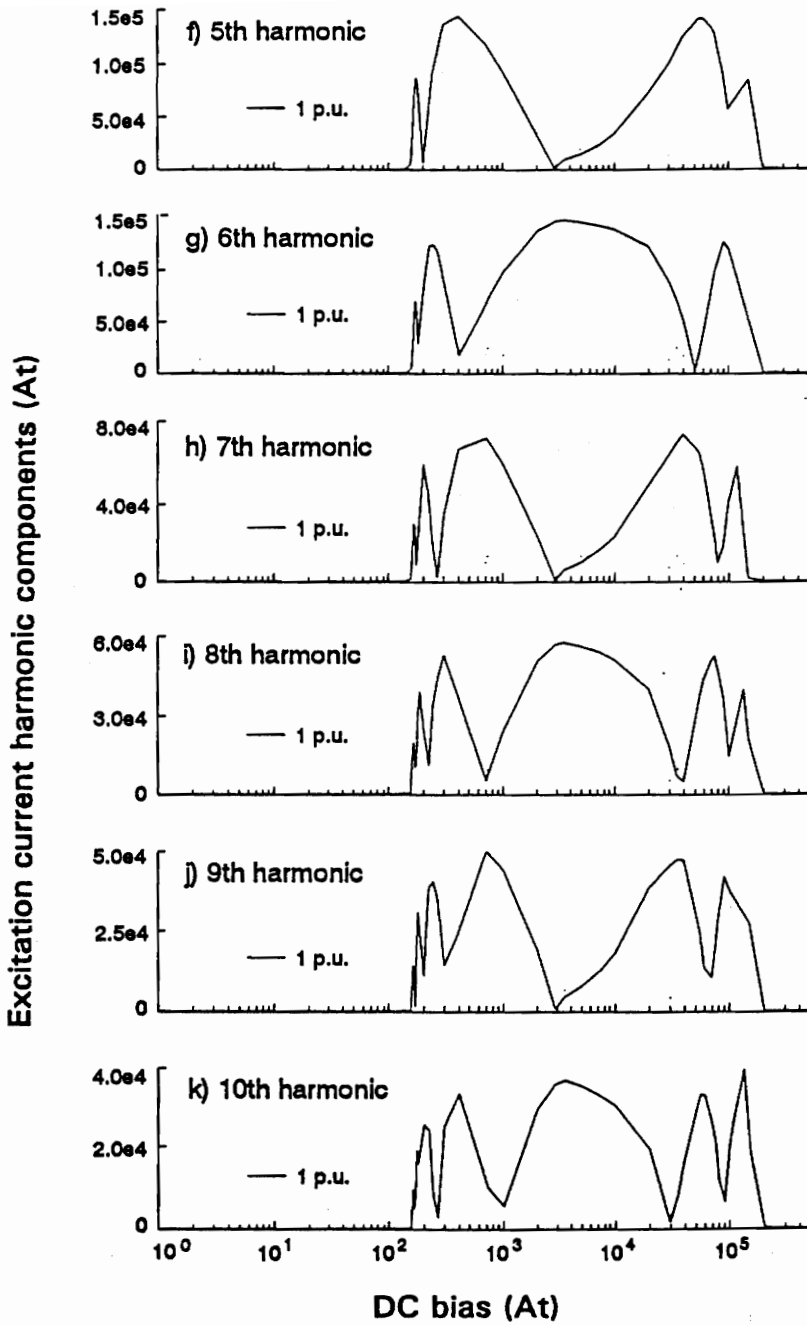


Figure 4.10 Harmonics in excitation current vs. dc bias for 1 p.u. ac voltage

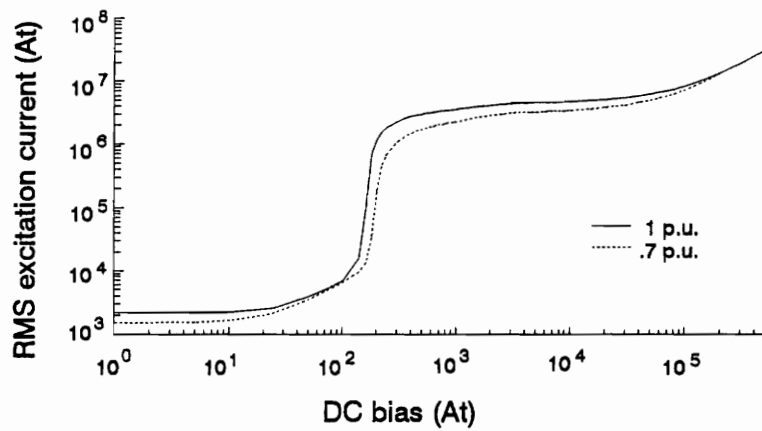


Figure 4.11 RMS excitation current vs. dc bias at 1 p.u. and 0.7 p.u. ac voltage.

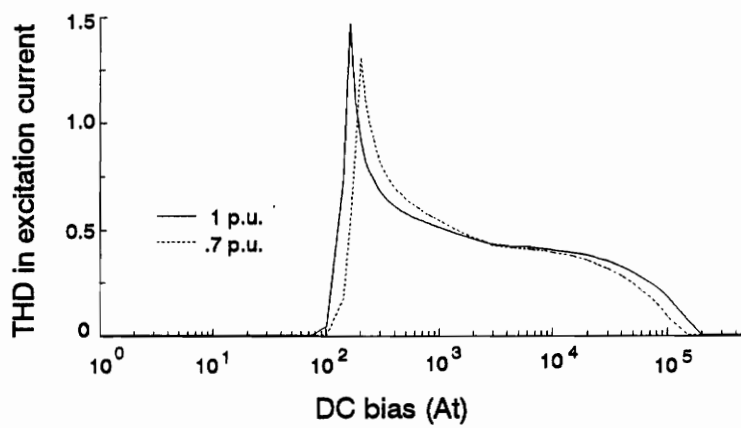


Figure 4.12 Total harmonic distortion (THD) in excitation current vs. dc bias at 1 p.u. and 0.7 p.u. ac voltages.

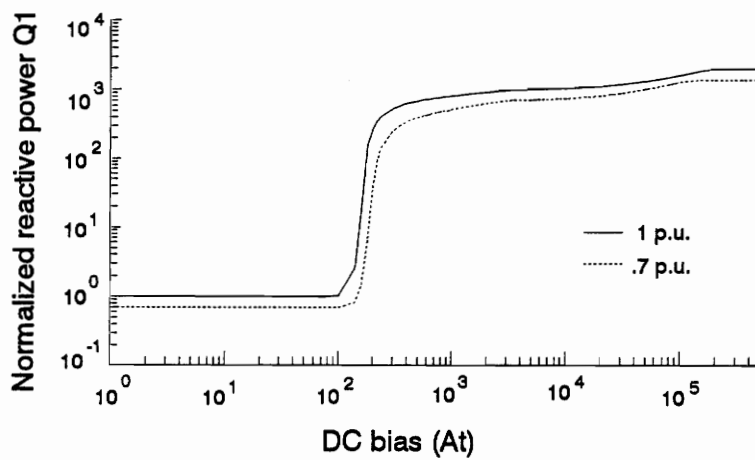


Figure 4.13 Normalized reactive power (Q1) vs. dc bias at 1 p.u. and 0.7 p.u. ac voltage.

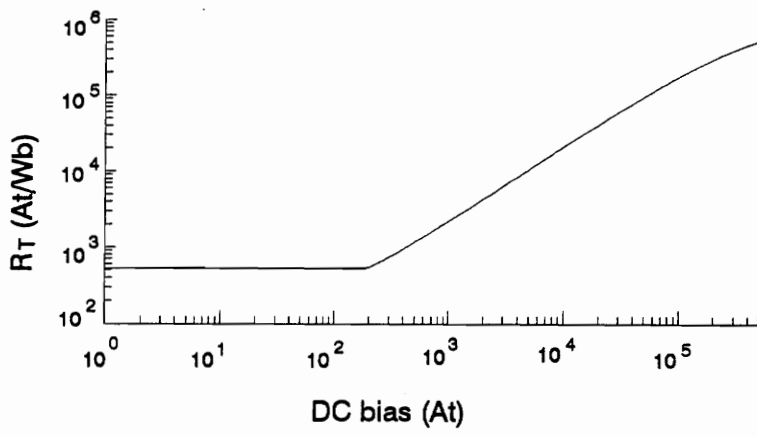


Figure 4.14 The total equivalent reluctance (R_T) vs. dc bias.

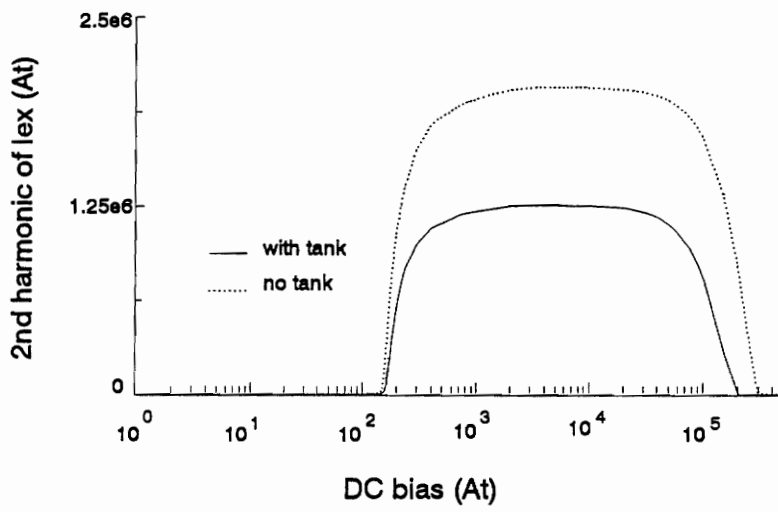


Figure 4.15 Comparison of 2nd harmonics in excitation currents

CHAPTER V. NO-LOAD AND LOADED TRANSFORMER SIMULATION

5.1 Introduction

An ideal transformer can transfer voltage and current linearly with a factor of its turns ratio. In practice, no transformer is ideal because of the losses in all the materials and the magnetic nonlinearity of the iron. The transformer magnetic circuit developed in the last chapter has taken the leakage field and the nonlinear magnetic property into consideration. Yet the material losses have not been included. Also, voltage drops on transformer winding resistances and leakage inductances are no longer negligible under dc operation due to increased excitation currents. This means that the flux inside the core is not necessarily sinusoidal. Therefore, a modified nonlinear equivalent Tee circuit is used to build a more completed transformer model. The effect of the load and how it affect the generation of harmonic excitation currents are examined.

A single phase transformer operation over a wide range of dc levels at no-load and various loading conditions is simulated. The sensitivity of the excitation current to each lumped component in the Tee circuit is examined in detail. Harmonics interaction with the rest of the power system is also studied with a simplified system representation.

5.2 Nonlinear Tee Circuit Model

5.2.1 The transformer equivalent Tee circuit

The equivalent Tee circuit for a single phase transformer given in figure 2.4 is redrawn on the right of figure 5.1. It consists of leakage inductances L_p and L_s , the nonlinear magnetizing inductance L_m , and ac winding resistances R_p and R_s , where subscripts 'p'

and 's' refer to primary and secondary windings respectively. The shunt resistance R_c represents core losses.

5.2.2 Nonlinear magnetizing inductance L_m

Due to the nonlinearity of the magnetic material, the magnetizing inductance L_m is not a constant but a nonlinear function of the magnetizing current. According to the Faraday's law of electromagnetic induction, a voltage $e(t)$ is induced in a N -turn coil such that:

$$e(t) = \frac{d\lambda(t)}{dt} = \frac{d\lambda(i)}{di} \frac{di(t)}{dt} \quad (5.1)$$

where, $\lambda(t)$ is the total flux linkage in the coil, and

$$L_m(i) = \frac{d\lambda(i)}{di} \quad (5.2)$$

is the incremental inductance. Therefore, the nonlinear magnetizing inductance can be characterized by a $\lambda \sim \text{mmf}$ curve.

Based on the transformer magnetic circuit model developed from last chapter, at any given mmf, the total flux linkage λ can be calculated. Consequently, the nonlinear magnetizing inductance L_m can be obtained using equation (5.2). Figure 5.2 gives an $L_m \sim \text{mmf}$ curve according to the result of the example transformer given in figure 4.1.

5.2.3 Leakage inductances

In spite of the magnetic nonlinearity of the iron core, the leakage flux is almost directly proportional to the currents producing them since the paths of the component fluxes are in air for a considerable portion of their length. Also, previous FEM studies have shown

that leakage inductance of the single phase transformer varies little under dc bias. Therefore, the leakage inductance L_p and L_s are considered as constants.

5.2.4 Losses

The core loss is the sum of the hysteresis loss and eddy current loss. The core loss component R_c is a function of the flux magnitude as well as the rate of the flux change. Since core loss calculation during saturation is not within the scope of this study, R_c is assumed to be constant. The core loss usually is 0.5 ~ 2% of the rated power. When the core loss component is negligible, the magnetizing current, which is the current flowing in the nonlinear magnetizing inductance, is equal to the excitation current.

The winding resistances R_p and R_s are also constants when skin effect and stray loss are ignored. The full load copper loss is also between 0.5% to 2% of the rated power under normal operation.

In general, the percentage of the core loss and the resistances decrease with the size increase of the transformer.

5.2.5 Graphical illustration

The nonlinear relationship of transformer voltage and excitation current is illustrated in figure 5.3, where dc biased sinusoidal flux results in a distorted magnetizing current. The current has a dc component I_{dc} . Let I_b be the dc bias current corresponding to the dc flux offset level due to the dc voltage input, and I_0 be the dc component of the distorted current when the zero reference level is moved to I_b . The following relationship holds:

$$I_{dc} (\text{GIC}) = I_b + I_0 \quad (5.3)$$

Figure 5.3 also shows that, when GIC (I_{dc}) is varied, dc bias current I_b and component I_0 (resulted from the horizontally unsymmetrical current) change simultaneously. In other word, if a transformer core is operating in the nonlinear region, any change of I_b will be accompanied by the change of the current waveform.

The values of rms and THD are used to provide information about the total effects of the dc bias level and the distortion of the excitation current waveform. THD is used to describe the total harmonic components in proportion to the fundamental component. Notice that, because the hysteresis loop is not considered in the excitation characteristic, the dc component I_0 can be considered proportional to the THD.

5.3 A Complete Circuit for Computation

5.3.1 Connection with the external network

If the output of a transformer only connects to a load, its output voltage can be reduced to any value which mainly depends on the saturation level of the transformer. However, when a power transformer is in service, it is not only connected with the source and the load, but also interconnected with other stations and devices through networking. Therefore, when the output voltage drops to a certain level, the external network will act like a source and supply power to the load and the transformer. Output voltage will be sustained at some level which is determined by the external network.

To represent the rest of the system connected to the transformer, an equivalent voltage source and a simplified equivalent circuitry is also connected to the same load terminal V_L , as shown on the left of figure 5.1. The external equivalent voltage source V_n is set equal to the secondary terminal voltage of the open-circuit transformer with a variable

angle. The voltage angle of V_n can be approximately determined from the power transformer equation,

$$\frac{V_o^2}{R_l} = \frac{|V_o||V_n|}{\omega(L_s + L_n)}(1 - \sin \delta) \quad (5.4)$$

where, V_o is the secondary terminal voltage of the open-circuit transformer. δ is the voltage angle of V_n . The rest of the parameters are chosen empirically such that [43],

$$C_n = 1/(\omega^2 L_n) \quad (5.5)$$

$$R_w = 25\omega L_n \quad (5.6)$$

$$R_n = 0.05\omega L_n \quad (5.7)$$

5.3.2 Computation of the nonlinear circuit

The circuit shown in figure 5.1 contains one capacitor and five inductors, one of which, L_m is nonlinear. To solve a circuit containing nonlinear devices, there are two major numerical methods; the time domain method and the harmonics balance method. The time domain method is chosen to solve the circuit due to its relative simplicity in programming.

The time domain method involves in an iterative process to solve a set of first order differential equations resulted from circuit analysis. State variables are first chosen to set up the differential equations. For the circuit being considered, the six state variables are i_p , i_s , i_l , i_n , v_w , and i_m . After selection of the state variables, the circuit laws lead the following differential equations:

$$V_{in} - V_m = L_p \frac{dI_p}{dt} + I_p R_p \quad (5.8)$$

$$V_m = L_m \frac{dI_m}{dt} \quad (5.9)$$

$$V_m - V_l = L_s \frac{dI_s}{dt} + I_s R_s \quad (5.10)$$

$$V_l = L_l \frac{dI_l}{dt} + I_l R_l \quad (5.11)$$

$$I_s - I_l = C_n \frac{dV_w}{dt} + I_n + \frac{V_w}{R_w} \quad (5.12)$$

$$V_w = L_n \frac{dI_n}{dt} \quad (5.13)$$

where all element representations are indicated in figure 5.1. The basic ideal of the time domain method is to use the finite difference approximation to replace the time derivatives in the differential equations (5.8) ~ (5.13). For an arbitrary function $f(t)$, its derivative with respect to time can be approximated by

$$\frac{df(t_n)}{dt} = \frac{f(t_n) - f(t_n - \Delta t)}{\Delta t} + O[\Delta t^2] \quad (5.14)$$

where Δt is the time increment, n indicates the number of iteration steps, and $O[\Delta t^2]$ is the higher order error term. It is not so difficult to verify that the error term approaches zero when the time increment approaches infinitesimal. Another concern in using the finite difference scheme to solve the differential equations is the stability. Since the circuit itself must satisfy the physical laws, the time increment is required to be small enough to avoid numerical errors in the solution process. When the circuit contains nonlinear devices, the issue of stability is particularly crucial. Since a large Δt leads to

unstable oscillation that breaks down the iteration process, a small Δt is chosen to maintain the stability of the finite difference scheme.

Based on the finite difference approximation, the following iteration equations are given,

$$I_p^n = I_p^{n-1} + \frac{\Delta t}{L_p} [V_{in} - (I_t^{n-1} - I_m^{n-1} - I_s^{n-1})R_c - I_p^{n-1}R_p] \quad (5.15)$$

$$I_m^n = I_m^{n-1} + \frac{\Delta t}{L_m} (I_p^n - I_m^{n-1} - I_s^{n-1})R_c \quad (5.16)$$

$$I_s^n = I_s^{n-1} + \frac{\Delta t}{L_s} [(I_p^n - I_m^n - I_s^{n-1})R_c - I_s^{n-1}R_s - V_n + V_w^{n-1} + (I_l^{n-1} - I_s^{n-1})R_n] \quad (5.17)$$

$$I_l^n = I_l^{n-1} + \frac{\Delta t}{L_l} [V_n - V_w^{n-1} - (I_l^{n-1} - I_s^n)R_n - I_l^{n-1}R_l] \quad (5.18)$$

$$V_w^n = V_w^{n-1} + \frac{\Delta t}{C_n} (I_l^n - I_s^n - \frac{V_w^{n-1}}{R_w} - I_n^{n-1}) \quad (5.19)$$

$$I_n^n = I_n^{n-1} + \frac{\Delta t}{L_n} V_w^n \quad (5.20)$$

The iteration starts with initial conditions ($n=0$) for the state variables. The initial conditions are calculated under the dc bias. The iteration continues until the steady state is reached.

5.4 No-load Excitation Current Simulation

5.4.1 No-load dc excitation

A 26kV/132kV, 7MVA single phase step-up transformer is used as an example. This is a scale down model of an actual 125 MVA power transformer [21]. The incremental

magnetizing inductance obtained from 3D finite element analysis is shown in figure 5.2. No-load condition is studied first. The primary linear circuit parameters are:

$$V_{ac}=26\text{kV (rms)}, \quad R_p = 0.5 \, \Omega, \quad L_p = 0.01 \, \text{H}, \quad R_c = 9.6 \, \text{k}\Omega$$

V_{ac} is the rms value of the sinusoidal ac voltage and V_{dc} the dc voltage which represents the earth surface potential. Both V_{ac} and V_{dc} are applied to the primary terminal V_{in} ($= V_{ac}+V_{dc}$). GIC is equal to the average (dc) component of the excitation current which is given by [9]

$$I_{dc} = \text{GIC} = V_{dc}/R_p \quad (5.21)$$

During normal operation, the excitation current is so small that the harmonic voltage drops on the primary impedance are negligible. The induced voltage V_m , which is the voltage across the magnetizing inductance in the Tee circuit, is almost equal to the applied sinusoidal voltage. Under dc operation, the excitation current increases drastically. The excitation current produces considerably amount of voltage drop on the primary impedance, which in turn, cause the waveforms of the induced voltage to differ from the applied sinusoidal voltage.

The waveforms of the excitation currents, the distorted magnetizing flux and induced voltage under different dc levels are shown in figure 5.4. Notice that the apparent inductance in equation (2.13) is used for the magnetizing flux calculation.

Complete variations of excitation current harmonics as a function of dc bias have been reported in chapter IV. The study was based on the assumption that the winding impedance and the core loss are negligible. However, under the effect of GIC, the transformer excitation current will increase significantly. As stated earlier, the previous assumption may not be able to offer satisfactory results anymore. Therefore, a more

complete transformer model as given in figure 5.1 is used. The effect of the winding impedance and the core loss are studied subsequently.

5.4.2 The effect of dc levels

Varying the dc level, the excitation current is simulated using the modeled parameters given above. The rms, I_p and THD of the excitation currents with respect to the dc level are given in figure 5.5. The simulation results show that the rms value of the excitation current has nearly a direct proportional relationship with the dc levels. The THD peaks at 8 A of dc, which corresponds to about 2 A dc bias current I_b .

Two important results has been observed. First, if winding impedance and core loss are not considered, the maximum THD occurs when the dc bias is at the knee region of the excitation characteristic. However, having both winding impedance and core loss represented in the circuit, the maximum THD appears before the dc bias reaches the knee of the excitation characteristic. In other word, varying the dc level, the THD reaches its maximum earlier when winding impedance and core loss are considered. Second, although the magnitudes of the harmonic components increase significantly in the nonlinear region operation, the distortion (or I_0) starts to decrease at some point. Therefore, when dc bias reaches a certain value which is still below the knee, the continuous increase of the dc level results only in the increase of the dc bias current I_b .

5.4.3 The effect of varying L_p and R_p

The winding impedances are determined by design data such as the conductor size, the geometrical arrangement, and space factors and operation conditions.

The leakage inductance L_p is varied and the effect is studied. When L_p increases while the input V_{dc} is fixed, the rms value of the excitation current decreases because the

equivalent impedance of the whole circuit increases, as shown in figure 5.6. In the mean time, the magnitude of the induced voltage also decreases due to voltage drop on R_p and L_p . This leads to the decrease of the THD and the increase of the dc bias I_b . Under 50 A dc injection, 50% decrease of L_p results in 50% increase of THD while 80% increase of L_p gives 50% decrease of THD.

The effects of the winding resistance R_p is studied subsequently. RMS and THD of I_{ex} versus R_p are shown in figure 5.7. Since dc injection is almost independent of R_p , the V_{dc} input has to be adjusted according to the values of R_p such that the dc level can remain the same. When R_p increases while keeping dc constant, both rms and THD of the excitation current decrease. The simulation results reveal that the sensitivity of the excitation current to the winding resistance increases rapidly as dc level increases. For example, when R_p is doubled, THD decreases 18% with 100 A dc and only 4% with 50 A dc. If R_p is one fifth of the original value, THD increases 6% under 100 A dc and only 1% under 50 A dc.

5.4.4 The effect of varying R_c

The core loss component R_c has very complicated nonlinear relationship with respect to the dc level. The nonlinear characteristic is not modeled in this study. However, varying the value of R_c indicates that the THD and rms of the excitation current are relatively stable under a wide range of R_c . The hypothetical test shows that, for a case of 50 A dc, THD only decreases 10% when R_c decreases more than 97% (or when the ratio of R_c/R_p is less than 25).

5.5 Effect of DC on a Loaded Transformer

5.5.1 Loaded transformer model

The simulation of the open-circuit transformer has shown that the excitation currents increase dramatically under dc injection. These currents in turn affect the winding loss and the core loss of the transformer. They also change the secondary terminal voltage due to the significant voltage drop on the winding impedance.

To investigate the transformer behavior serving a load and connecting to the power system grid, transformer model of figure 5.1 is used. The inductive load Z_L has a 0.8 power factor. The value of the voltage source V_n is set equal to the secondary terminal voltage of the open-circuit transformer with a variable angle from 0 to -9 degrees. The secondary parameters are:

$$\begin{array}{lll} n \text{ (turns ratio)} = 5, & R_s = 0.5 \Omega, & L_s = 0.01 \text{ H} \\ R_L \text{ (rated)} = 77 \Omega, & L_L \text{ (rated)} = 0.15 \text{ H}, & L_n = 0.004 \text{ H} \\ R_n = 0.0754 \Omega, & C_n = 70 \mu\text{F}, & R_w = 37.5 \Omega \end{array}$$

5.5.2 The effect of load on excitation current

THD and rms values of the excitation current are found and given in figure 5.5. It is seen that the excitation currents change slightly under dc operation in both the open circuit and the full load situations. Some differences are observed in the THD curves. The voltage drop on the primary winding impedance caused by the load current seems to have some moderate effect on the excitation current.

5.5.3 The effect of dc on the load

THD and rms values of the secondary current I_s are given in figure 5.8. It is seen that rms values of the secondary currents increase during dc operation. THD of the secondary current peaks at the same dc level as that of the excitation current.

It is desirable that the rated voltage is supplied to the load and maintained as constant as possible. However, under dc excitation, the voltage drops on both the primary and secondary winding impedance increase due to the increase of excitation currents. As a result, the voltages at the secondary terminal decrease in both the open circuit and loading conditions. This voltage also contains harmonics if the dc level is large enough, but the voltage distortion is much less significant than the current.

The losses P_{loss} in a transformer include the core loss, the copper loss due to the winding current, and the stray loss due to eddy currents induced by the leakage fluxes in the windings, tank, clamps and various parts of the structure. The transformer efficiency is defined by the equation

$$\eta = \frac{P_{out}}{P_{in}} \times 100\% = \frac{P_{out}}{P_{out} + P_{loss}} \times 100 \quad (5.22)$$

where P_{out} and P_{in} are the output and input power respectively. Figure 5.9 shows that the efficiency decreases rapidly as the dc level goes up.

5.5.4 Current waveforms

The current waveforms when Z_L is equal to half of the rated load and is connected to a system voltage (V_n at angle $= -4.5$ degree) is shown in figure 5.10. The dc level is at 50

A. Because the majority of the excitation current harmonics flow into the system instead of the local load Z_L , there is heavy distortion in I_n .

Excitation current harmonics may also coincide with power system resonance frequencies. A tuned system with resonance frequency around 300 Hz was simulated. The value of L_n , C_n , R_n and R_w , as given in the equations (5.4 ~ 5.6), are selected to reflect equivalent system impedance. Resonance excited by the 5th harmonic of transformer magnetizing current was observed.

5.6 Conclusions

At no load, varying the dc level, THD of the excitation current reaches its maximum value when dc bias is right below the knee of the excitation curve. THD decreases when the operation point is moved towards the linear or the heavy saturation regions. Including the winding impedances and core loss component, THD will reach its maximum value earlier.

The excitation current is relatively stable when the core loss R_c varies. Also, the change of the excitation current due to the variation of the primary winding resistance R_p within reasonable range is insignificant. However, the harmonic distortion and the rms value of the excitation current decrease rapidly as the primary leakage inductance L_p increases. The higher the dc level, the larger the decreasing rate for THD and rms. Therefore, it is necessary to include the winding impedance especially the leakage inductance in the excitation current simulations in order to achieve desired accuracy. On the other hand, the core loss during GIC can be negligible for an acceptable error.

Variation of the load has little effect on the excitation current. The load voltage, current and efficiency all decrease monotonically as the dc level increases.

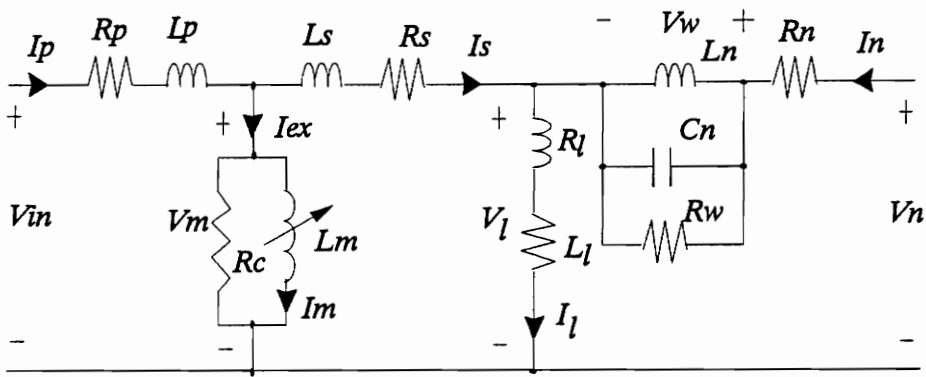


Figure. 5.1 Equivalent Tee circuit of a single phase transformer and a simplified external system representation

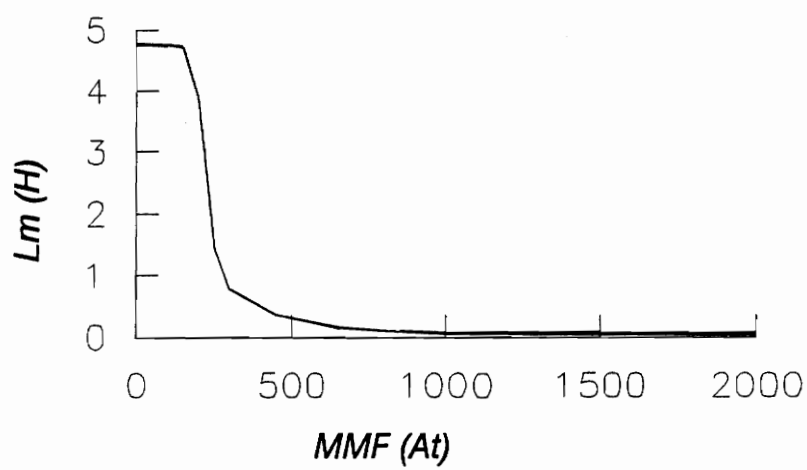


Figure 5.2 Nonlinear magnetizing inductance of the example transformer, L_m

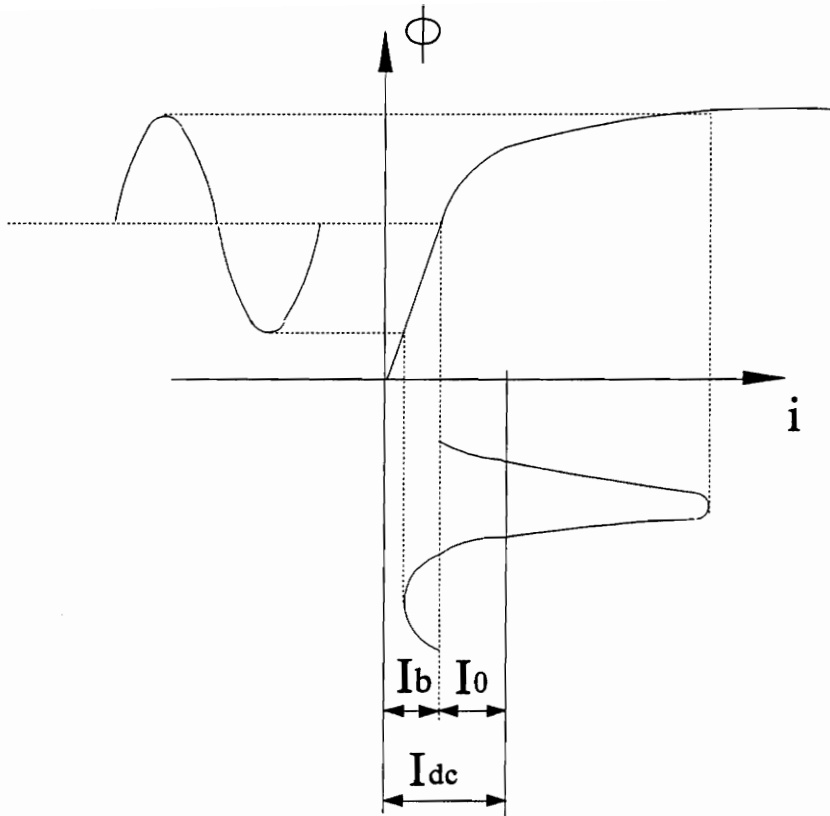


Figure 5.3 An illustration of the nonlinear excitation characteristics

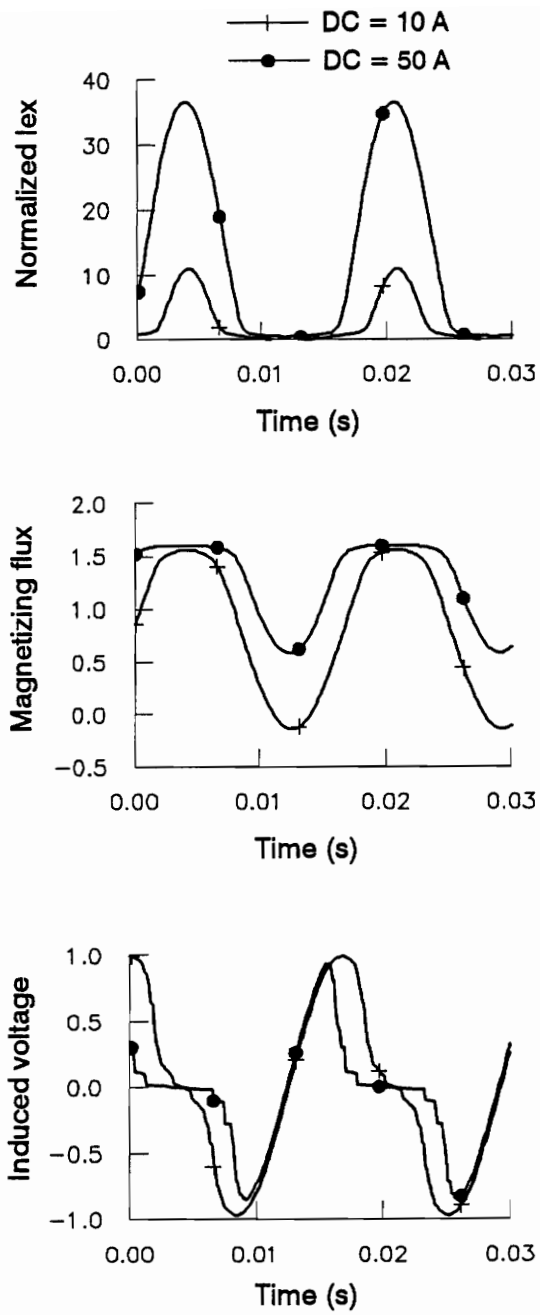


Figure 5.4 Waveforms of excitation current, magnetizing flux and induced voltage under different levels of dc injection

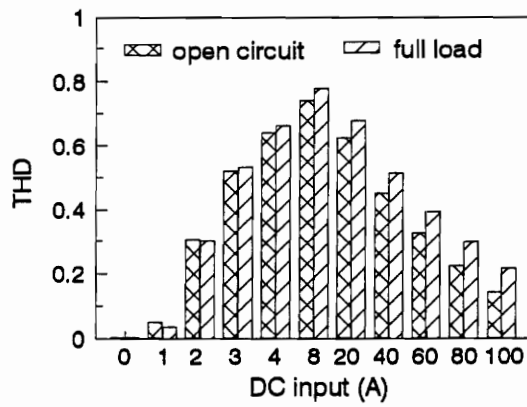
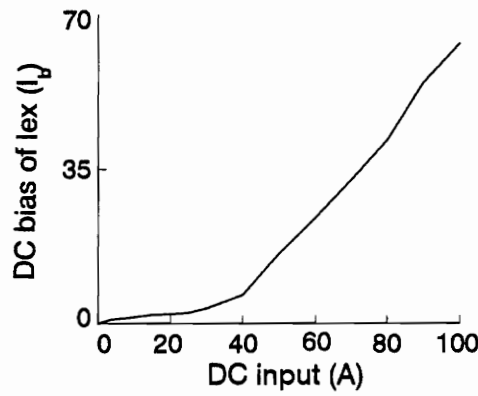
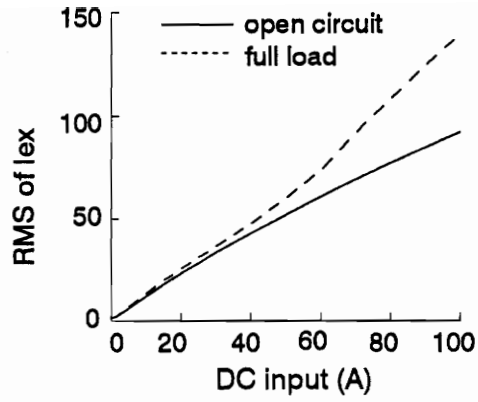


Figure 5.5 RMS, THD and dc bias (I_b) of the excitation currents vs. dc levels

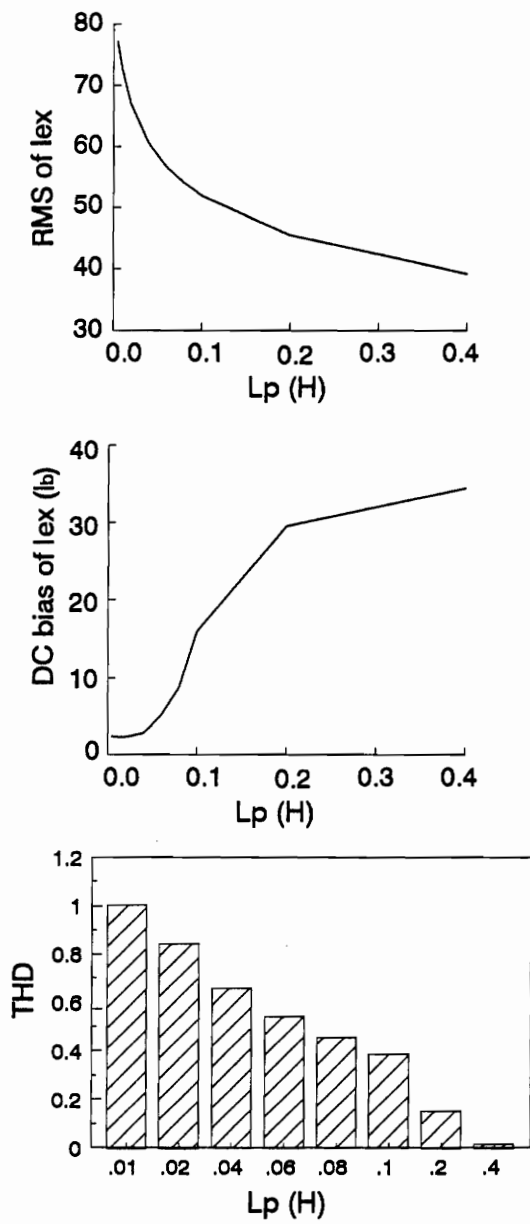


Figure 5.6 RMS, THD and dc bias (I_b) of the excitation currents vs. L_p (normalized)

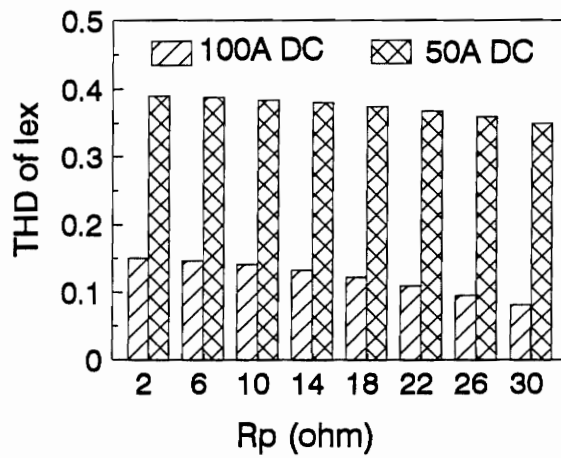
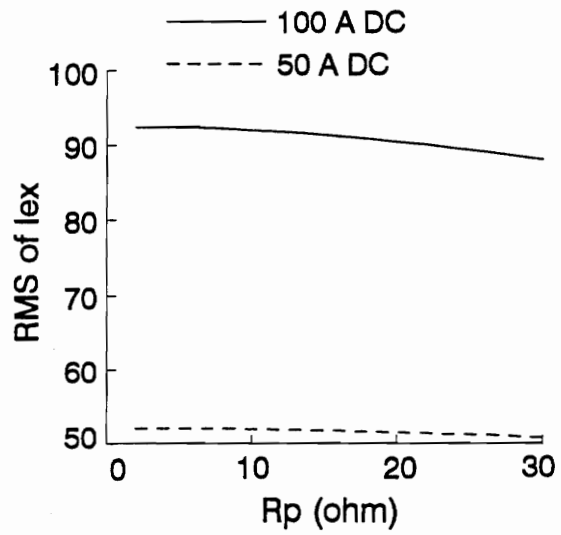


Figure 5.7 RMS and THD of excitation currents vs. R_p (normalized)

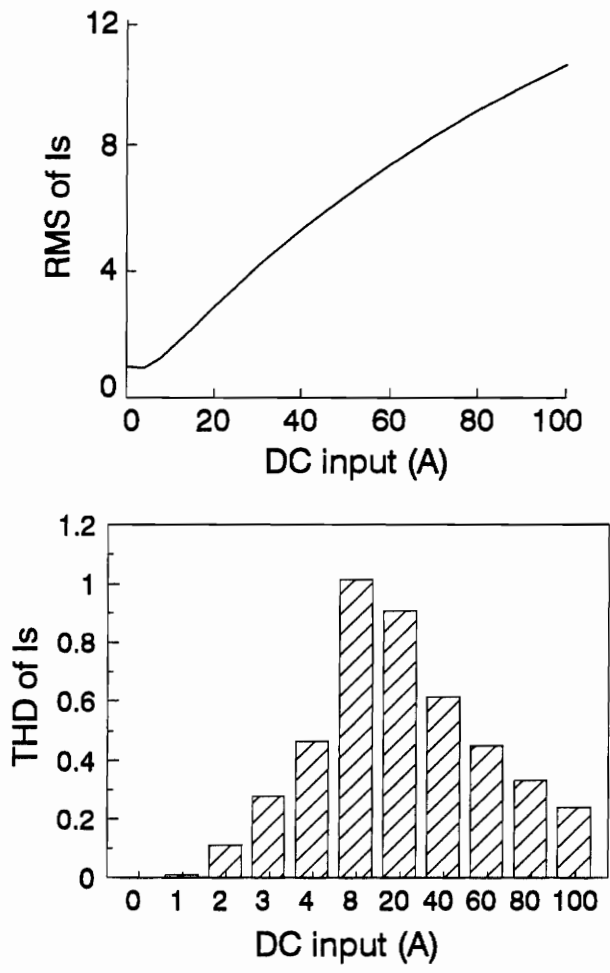


Figure 5.8 RMS and THD of secondary currents vs. dc levels (normalized)

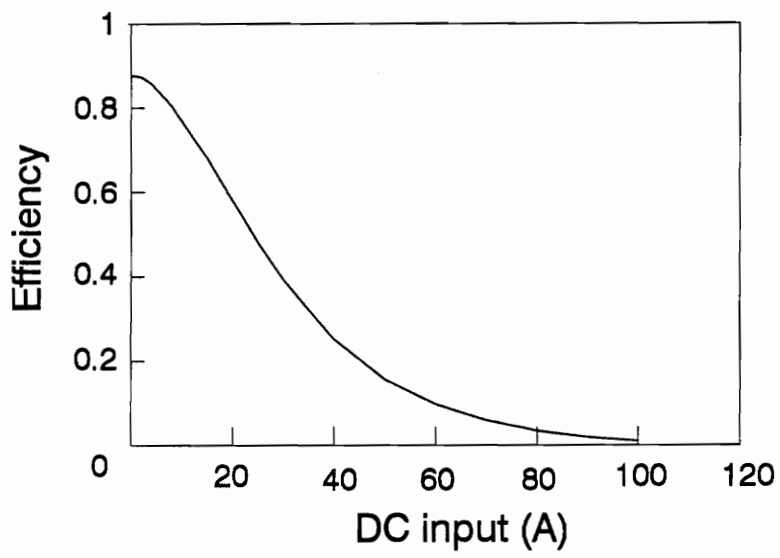


Figure 5.9 Efficiency of the transformer vs. dc levels

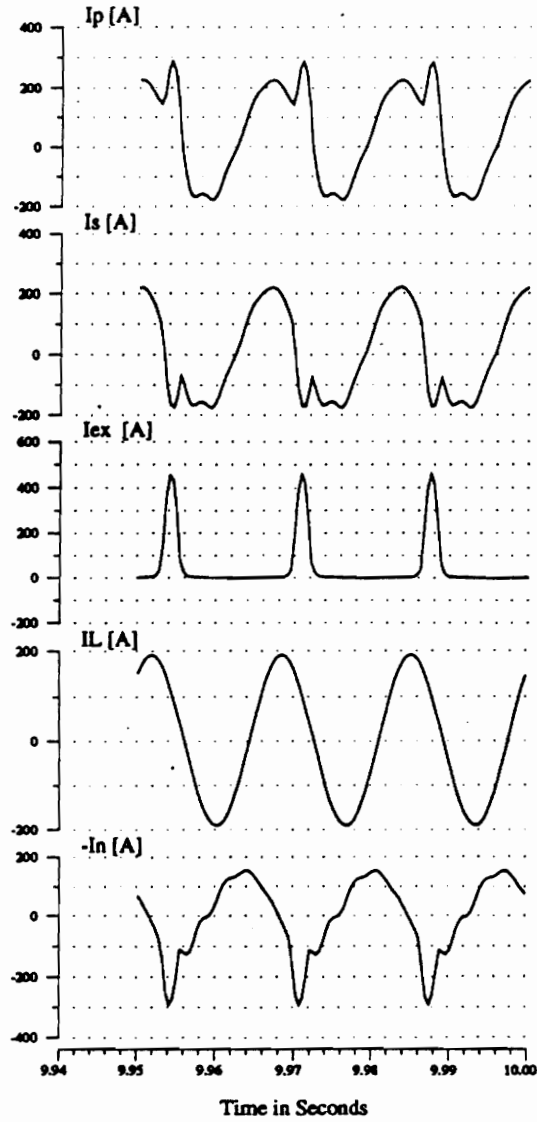


Figure 5.10 Waveforms of currents on the primary (I_p), secondary (I_s), excitation (I_{ex}), load (I_L), and system (I_n)

CHAPTER VI. SMALL SCALE TRANSFORMER DC EXCITATION TEST

6.1 Laboratory Experiments

An experiment is performed to measure the open circuit excitation current of a small scale single phase transformer under dc injection. It is hoped that the dc injection responses of the small scale transformer could reveal some information of power transformers to some degree.

6.1.1 Experimental setup

A single phase matching transformer is used in this test. It is rated at 6 VA with several voltage taps over a wide range of voltage ratings. The winding arrangement is shown in figure 6.1. The core is an EI core made from M6 grade material. It has 6 inches length of magnetic path and is contained in a sealed box which is served as a tank. The box is made of mild steel of M19 grade material and is filled with epoxy. The transformer including the box is in 3 x 3.5 x 1.5 cubic inches.

The experimental setup is given in figure 6.2. An autotransformer serves as the ac input of the matching transformer. Only no-load test is performed. The input is applied between taps 4 and 9 with taps 7 and 8 short circuited such that the voltage rating for this input is 120 V. Since the transformer secondary is open, there is no load-current in the circuit. The voltage measured by the TEKTRONIX 7854 oscilloscope across a 1 Ω resistor corresponds to the excitation current of the transformer. Because the scope shares the common ground with the system, the potential difference between the two ends of the resistor is pick up using the add function. The scope is connected to a digital data acquisition system. One hundred sampling points are chosen for averaging.

6.1.2 Experimental procedures

The experimental procedures are given as follows:

a) Set the dc source to zero. Slowly increase the ac signal and record the readings of the voltmeter and the amp-meter. The relationship between the primary voltage (V_p) and primary current (I_p) is obtained as shown in figure 6.3. This curve shows a nonlinear relationship which reflects the core material saturation characteristics.

b) Keep the dc input at zero. Increase ac voltage until the transformer operates close to the knee of the v-i curve without dc bias, which in this case $V_{rms} = 65$ V. The excitation current waveform is not sinusoidal but symmetric as shown in figure 6.4. Pure sinusoidal waveform is not observed due to the hysteresis phenomenon of the magnetic core. The waveform is recorded.

c) Leave the ac voltage unchanged. Increase the dc input such that part of the ac voltage cycle has reached the nonlinear region of the v-i curve because of the dc bias. At this time, the excitation current waveform is no longer symmetric. The waveforms are recorded.

d) Repeat step "c)" by further increasing the dc value. The excitation waveforms for each increasing dc input are recorded until they are completely distorted. Stop when the transformer becomes very hot and noisy.

6.2 Test Results

A set of data for the excitation current under different dc inputs have been recorded. Figure 6.5 shows some of the excitation current waveforms. Fourier transformation is

performed such that a spectrum of harmonic components under dc biases is obtained. The relationship of each harmonic component and the input dc level is given in figure 6.6.

Figure 6.6 shows that the magnitudes of the harmonics are still rising with the increase of dc bias before the test has to stop. The first peaks of all of the harmonics have not been reached when the transformer starts to smell burn. The dc bias is still below the knee and is far away from the heavy saturation simulated by the transformer model. However, it is possible that GIC can reach to very high level which in turn can bias a transformer at very heavy saturation region. Therefore, GIC can be very dangerous to transformers.

It is also noticed that, although the simulation results show that the magnitudes of the harmonics decrease with the increase of harmonic order, it may not be necessarily true in the reality. In the simulation, the B-H curve is approximated as a straight line at the so called linear region. The excitation current is an ideal sinusoidal waveform when no dc bias is applied. In practice, the excitation current is always somewhat distorted even during normal operation because of the hysteresis loop in the B-H curve. Therefore, the trends may not be obvious when comparing the magnitudes of the different harmonic orders.

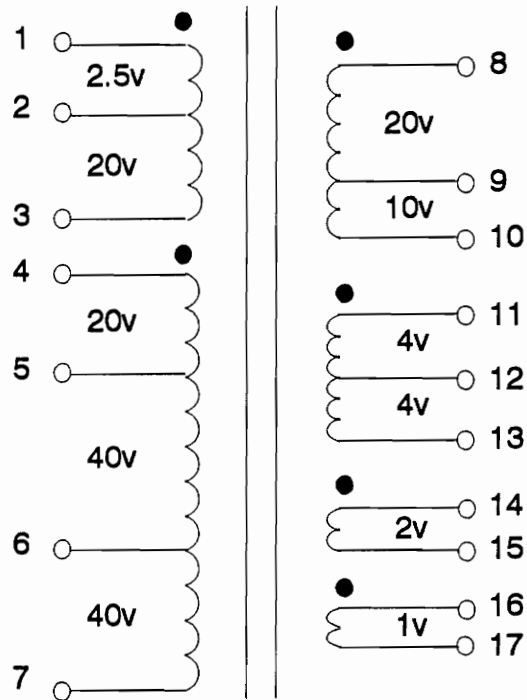


Figure 6.1 Winding arrangement of the experimental transformer

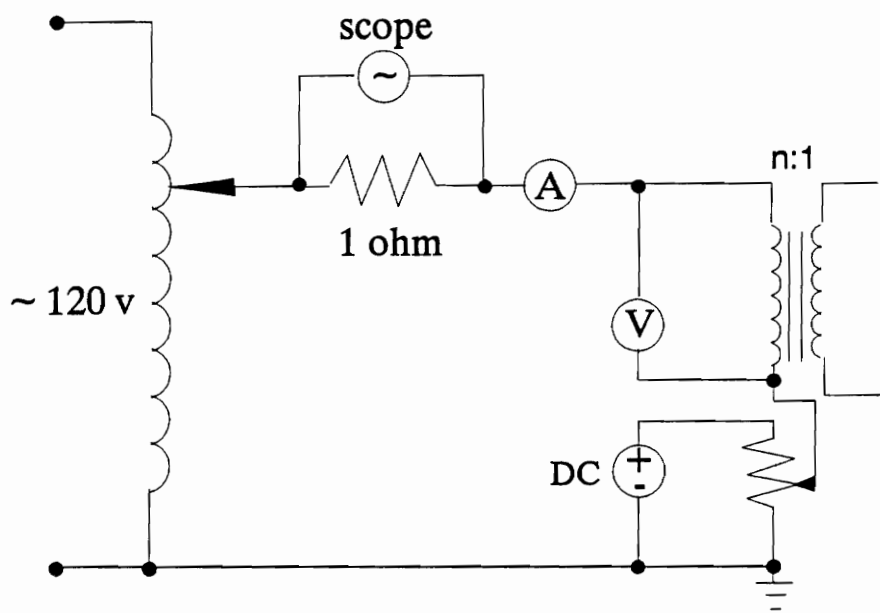


Figure 6.2 The experimental setup for excitation current measurement under dc bias

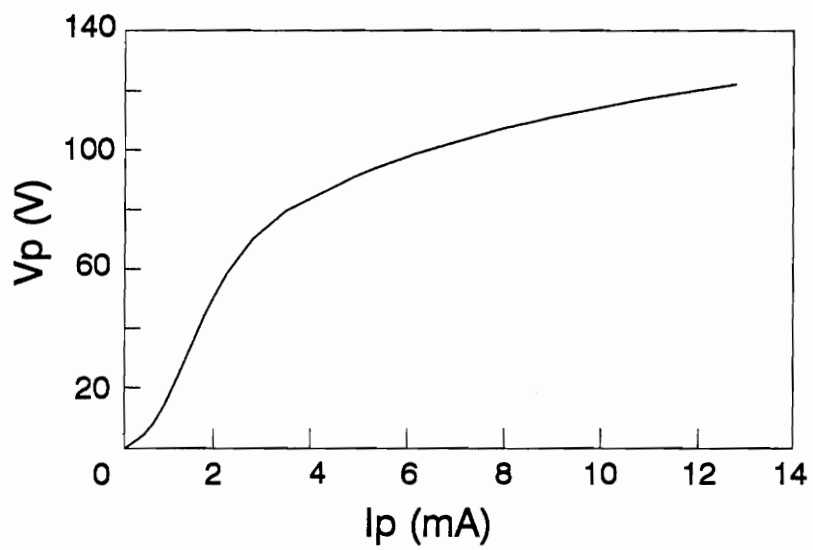


Figure 6.3 Primary current vs. primary voltage

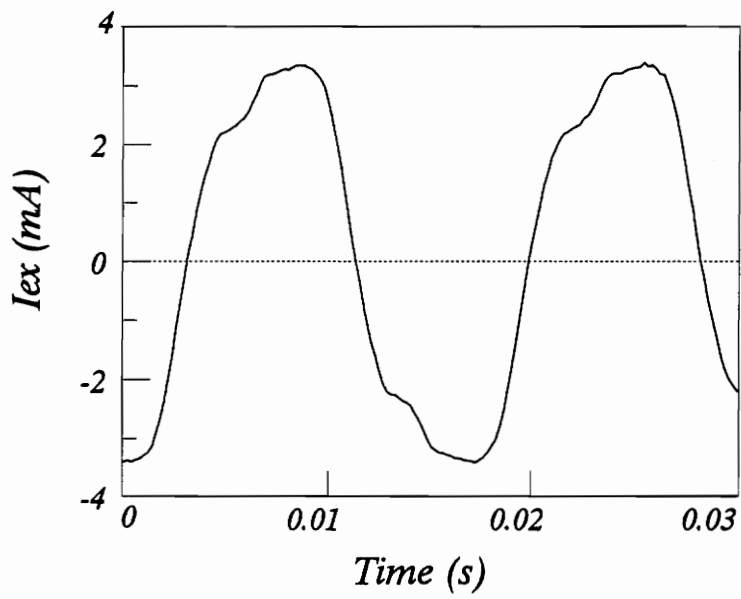


Figure 6.4 Excitation current waveform without dc bias

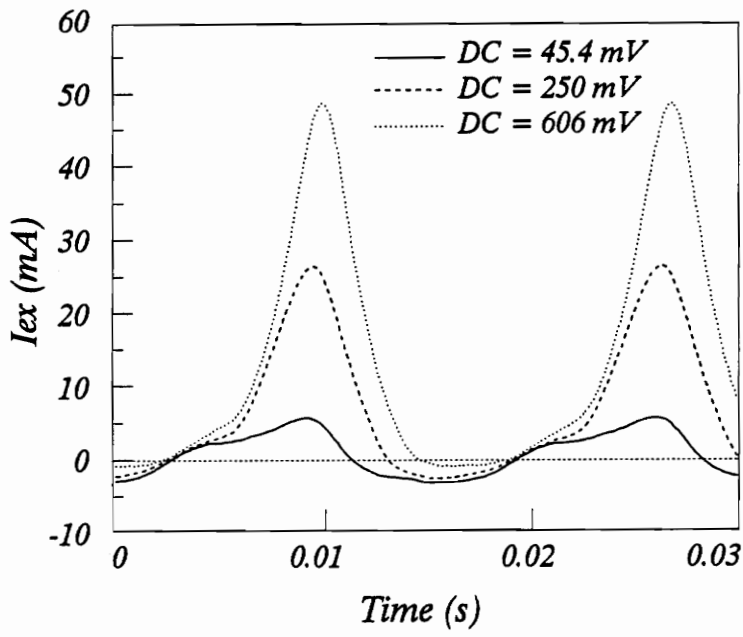


Figure 6.5 Excitation current waveforms under dc bias

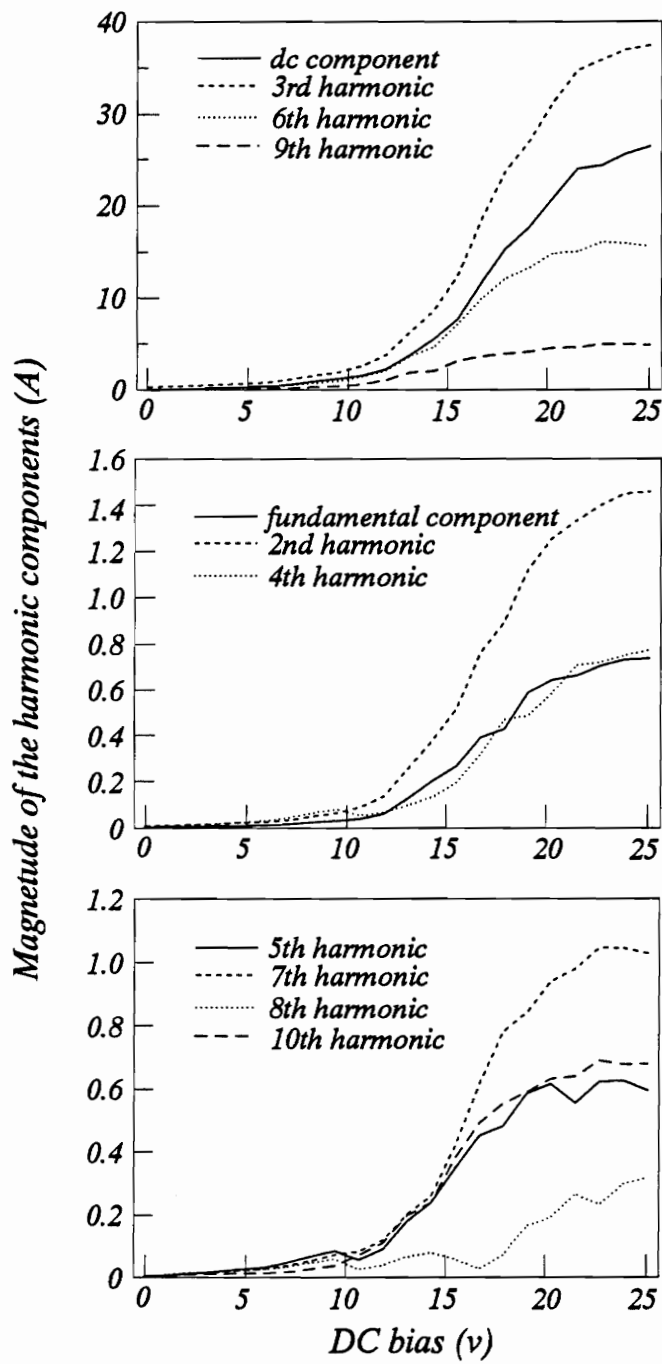


Figure 6.6 Harmonic components vs. dc bias

CHAPTER VII. HARMONICS IN THREE PHASE TRANSFORMER BANKS

7.1 Introduction

Nearly all electrical energy is generated in three phase generators and transmitted over three phase transmission lines. Power transformations in three phase systems can be accomplished by either banks of single phase transformers or three phase transformers.

When a transformer bank is in wye connection with its neutral grounded, it might link very high ESP with the station on the other end during a GMD. Thus the quasi-dc currents (GIC) can enter the transformers and bias the transformer cores. Single phase transformer half cycle saturation and its harmonic generation have been discussed in detail in the previous chapters. The characteristics of the three phase transformers may differ from those of a similarly connected bank of single phase transformers. Since only single phase nonlinear magnetic circuit has been developed, only single phase transformer banks are studied subsequently.

7.2 Three Phase Circuit Analysis

7.2.1 Three phase circuit models

The wye connections with grounded neutrals provide ways for GIC entering power systems. Therefore the three phase arrangements facing the risk of GIC invasion must have at least one side of the transformers connected in wye with its neutral grounded. The following three phase transformer connections are subjected to GIC saturation:

1. Y-Y connection with neutrals grounded on both sides.

2. Y-Y connection with one isolated neutral.
3. Y- Δ connection with grounded neutral.

In this study, the three phase connections are accomplished by using banks of single phase transformers. The saturation model of a single phase transformer given in figure 2.4 is used, except an ideal transformer with turns ratio n is added to isolate the secondary from the primary (figure 7.1).

Since the operation of Y-Y connection with grounded neutrals on both side is very similar to that of single phase transformer, only Y-Y connection with one isolated neutral and Y- Δ connection with grounded Y neutral are studied. Consider each identical single phase circuit given in figure 7.1 as a two port network, figure 7.2.a shows the model of the Y-Y transformer bank and its load. Y- Δ connection with load is illustrated in figure 7.2.b. These are the three phase nonlinear circuit models being used in the simulation. Each phase is indicated by subscripts a, b, and c. For convenience of calculation, each dc input of the three phases is connected to a dc voltage source. In reality, the GIC is injected from the grounded neutral.

7.2.2 Harmonic balance method

Both time domain and frequency domain analyses can be used to solve the nonlinear circuits of figure 7.2. The time domain analysis involves solving a system of integro-differential state equations. It has the advantages of dealing with transient and nonlinear behaviors of a system. However, it suffers from complexity and computational intensity when a circuit has many linear and nonlinear inductive and capacitive components. It would require extensive CPU time to solve the circuits of figure 7.2 in time domain programs such as EMTP. In contrast, the frequency domain analysis is known to be most effective in steady-state analysis of a linear system because of its simplicity and efficiency. The harmonic balance method makes use of capabilities of the time domain

analysis to handle nonlinear circuits and the frequency domain to carry out steady state analysis. When only steady state response is required, as in this case, harmonic balance method can be an effective way for complicated nonlinear circuit analysis [53].

The basic idea of the harmonic balance method is to divide the system containing nonlinear and linear elements into two sets of subsystems; nonlinear subsystems and linear subsystems. The nonlinear subsystems contain nonlinear elements, where the time domain analysis is applied. The nonlinear subsystem can also contain linear elements. The linear subsystems contain only linear elements, where the frequency domain analysis is utilized. Separation of the two subsystems S_l (linear) and S_n (nonlinear) are realized by introducing an equivalent current source $i_x(t)$ and an equivalent voltage source $v_y(t)$ at the interfacing terminals. Starting with an initial value $i_x(t)^0$, an iteration process between time domain and frequency domain updates $i_x(t)$ and $v_y(t)$ until,

$$|i_x(t) - i_y(t)^*| \leq \varepsilon \quad (7.1)$$

where, $i_y(t)^*$ is the current resulted from the voltage source $v_y(t)$. Whether the current source $i_x(t)$ or the voltage source $v_y(t)$ be used for the nonlinear subsystem S_n can be arbitrary or be determined by the property of the nonlinear subsystem.

Figure 7.3 shows the nonlinear subsystem S_n and part of the linear subsystem S_l for Y-Y or Y- Δ three phase transformer bank models. This nonlinear subsystem includes a current source $i_n(t)$ in parallel with the nonlinear inductance L_m and the core loss component R_c . There are two reasons in choosing this nonlinear subsystem configuration:

1) To avoid the infinite integration due to a voltage source connected between the nonlinear inductance. If the source across L_m is a voltage source $v_n(t)$ instead of a current source $i_n(t)$, the current resulted from $v_n(t)$ would be,

$$i_n(t)^* = \frac{\int_0^T V_n(t) dt}{L_m} + i_n(t)^0 \quad (7.2)$$

where T is the cycle and $i_n(t)^0$ is the initial value. Different $i_n(t)^0$ will give different $i_n(t)^*$ regardless of the source $v_n(t)$.

2) To convert differentiation into integration which is more numerical stable. The conversion is accomplished by including the parallel resistive component R_c in the nonlinear subsystem. The magnetizing current $i_m(t)$ is calculated by,

$$i_m(t)^{k+1} = i_m(t)^k + \frac{(i_n(t) - i_m(t)^k)R_c}{L_m} dt \quad (7.3)$$

and,

$$V_n(t)^* = (i_n(t) - i_m(t))R_c \quad (7.4)$$

where $v_n(t)^*$ is the voltage across the current source $i_n(t)$. Subscript k indicates the k -th iteration.

One concern related to iteration process is convergence. Mathematically, an iteration may be speed up to reach the convergence by introducing an overrelaxation parameter γ , leading to a so-called overrelaxation iteration. The parameter γ is between 0 and 1 and an optimal value is based on experience as well as trial and error. After adopting the overrelaxation iteration process, The solution process can be summarized as follows:

- (i) Given an estimated value of $i_n(t)^0$ at the interfacing terminal. Subscript n refers to the parameters in the nonlinear subsystem.
- (ii) Calculate the voltage $v_n(t)^*$ from the current $i_n(t)^0$ in the nonlinear subsystem S_n .

(iii) Let $v_1(t)^0 = v_n(t)^0$. Calculate $V_1(j\omega)^0$ from $v_1(t)^0$ using Fourier transformation. Where j is the harmonic order and $\omega = 2\pi f$. Subscript 1 indicates the parameters in the linear system.

(iv) Calculate $I_1(j\omega)^0$ from $V_1(j\omega)^0$ using linear analysis in the frequency domain.

(v) Calculate $i_1(t)^*$ from $I_1(j\omega)^0$ using inverse Fourier transform.

(vi) Compare $i_1(t)^*$ and $i_n(t)^0$:

$$|i_1(t)^* - i_n(t)^0| = \varepsilon \quad (7.5)$$

(vii) If ε is greater than a specified tolerance, return to step (ii) using a new value $i_n(t)^1$ in place of $i_n(t)^0$, $i_n(t)^1$ is given by

$$i_n(t)^1 = \gamma i_1(t)^* + (1 - \gamma) i_n(t)^0 \quad (7.6)$$

or more generally by

$$i_n(t)^k = \gamma i_1(t)^* + (1 - \gamma) i_n(t)^{k-1} \quad (7.7)$$

where the superscript k indicates the k -th iteration. If ε reaches a specified tolerance, the nonlinear analysis stops.

7.3 Three Phase Harmonics

7.3.1 Phase relations among the harmonics

If the single phase transformers in a three phase bank are identical and the line voltages are balanced, the waveforms of the excitation currents in the transformers are identical but differ in phase by 120° .

When the third harmonic components present in the three phase circuits, each of them also differs in phase by one third of a cycle. In other words, their phase order is shifted by three third of one, or a whole, third harmonic cycle. Thus the third harmonic components are in phase and they are zero sequence components. For the same reason, it can be shown that all multiples of the third harmonic behave in a three phase circuit in the same way as do the third harmonics.

The 5th harmonic in the three phase circuits differs in phase by five third of a fifth harmonic cycle. When the fundamental component i_{ab1} lags the fundamental component i_{ca1} by one third of a cycle, the fifth harmonic component i_{ab5} leads the fifth harmonic component i_{ca5} by one third of a fifth harmonic cycle. Thus the phase order of the fifth harmonics is the reverse of the phase order of the fundamentals. They are negative sequence components.

The phase order of the other harmonics can be shown accordingly. The phase relations can be summarized in table 7.1.

It can be readily shown that there is no zero sequence component in the line currents for both wye with isolated neutral and delta connections. The zero sequence components can not exist in the wye windings, and therefore in the line currents, when there is no return path through its neutral. In the delta connection, however, the zero sequence components simply circulate within the delta windings but do not appear on the lines.

Because of the absence of zero sequence currents, the effective value of the no load line currents is less than $\sqrt{3}$ times the effective value of excitation currents in the delta windings. Let $I_{\phi\Delta}$ be the effective value of the excitation currents in the windings, then

$$I_{\phi\Delta} = \sqrt{I_{\phi\Delta c}^2 + I_{\phi\Delta 1}^2 + I_{\phi\Delta 2}^2 + I_{\phi\Delta 3}^2 + I_{\phi\Delta 4}^2 + I_{\phi\Delta 5}^2 + I_{\phi\Delta 6}^2 + \dots} \quad (7.8)$$

Table 7.1 Phase relations among the harmonics in three phase circuits

Harmonic	Phase order	Symmetrical component
1, 4, 7, 10, 13, 16, etc.	abc	positive sequence
2, 5, 8, 11, 14, 17, etc.	cba	negative sequence
3, 6, 9, 12, 15, 18, etc.	in phase	zero sequence

where $I_{\phi\Delta i}$ is the effective values of the harmonic components in the three identical transformers. Notice that even harmonics may present due to dc saturation. The effective value of the line currents I_{line} is,

$$I_{line} = \sqrt{3} \sqrt{0 + I_{\phi\Delta 1}^2 + I_{\phi\Delta 2}^2 + 0 + I_{\phi\Delta 4}^2 + I_{\phi\Delta 5}^2 + 0 + \dots} \quad (7.9)$$

or,

$$I_{line} = \sqrt{3} \sqrt{I_{\phi\Delta}^2 - I_{\phi\Delta dc}^2 - \sum I_{\phi\Delta 3n}^2} \quad (7.10)$$

A 132kV/26kV, 7MVA step-down single phase transformer is used as an example. The incremental magnetizing inductance is given in figure 5.2. The primary linear circuit parameters are: $V_{ac}=132\text{kV}$ (rms), $R_p = 12.5 \Omega$, $L_p = 0.25 \text{ H}$, $R_c = 240 \text{ k}\Omega$ referred to 132kV side. The secondary parameters are: $R_s = 0.5 \Omega$, $L_s = 0.01 \text{ H}$, Z_L (rated) = 77Ω , turns ratio $n = 5$.

7.3.2 Balanced Y-Y connection

Balanced Y-Y connection was simulated first, see figure 7.2.a. As the dc bias increases, more harmonics are observed in the excitation currents. The trend is identical to that of a single phase transformer. When rated inductive load are used, small amount of excitation harmonics enters the load side. The harmonics in the excitation currents are mainly supplied by the primary currents. Thus the primary currents have similar harmonic pattern as the excitation currents.

In order to find out how different types of load affect the harmonics appeared in the secondary, rated capacitive loads are also used. Increased harmonics are observed as the power factor decreases (except the third harmonic and its multiples). Figure 7.4 shows

the magnitudes of the harmonics when 50 A per phase balanced dc is applied. Some observations are given below:

1) The harmonic contents in the excitation currents are identical regardless of change in power factors.

2) The harmonic contents in the excitation currents can be supplied from the primary and secondary. Because third harmonic and its multiples can not exist in the secondary, they have to come from the primary.

3) When the transformer cores are operating in the nonlinear region, the secondary currents and primary currents may not be in phase. Therefore, the difference of the magnitudes of each harmonic in the primary and secondary may not equal to the magnitude of the corresponding harmonic in excitation currents.

4) Because of resonance between the load capacitor and the winding inductance, the fifth harmonic shows relatively higher magnitude (A calculation shows a series resonance occurs at around 300 Hz). When the load becomes more capacitive, the circuit will reach to a point where oscillation occurs around the fifth harmonic. Figure 7.5 shows the waveforms of the secondary line current under 50 A per phase dc injection at two different load power factors.

The effect of rated capacitive loads with 0.8 power factor is compared with the inductive loads with the same power factor. On the secondary side, except the second harmonic for the inductive loads (which is 50% of that of the capacitive loads), all higher order harmonics of the inductive loads are negligibly small. Remember that the harmonics in the excitation currents are identical for the two different loading conditions. This means, for inductive loads, most harmonics enter the primary side.

7.3.3 Balanced Y- Δ connection

With the same dc input (50 A per phase), the Y secondary is replaced by the Δ connection with balanced loads. The simulation results show that the excitation currents stay unchanged. When the loads are inductive, the harmonics in the primaries are very close to those in the excitation currents.

Harmonics in the primary and secondary windings of the Y- Δ are very similar to those of the Y-Y connection, except the third harmonic and its multiples. It is interesting to point out that almost all the third harmonic and its multiples are supplied by the Δ windings while they are entirely supplied by the primaries in the case of a Y-Y connection. Therefore, in the Y- Δ connection, there is hardly any third harmonic injected into the system.

Figure 7.6 shows the waveforms of the delta winding current and the line current under balanced load with 0.25 leading power factor. Missing zero sequence components in the line is not the only reason that the two waveforms differ. The presence of the negative sequence components is another reason. Because of the reversed phase order of the negative sequence currents, the phase relation between the positive sequence and the negative sequence of the line currents differs from the phase relation between these components of the delta winding currents.

7.3.4 Unbalanced Conditions

Unbalanced load

For both Y-Y and Y- Δ connections, the load on phase a was reduced by half and harmonics in the primary, secondary, and excitation currents were observed. The

unbalance in the load hardly affects the excitation current in either connections as shown in figure 7.7 (which is for the Y- Δ connection under 50A/phase dc). Figure 7.8 gives the current waveforms for the excitation, primary, and secondary currents. Again, the unbalance appears in all three but the excitation current.

Unbalance dc excitation

When unbalanced dc injection is simulated, V_{dci} ($i = a,b,c$) in figure 7.3 is changed accordingly to simulate the unbalanced GIC input caused by difference in system line impedances.

For both Y-Y and Y- Δ connections, the dc in phase a was reduced 30% ($I_{dca} = 35A$). Harmonics in the primary, secondary, and excitation currents were observed. The unbalance in dc changed the excitation current in phase a as expected. However, the unbalanced dc hardly affects the secondary line current for both connections. Figure 7.9 gives waveforms of the excitation, primary, and secondary currents for the Y-Y connection. The unbalance appears in all three of the current waveforms.

7.4 Conclusions

The study extends the work of previous efforts in characterizing transformer generated harmonics under GIC. Calculation of harmonics from dc biased three phase transformer banks were performed using the piecewise harmonic balance technique. The study provides a preliminary understanding of the excitation current harmonics of three phase transformer banks under GIC.

Harmonic characteristics of the Y-Y (with one grounded neutral) and Y- Δ three phase bank and single phase connections are compared. As expected, there is no difference in

the excitation currents between the three configuration. The only variations are introduced by the different paths for the third harmonic and its multiples. That is, the third harmonic and its multiples can not exist in the ungrounded wye windings and the line currents on the delta side.

The study also provides information on how excitation current harmonics will be shared between the primary and secondary of the three phase transformer banks. In the model, the impedance on the primary includes only the transformer winding resistance and leakage inductance, thus, the distribution of the harmonics between the primary and secondary side depends on the equivalent load seen by the transformer secondary. As this load changes from inductive to capacitive, the amount of harmonics in the secondary increase with the corresponding changes in the primary winding. Resonance was also observed in the simulation which occurred around the 5th harmonic.

The unbalance of the load hardly affects the excitation current. The unbalanced dc hardly affects the secondary line current for both connections, but it changes the excitation in the affected phase, as expected. In general, very little effect on the excitation current is observed due to load variations.

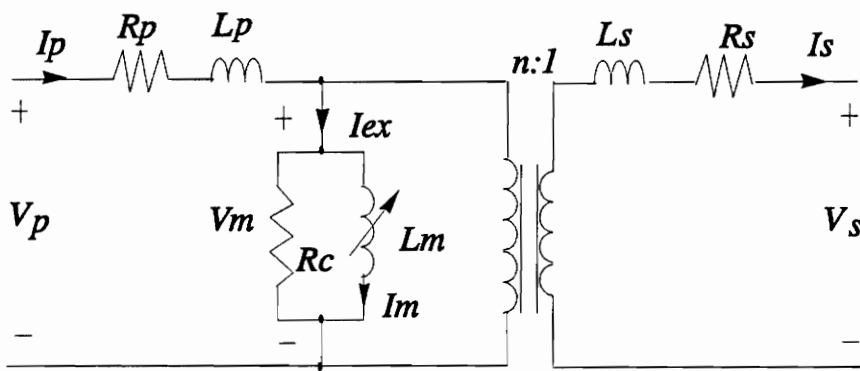


Fig. 7.1 Equivalent Tee circuit of a single phase transformer

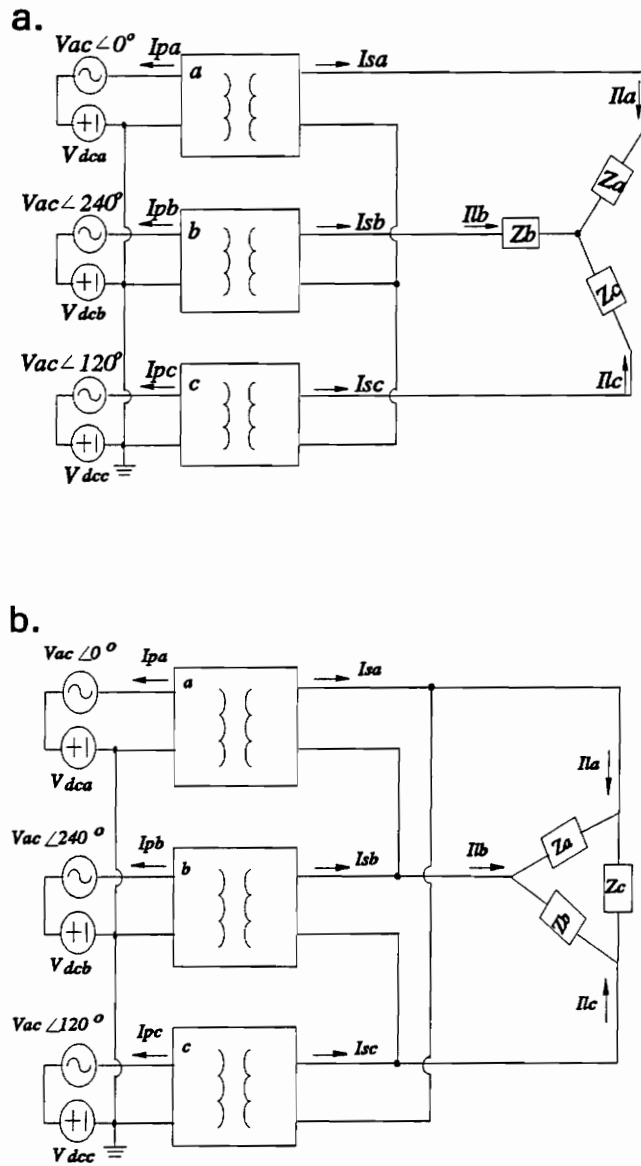


Fig. 7.2 Model of the a) Y-Y bank with one grounded neutral
 b) Y- Δ bank with grounded neutral

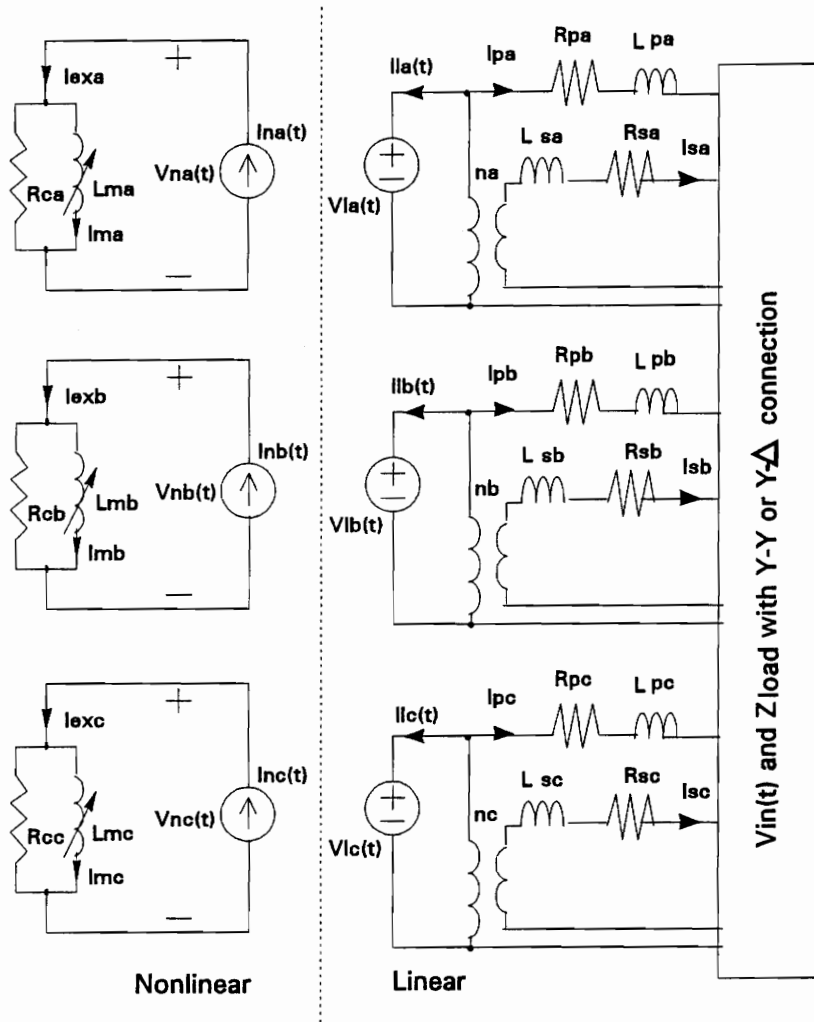


Fig. 7.3 Model circuits separated into nonlinear and linear subsystems

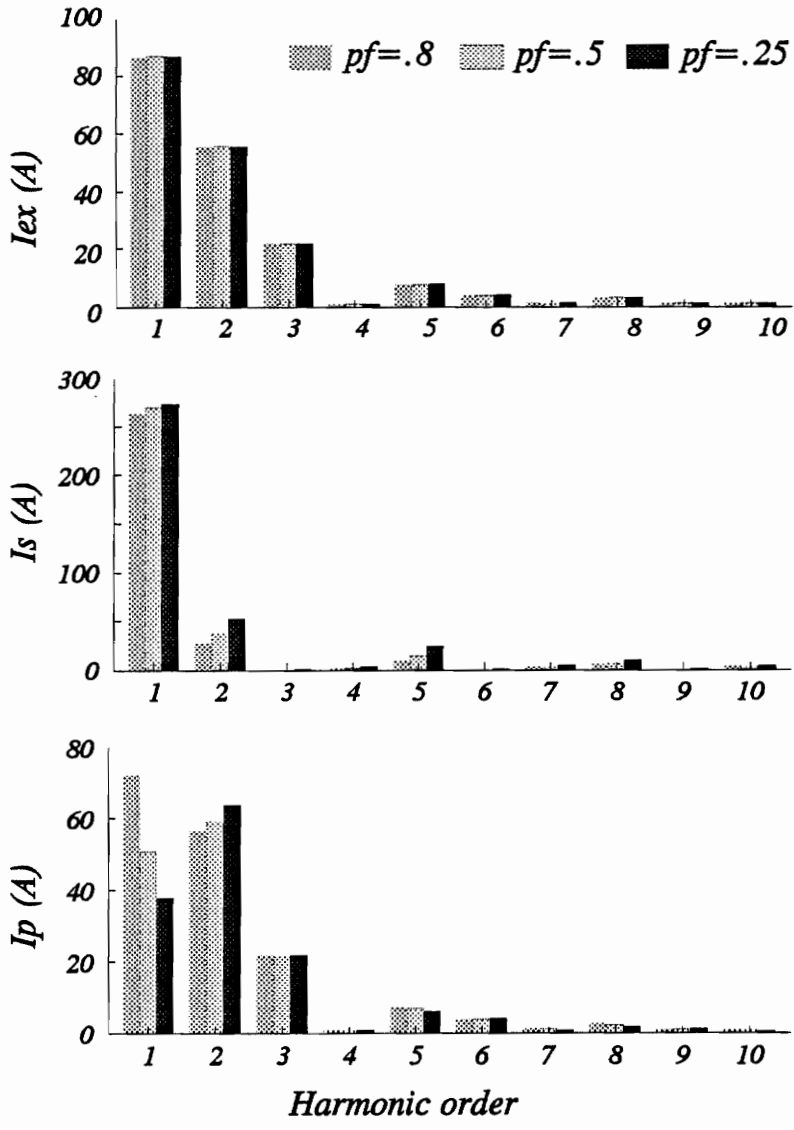


Fig. 7.4 Harmonic distribution of balanced Y-Y with various power factors under 50A/phase dc.

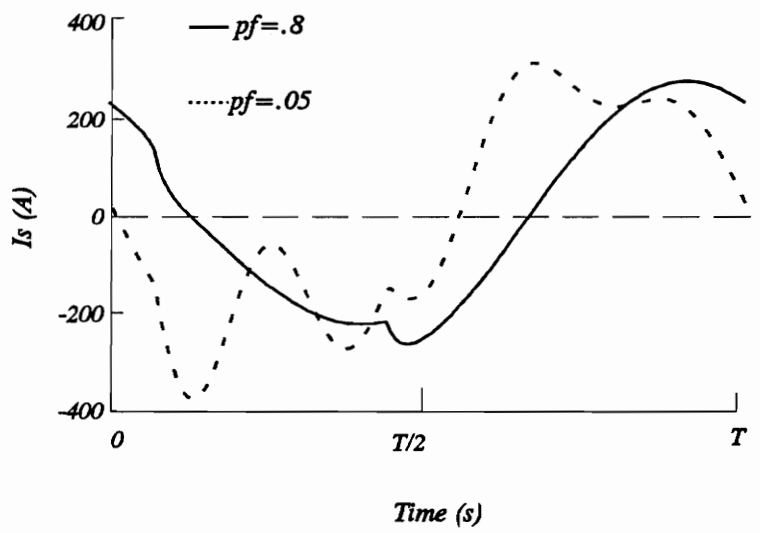


Fig. 7.5 Secondary line currents of balanced Y-Y under 50A/phase dc.

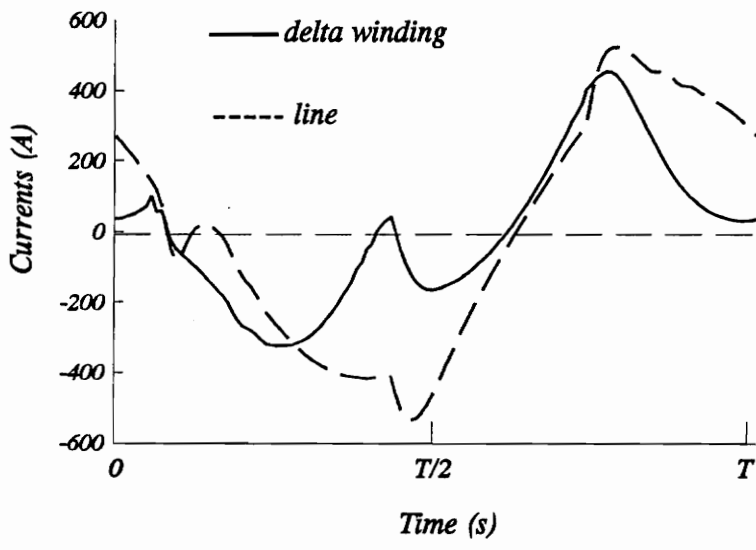


Fig. 7.6 Waveforms of delta winding and line currents under balanced capacitive loads (50A/phase dc).

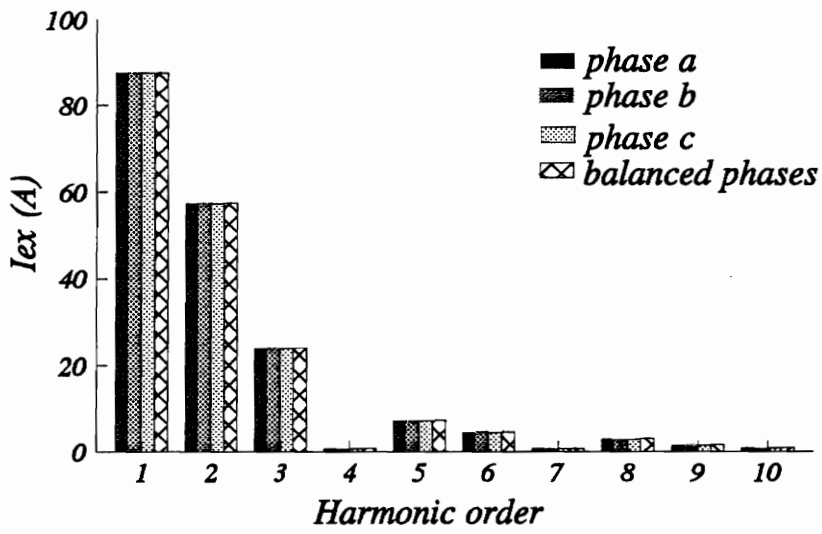


Fig. 7.7 Excitation current harmonics of the Y- Δ connection under unbalanced capacitive load ($Z_a = 2Z_b = 2Z_c$, pf = 0.25, 50A/phase dc).

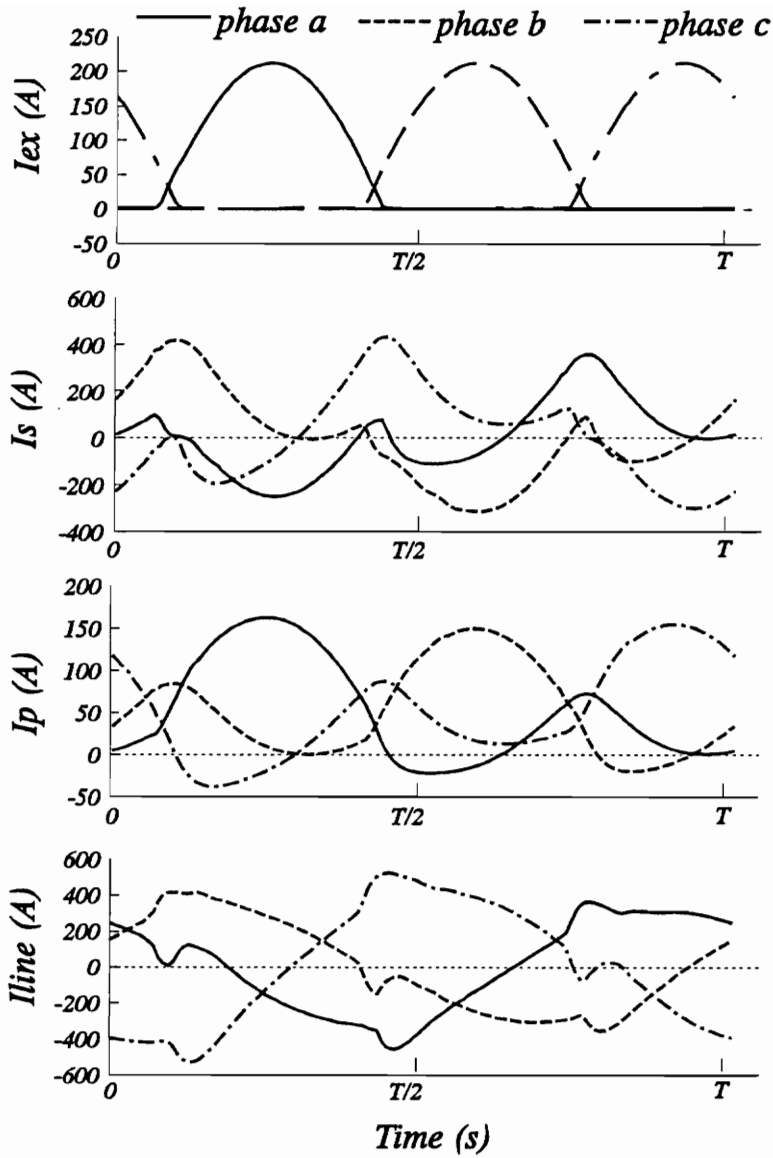


Fig. 7.8 Excitation, primary, secondary winding and line current waveforms for the Y- Δ connection under unbalanced capacitive load ($Z_a = 2Z_b = 2Z_c$, pf = .25, 50A/phase dc).

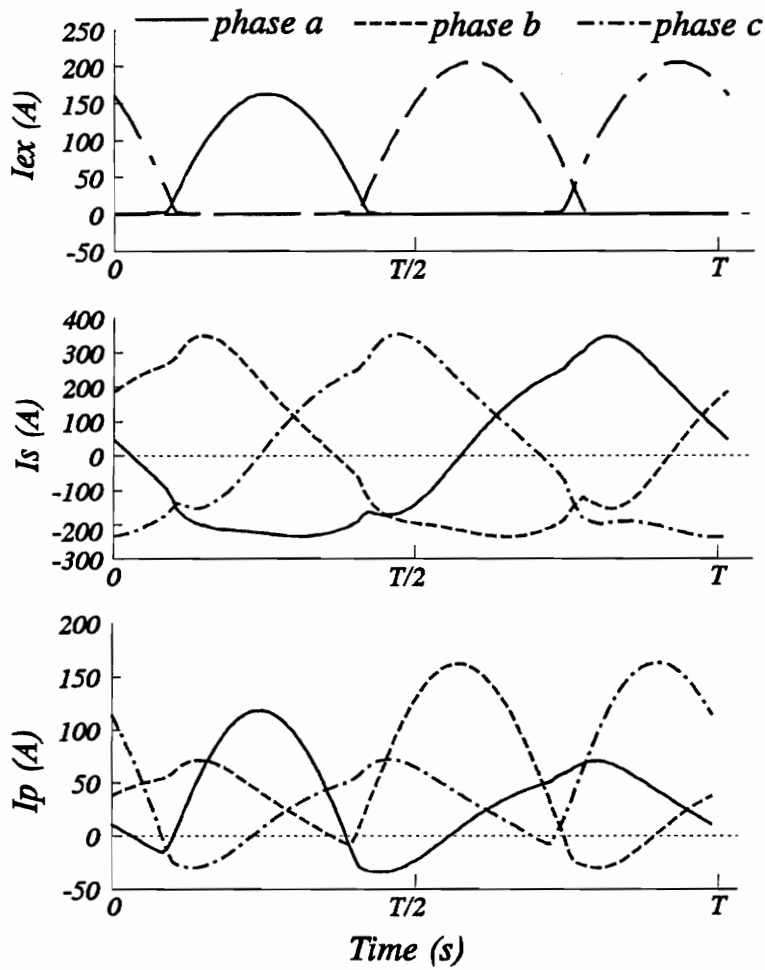


Fig. 7.9 Excitation, primary, and secondary current waveforms for the Y-Y connection under unbalanced dc ($I_{dcb} = I_{dcc} = I_{dca}/0.7 = 50\text{A}$, $\text{pf} = .25$).

CHAPTER VIII. CONCLUSIONS AND FUTURE STUDY

8.1 A Summary of the Present Work

The dc magnetization for different transformer core designs is systematically studied using 2D and 3D finite element analysis. Based on the finite element analysis results, a single phase transformer magnetic circuit model is developed for a wide range of dc operation. Harmonic characteristics generated from the transformer model under dc bias are also studied. A nonlinear curve of the magnetizing inductance derived from the transformer magnetic circuit model is used to replace the linear magnetizing inductance of the conventional equivalent Tee circuit. The sensitivity of the transformer winding impedances and the core loss on the excitation characteristics are examined. The saturated transformer under no-load and varies loading conditions is simulated. Excitation harmonics from dc biased three phase transformer banks with different types of equivalent loads are calculated. The effect of both unbalanced dc excitation and unbalanced loads are investigated.

8.2 Conclusions from the FEM Analyses

The FEM analyses described in this dissertation has provided new findings regarding GIC susceptibility of different transformer core configurations, both confirmed and modified some early predictions based on analytical approaches.

The study concludes that all single phase and three phase designs are susceptible to GIC. A transformer core saturation pattern is determined mainly by its core configuration. A three phase three leg core design could also reach saturation and become susceptible if the dc bias is increased further. It will also be susceptible if unbalanced GIC currents in

the three phases become significant. The three phase conventional core design in this study seems to have less heating risk in the tank since H (dc) outside the core is low. Including the transformer tank in the simulation proves to be necessary. The results show that the magnetic field intensity outside the core with tank is much higher than without tank.

When a single phase transformer is under dc bias, the leakage flux distribution contributed by the load current changes very little. It is unlikely to introduce additional heating loss from what is normally there before saturation. The major source of possible stray flux heating is very likely from the magnetizing current. It contains higher harmonics and has an increased effective value under saturation. Although different winding configurations demonstrate various distribution pattern of leakage flux even for the same core design, their effect on the stray flux heating during saturation is very small due to the same reason.

2D simulations have been compared with 3D simulations. On the symmetric planes, 2D and 3D simulations show very similar results. This proves that 2D simulation can also provide useful information.

8.3 Modeling and the Results

An improved method of modeling transformer excitation during SMD/GIC based on the results of 3D finite element magnetic flux distribution analysis is developed. A step further from previous studies, the described method uses 3D FEM analysis results at different levels of dc mmf bias to determine the equivalent magnetic circuit structure, the number of linear and nonlinear reluctances and their parameters required. Again, FEM analysis results over a broad operation range are used to establish the validity of the model.

The lumped magnetic circuit model is used to simulate transformer excitation currents during different levels of dc operations. The circuit is solved using a time domain iterative programming method. The output gives magnetic field density (or total flux) in each circuit branch. Magnetizing currents could be derived at any time instant of a power cycle. FEM results and the equivalent magnetic circuit generated results (B and flux at different locations of the core) show a close match of mostly around 1% over a wide range of operation. The mismatch could reach 8% in very few segments of the core for knee region dc bias.

This model has included the effect of the tank in the study. One comparison shows that flux decreases by 14% in the center leg if the tank is not considered during saturation. For a case with 1×10^5 At dc bias, the total harmonic distortion (THD) in the excitation current changes from 0.1779 with tank to 0.2673 without tank, a 50% difference.

The harmonic characteristics of the single phase transformer excitation current under dc bias over an extended range have been simulated. The following observations can be made for this particular type of transformer:

- The rms value, the dc component (I_{dc}), and the fundamental component of excitation current increase monotonically with respect to dc bias level, with the exception that the fundamental will stay at a fixed level after certain high dc bias value. The trends of increase generally resembles the B-H characteristics of the magnetic materials.
- Harmonics begin to appear at a relatively low dc bias, and each harmonic will follow a certain pattern as the dc bias increases. As the order of harmonics increases, phase-shift becomes more frequent, and their patterns become more complicated.

- All harmonics except the dc and fundamental components will disappear eventually with the increase of dc bias. This may or may not be observed during a GMD since GIC may not reach such a high level.

- The second harmonic peaks only once as the dc bias level increases. The third harmonic shows two peaks with the increase of dc bias. The fourth harmonic also shows a clear pattern with two sharp peaks and a rather flat one in the middle. The number of peaks in each harmonic is somewhat in proportion to the harmonic order, not necessarily following a one-to-one correspondence.

- All harmonic levels tend to decrease if voltage reduction (or under excitation) is implemented. Also the peaks move closer toward each other with reduced ac system voltage. The amount of change may not be significant enough to justify voltage reduction action during a geomagnetic disturbance as in the case of this example.

- DC saturated transformers are seen as reactive power sinks and significant harmonic sources. The reactive power consumption increases with respect to dc bias level, the trend follows exactly the shape of the fundamental component of excitation current.

- THD reaches a maximum of 140% for a dc bias close to the knee of the B-H curve, it drops sharply and holds at around 40% for a very wide range of dc bias.

Simulation of the modified nonlinear Tee circuit shows that, at no load, varying dc level, THD of the excitation current reaches its maximum value when dc bias is right below the knee of the excitation curve. THD decreases when the operation point is moved towards the linear and the saturation regions. Including the winding impedances and core loss component, THD will reach its maximum value earlier.

The excitation current is relatively stable when the core loss R_c varies. Also, the change of the excitation current due to the variation of the primary winding resistance R_p within reasonable range is insignificant. However, the harmonic distortion and the rms value of the excitation current decrease rapidly as the primary leakage inductance L_p increases. The higher the dc injection, the larger the decreasing rate for THD and rms. Therefore, it is necessary to include the winding impedance especially the leakage inductance in the excitation current simulations in order to achieve desired accuracy. On the other hand, the core loss during GIC can be negligible for an acceptable error.

Variation of the load has little effect on the excitation currents. The load voltage, current and efficiency all decrease monotonically as the dc level increases. The voltage regulation increase with dc level for a fixed load.

Harmonic characteristics of the Y-Y (with one grounded neutral) and Y- Δ three phase bank and single phase connections are compared. As expected, there is no difference in the excitation currents between the three configuration. The only variations are introduced by the different paths for the third harmonic and its multiples. That is, the third harmonic and its multiples can not exist in the ungrounded wye windings and the line currents on the delta side.

In the models of the three phase transformer banks, the impedance on the primary includes only the transformer winding resistance and leakage inductance, thus, the distribution of the harmonics between the primary and secondary side depends on the equivalent load seen by the transformer secondary. As this load changes from inductive to capacitive, the amount of harmonics in the secondary increase with the corresponding changes in the primary winding. Resonance is also observed in the simulation which occurred around the 5th harmonic.

The unbalance of the load hardly affects the excitation current. The unbalanced dc hardly affects the secondary line current for both connections, but it changes the excitation in the affected phase, as expected. In general, very little effect on the excitation current is observed due to load variations.

8.4 Significance and Future Study

The conclusions drawn from this study may not be directly applicable to other transformer configurations. However, the method and approach as well as the principal trends observed are considered general.

The FEM analysis helps to reveal and confirm the fundamental transformer stray flux heating mechanism and provide information for predicting future transformer heating possibilities with respect to different designs and core configurations. It is hoped that the classification of the GIC subjected transformers in the igneous rock zone by their potential risk factors may become possible.

Also, the knowledge of harmonics produced by dc biased transformers will be valuable resources in many applications. For example, triggers of monitor and alarm devices could make use of the property of the harmonic components as a saturation indicator. Intelligent protective relays could be designed using one or several harmonic components to distinguish between a transformer internal fault, an inrush current, or a GMD strike. Restraint functions based on the properties of harmonics from a GIC saturated transformer could be implemented on some capacitor protective relays to block unwanted triggering during a GMD.

It is suggested that future work will include eddy loss analysis using actual transformer design data. Better methods of combined application of dc and large ac excitations in

FEM study will be investigated. More structural details and core laminations may be considered in the problem. Thermal study will be performed based on knowledge of eddy losses analysis.

To simulated transformer excitation currents using the equivalent circuit, models of winding impedances and core loss based on FEM analysis will be developed. These models will take leakage flux, stray loss, eddy loss and hysteresis loss into consideration and they may be nonlinear components with respect to dc bias level.

Future study will also involve three phase transformers of both core and shell form designs.

APPENDIX. ELECTROMAGNETIC SOLVER

a.1 Numerical Approaches

a.1.1 Maxwell's equations

Because a transformer is an electromagnetic device, its behavior is governed by the electromagnetic fields which obey Maxwell's equations. Maxwell's equations can be given in differential forms or their alternative integral forms. The differential forms of Maxwell's equations are rewritten below,

$$\nabla \times H = J + \frac{\partial D}{\partial t} \quad (\text{a.1})$$

$$\nabla \times E = -\frac{\partial B}{\partial t} \quad (\text{a.2})$$

$$\nabla \cdot B = 0 \quad (\text{a.3})$$

$$\nabla \cdot D = \rho \quad (\text{a.4})$$

where B and H are the magnetic flux density and the magnetic field intensity, respectively. D and E are the electric flux density and the electric field intensity, respectively. J is the current density and ρ is the material resistivity.

Maxwell's equations are the most fundamental mathematical expressions of the physical phenomenon of the electromagnetic fields. In order to predict the performance of a transformer, it is always necessary to study the electromagnetic fields inside the transformer. The fields can be solved mathematically through the Maxwell's equations.

a.1.2 Numerical approach

If a device in the field has a simple shape such as sphere, its field solutions can be given analytically by solving the Maxwell equations mathematically. However, when a device has an irregular shape like power transformer core, elaborate mathematics have to be made to solve the Maxwell equations. Solution concepts such as series expansions, separation of variables, Legendre polynomials, Bessel functions, Schwarz-Christoffel transformations, Laplace transforms, have to be used. By these methods, not only the solution of the electromagnetic field inside a complex device is a lengthy process, it is also the case that no closed form solution is possible without making drastic simplifying assumptions on device geometry, current and charge distributions, and so on. As a consequence of these assumptions, the solution may not be reliable and sometimes can be erroneous. In addition, human error is another source of inaccuracy because a slight mistake is common and difficult to detect in a several page derivation.

Fortunately, with the help of digital computer, high order equations with large complexity can be solved using simple numerical approximation schemes. Although these schemes are called approximation methods, it is possible to increase the accuracy as much as desired, at the cost of some additional time and storage spaces. In fact, only for simple problem shape it is true that approximate solutions may be less accurate than the closed form solutions from classical analysis. When it comes to large problems involving complex geometries, however, closed form solutions are just not possible and only numerical schemes will do the job. With the sophisticated software packages now available for field computation, one may even go so far as to hazard the assertion that numerical schemes are generally superior to, and are therefore preferable to, classical methods.

a.2 Finite Element Method

a.2.1 Introduction to finite element method

Finite element method (FEM) is one of the two major classes of numerical methods, namely finite difference method (FDM) and FEM, for partial differential equations (PDE). The standard FEM is a special form of Galerkin method developed in 1915. FEM was first proposed by Courant in 1943 and rediscovered by engineers and physicists in 1950s, since then FEM has become more and more popular. A systematic theoretical study of FEM started in 1960s. However, it was not until the late 1960s (1967) that FEM was first applied in electromagnetics by Winslow.

A framework of FEM can be given as follows:

1. Given the field equation (elliptic equation) and its boundary conditions.
2. Converted the original second order boundary value problem into the first order variational formulation according to the energy minimization principle.
3. Descritized the infinite dimensional problem into a set of finite dimensional algebraic equations (constructions of the finite element space and finite element equations).
4. Solved the coefficient matrix of the algebraic equations (finite element equations).
5. Implemented the methods on computers.
6. Analyzed the methods (error estimates)

3.2.2 The original boundary value problem

Although the Maxwell's equations are universal in solving the electromagnetic problems, they encounter at least two inconveniences when the vector fields B or H are solved for a complicated geometry. First, the vector fields have multivalues along material interfaces

(boundaries) where they undergo discontinuities. The discontinuities at the boundaries are such that

$$H_{t1} = H_{t2} \quad (\text{a.5})$$

$$B_{n1} = B_{n2} + J_s \quad (\text{a.6})$$

where H_t and B_n are the tangential component of the field intensity and the normal component of the flux density, respectively. J_s is the surface current density. Second, there are two equations (coupled equations) being solved simultaneously for the vector fields. When numerical approximation is employed, the variable is often overdetermined. Consequently, neither equation is exactly satisfied. The answer has to try to satisfy both equations in some optimal manner.

Fortunately, the above problems can be solved by introducing a new variable called potential. In magnetics, the magnetic vector potential A is derived from the properties of the nondivergence of magnetic flux. So that,

$$B = \nabla \times A = u_x \left[\frac{\partial A_y}{\partial z} - \frac{\partial A_z}{\partial y} \right] + u_y \left[\frac{\partial A_z}{\partial x} - \frac{\partial A_x}{\partial z} \right] + u_z \left[\frac{\partial A_x}{\partial y} - \frac{\partial A_y}{\partial x} \right] \quad (\text{a.7})$$

Substitute this into the Maxwell's equations and using equation (2.6), and the relation

$$D = \epsilon E \quad (\text{a.8})$$

we have,

$$\nabla \times \nabla \times A = \mu J + \mu \epsilon \frac{\partial}{\partial t} \left(-\nabla V - \frac{\partial A}{\partial t} \right) \quad (\text{a.9})$$

where, V is the electric scalar potential which is defined as

$$E = -\nabla V - \frac{\partial A}{\partial t} \quad (\text{a.10})$$

Equation (a.9) can be rearranged using the vector identity

$$\nabla^2 A - \mu\epsilon \frac{\partial^2 A}{\partial t^2} = -\mu J + \nabla(\nabla \cdot A + \mu\epsilon \frac{\partial V}{\partial t}) \quad (\text{a.11})$$

For the vector A to be unique and therefore determinable, its divergence in addition to its curl has to be defined. The divergence of A is liberty chosen such that

$$\nabla \cdot A + \mu\epsilon \frac{\partial V}{\partial t} = 0 \quad (\text{a.12})$$

Therefore, equation (a.11) becomes

$$\nabla^2 A - \mu\epsilon \frac{\partial^2 A}{\partial t^2} = -\mu J \quad (\text{a.13})$$

This is called the time variant Poisson equation. Thus, by switching to the vector potential, a discontinuous unknown can be replaced by a continuous one which governed by one equation.

Proper boundary conditions have to be assigned to the problem space in order to obtain unique solution. There are two common boundary conditions, namely, Dirichlet and Neumann boundary conditions. Dirichlet condition is defined such that the potential along the boundary is specified while Neumann boundary means that the normal gradient of the potential is specified. It is very important to remember that the flux flows normal to equipotentials in electric field and along equipotentials in magnetic field.

When a problem is solved over an infinitely large area, some special techniques such as ballooning have to be employed. Balloon boundary condition simulates open boundary conditions by modeling the background as extending to infinity at which the vector potential goes to zero. However, it is not always possible or economical to solve problems over an infinitely large area. A boundary at infinity has to be placed at a finite distance. This approximation leads to the potential drop to zero faster and results in slightly higher field densities. Fortunately, the concept of symmetry can be applied to many problems to reduce the solution regions. Symmetry may result in a Neumann boundary or a Dirichlet boundary. Once a symmetric plane is defined, only half of the problem needs to be modeled.

a.2.3 Solving Poisson's equation using FEM

When 3D problem is encountered, three components (x, y, z) of the vector potential must be solved at each point in space. A great simplification arises in 2D problems where the magnetic flux will be on the xy plane and the vector potential A will have only the z -component.

In order to illustrate the basic principle of the finite element method applied to solve the electromagnetic problems, the 2D Poisson's equation is taken as an example. For a 2D homogeneous system, the Poisson's equation is given by

$$\nabla^2\phi(x,y) = f(x,y) \quad \text{within a region } R. \quad (\text{a.14})$$

$$\phi|_c = u(s) \quad (\text{a.15})$$

where $u(s)$ is the value of f along the boundary c of the region R .

The fundamental idea of the finite element method is to replace continuous functions with polynomials. Mathematically, the finite element method is based on variational method, where a variational expression for a specific problem needs to be sought. For an electromagnetic problem, a variational expression can be found based on the fact that potential function satisfies the Poisson's equation when the energy of the system is minimized. In other words, in order to solve the problem defined by the second order Poisson's equation and its associated boundary condition, (a.14) and (a.15), one turns to solve a problem instead given by the total system energy subjected to minimization.

The finite element method involves dividing the simulation region R into a number of small elements. This process is called meshing. The small elements usually are triangles because the triangles can fit irregular geometry better than rectangular elements. Suppose that within an triangular element e shown in figure a.1, the potential function is continuous. At its three vertices, the potential values are represented by f_i , f_j , and f_k . Assuming that the potential function $f^e(x,y)$ within that element can be approximated by a linear polynomial

$$\phi^e(x,y) = ax + by + c \quad (\text{a.16})$$

where a, b, and c are constants to be determined. Since f_i , f_j , and f_k are values of the $f^e(x,y)$ at the vertices, they should satisfy the above equation, leading to the following

$$\phi_i(x_i, y_i) = ax_i + by_i + c \quad (\text{a.17})$$

$$\phi_j(x_j, y_j) = ax_j + by_j + c \quad (\text{a.18})$$

$$\phi_k(x_k, y_k) = ax_k + by_k + c \quad (\text{a.19})$$

The three constants can be solved and represented in terms of the nodal potential values and the nodal coordinates, that is

$$a = \frac{1}{\Delta} \begin{vmatrix} \phi_i & y_i & 1 \\ \phi_j & y_j & 1 \\ \phi_k & y_k & 1 \end{vmatrix} \quad (\text{a.20})$$

$$b = \frac{1}{\Delta} \begin{vmatrix} x_i & \phi_i & 1 \\ x_j & \phi_j & 1 \\ x_k & \phi_k & 1 \end{vmatrix} \quad (\text{a.21})$$

$$c = \frac{1}{\Delta} \begin{vmatrix} x_i & y_i & \phi_i \\ x_j & y_j & \phi_j \\ x_k & y_k & \phi_k \end{vmatrix} \quad (\text{a.22})$$

Substituting the resultant a, b, and c expressions back to equation (a.16) leads to a matrix representation of the potential function $f^e(x,y)$ of the element e

$$\phi^e(x,y) = \begin{bmatrix} K_{11} & K_{12} & K_{13} \\ K_{21} & K_{22} & K_{23} \\ K_{31} & K_{32} & K_{33} \end{bmatrix}^e \begin{bmatrix} \phi_i \\ \phi_j \\ \phi_k \end{bmatrix}^e = [K]^e \begin{bmatrix} \phi_i \\ \phi_j \\ \phi_k \end{bmatrix}^e \quad (\text{a.23})$$

where $[K]^e$ is 3x3 and is called the shape function matrix. The energy J^e of the element e is given in terms of the potential function $f^e(x,y)$

$$J^e = \left(\frac{1}{2} \vec{D} \cdot \vec{E} \right) * \Delta R = \frac{\epsilon}{2} [\nabla \phi^e]^2 * \Delta R \quad (\text{a.24})$$

where ϵ is dielectric constant. ΔR is the area of the element. The total energy of the system is the sum of the energy at each elements, which is equation (a.24). The minimization of the total energy gives rise to a set of linear equation

$$[A][\phi] = [b] \quad (\text{a.25})$$

where matrix $[A]$ is called the coefficient matrix. The column vector $[f]$ contains all nodal potential values to be solved. $[b]$ is a column vector containing the enforcing function and boundary conditions. Note that the coefficient $[A]$ is obtained by augmenting the shape matrix at each element and then adding up all shape matrices. The potential values at each vertex of the elements can then be obtained by solving the linear equation. The resultant potentials can be used to calculate other field quantities such as capacitance and inductance.

There are several remarks worthy of being mentioned as follows:

(a) The finite element method turns a continuous second order Poisson's equation, which is difficult to solve in many practical cases, into a set of first order linear equations, which can be solved relatively easily. That is, the finite element method allows for the conversion of $\nabla^2\phi$ to $[\nabla\phi]^2$ such that the potential function $\phi(x,y)$ can be represented by a simple first order trial polynomial function. This process is an approximation. The simulation results obtained by the finite element method are approximated ones and therefore contain unavoidable errors.

(b) The finite element method allows the energy-related quantities such as power loss, capacitance and inductance to have higher accuracy than the potential. For example, if the obtained potential values have accuracy of order k , then the energy-related quantities will have accuracy of order k^2 . This is due to the term $[\nabla\phi]^2$ involved in the energy minimization.

(c) The coefficient matrix is a sparse matrix containing a lot of zero matrix elements. Also, the matrix is symmetrical. These features should be exploited in solving the linear equation in order to increase the simulation efficiency. In addition, the matrix depends on the way the simulation region R is divided and on the material properties of the region.

The implementation of the finite element method consists of the following steps:

- (1) Define the simulation objects, simulation region and material properties;
- (2) Divide the region into triangular elements (making meshes);
- (3) Calculate the shape function matrix in each element;
- (4) Form the global coefficient matrix;
- (5) Impose boundary conditions;
- (6) Solve the linear equation using methods such as conjugate gradient method;
- (7) Derive field quantities from the resultant potentials.

a.3 FEM Solver

Several commercial electromagnetic solvers using finite element method are available to solve complicated 2D and 3D geometry. These solvers can give different field quantities in the whole problem region. ANSOFT is the FEM solver which has been used throughout this dissertation.

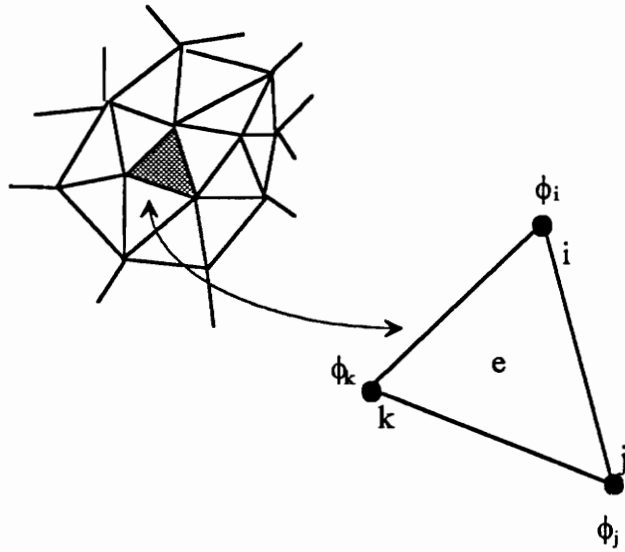


Figure a.1 A portion of the 2D meshes

BIBLIOGRAPHY

- [1] D. Larose, "The Hydro-Quebec System Blackout of March 13, 1989," IEEE Special Panel Session Report, 90TH0291-5 PWR.
- [2] V. D. Albertson, "Geomagnetic Disturbance Causes and Power System Effects" IEEE Special Panel Session Report, 90Th0291-5 PWR.
- [3] V. D. Albertson, "Measurement and Instrumentation for Disturbance Monitoring of Geomagnetic Storm Effects," IEEE Special Panel Session Report, 90TH0291-5 PWR.
- [4] V. D. Albertson, J. A. Van Bellen, "Electric and Magnetic Fields at the Earth's Surface Due to Auroral Currents," IEEE Trans. on Power Apparatus and Systems Vol. PAS-89, No. 4, April 1970.
- [5] J. G. Kappenman, V. D. Albertson, "Bracing for the Geomagnetic Storms," IEEE Spectrum, March 1990.
- [6] D. H. Boteler, "Geomagnetically Induced Currents: Present Knowledge and Future Research," IEEE Trans. on Power Delivery, 93 WM 063-8 PWRD.
- [7] C. C. Balch, "Real-Time Monitoring and Predicting of Geomagnetic Activity," IEEE Special Panel Session Report, 90TH0291-5 PWR.
- [8] R. J. Ringlee, J. R. Steward, "Geomagnetic Effects on Power Transformers," IEEE Special Panel Session Report, 90TH0291-5 PWR.
- [9] E. L. Harder, "Effect of Direct Current in Transformer Windings," The Electric Journal, October, 1930.
- [10] J. G. Kappenman, D. L. Carlson, G. A. Sweezy, "GIC Effects on Relay and CT Performance," IEEE Special Panel Session Report, 90TH0291-5 PWR.
- [11] R. L. Leshner, J. W. Porter, R. T. Byerly, "SUNBURST -- A Network of GIC Monitoring Systems," IEEE Trans. on Power Delivery, 93 WM 064-6 PWRD.
- [12] "Geomagnetic Disturbance Effects on Power Systems," A Report prepared by the IEEE Transmission and Distribution Committee Working Group on Geomagnetic Disturbances and Power System Effects.

- [13] A. P. S. Meliopoulos, E. N. Glytsis, G. J. Cokkinides, M. Rabinowitz, "Comparison of SS-GIC and MHD-EMP-GIC Effects on Power Systems," IEEE Trans. on Power Delivery, 93 WM 065-3 PWRD.
- [14] H. C. Tay, G. W. Swift, "A Novel Method of Detecting Asymmetrical Transformer Core Saturation Due to GIC," IEEE Trans. on Power Apparatus and Systems, Vol. PAS-103, No. 1, January, 1984.
- [15] V. D. Albertson, "Mitigation Techniques to Block GIC," IEEE Special Panel Session Report, 90TH0291-5 PWR.
- [16] T. H. Harrison, B. Richardson, "Transformer Loss Reductions," International Conference on Large High Voltage Electric Systems, Paris, 1988.
- [17] R. A. Walling, A. H. Khan, "Characteristics of Transformer Exciting-Current During Geomagnetic Disturbances," IEEE/PES, 91 WM 095-0 PWRD.
- [18] P. R. Gattens, R. Girgis, R. Nevins, "Investigation of Transformer Overheating Due to Solar Magnetic Disturbances," IEEE Special Panel Session Report, 90TH0291-5 PWR.
- [19] J. G. Kappenman, V. D. Albertson, N. Mohan, "Current Transformer and Relay Performance in the Presence of Geomagnetically-Induced Currents," IEEE Trans. on Power Apparatus and Systems, PAS-100, (2).
- [20] N. Mohan, J. G. Kappenman, V. D. Albertson, "Harmonics and Switching Transients in the Presence of Geomagnetically-Induced Currents," IEEE Trans. on Power Apparatus and Systems, PAS-100, (2).
- [21] "High-Voltage Direct-Current Converter Transformer Magnetics," EPRI EL-4340, Project 1424-3, Final Report, December 1985.
- [22] V. D. Albertson, J. G. Kappenman, N. Mohan, G. A. Skarbakka, "Load-Flow Studies in the Presence of Geomagnetically-Induced Currents," IEEE Trans. on Power Apparatus and Systems, Vol. PAS-100, No. 2, February 1981.
- [23] A. P. B. Joosten, J. Arrillaga, C. P. Arnold, N. R. Watson, "Simulation of HVDC System Disturbances with Reference to the Magnetizing History of the Converter Transformers," IEEE Trans. on Power Delivery, 89 SM 795-6 PWRD.
- [24] R. A. Walling, A. H. Khan, "Solar-Magnetic Disturbance on Power System Performance and Security," EPRI GIC Workshop Report, 1990.

- [25] L. Bolduc, J. Aubin, "Effects of Direct Currents In Power Transformers, Part I. A General Approach, Part II, Simplified Calculations for Large Transformers," Electric Power Systems Research, Vol. 1, 1978.
- [26] W. J. McNutt, "The Effect of GIC on Power Transformers," IEEE Special Panel Session Report, July 1990.
- [27] W. Xu, T. G. Martinich, J. H. Sawada, Y. Mansour, "Harmonics From SVC Transformer Saturation With Direct Current Offset," IEEE Trans. on Power Delivery, 93 SM 404-4 PWRD.
- [28] W. Pasco, E. T. Norton, S. L. Nilsson, "High Voltage Direct Current Converter Transformer Magnetics," EPRI Report EL-4340, Research Project 1424-3, December 1985.
- [29] H. C. Tay, G. S. Swift, "On the Problem of Transformer Overheating due to Geomagnetically Induced Currents," IEEE Trans., Vol. PAS-104, No.1, Jan. 1985.
- [30] N. Takasu, T. Oshi, et. al., "An Experimental Analysis of DC Excitation of Transformers by Geomagnetically Induced Currents," IEEE Trans. on Power Delivery, 93 SM 393-9 PWRD.
- [31] J. G. Kappenman, "Transformer DC Excitation Field Test & Results," IEEE Special Panel Session Report, 90TH0291-5 PWR.
- [32] E. F. Fuchs, M. A. S. Masoum, D. J. Roesler, "Large Signal Nonlinear Model of Anisotropic Transformers for Nonsinusoidal Operation, Part I: i - v Characteristic," IEEE Trans. on Power Delivery, Vol. 6, No. 1, January 1991.
- [33] M. A. S. Masoum, E. F. Fuchs, D. J. Roesler, "Large Signal Nonlinear Model of Anisotropic Transformers for Nonsinusoidal Operation, Part II: Magnetizing and Core-Loss Currents," IEEE Trans. on Power Delivery, Vol. 6, No. 4, October 1991.
- [34] R. S. Girgis, C. D. Ko, "Calculation Techniques and Results of Effects of GIC Currents as Applied to Two Large Power Transformers," IEEE Trans. on Power Delivery, Vol. 7, No. 2, April 1992.
- [35] R. Yacamini, J. C. de Oliveira, "Harmonics Produced by Direct Current in Converter Transformers," PROC. IEE, Vol.125, No. 9, September 1978.
- [36] R. Feinberg, *Modern Power Transformer Practice* (John Wiley & Sons, Inc., New York, 1979)

- [37] J. M. Christini, R. S. Girgis, "Effects of Stray DC Currents on the Performance of Large Core Type Transformers," Proceedings of the American Power Conference, 1992.
- [38] C-D. Ko, R. S. Girgis, "Analysis of Core-Form Transformer Performance Under the Effects of Geomagnetically Induced Currents," Proceedings of the American Power Conference, 1992.
- [39] A. E. Emanuel, "Powers in Nonsinusoidal Situations - A Review of Definitions and Physical Meanings," IEEE Trans. on Power Delivery, Vol. 5, No. 3, July 1990.
- [40] J. Arrillaga, D.A. Bradely, P.S. Bodger, *Power System Harmonics* (John Wiley & Sons, New York, 1985)
- [41] W. Shepherd, P. Zand, *Energy Flow and Power Factor in Nonsinusoidal Circuit* (Cambridge University Press, 1979)
- [42] Department of Electrical Engineering, MIT, *Magnetic Circuits and Transformers* (John Wiley & Sons, New York, 1943).
- [43] Discussion with Mr. R. A. Walling at GE Industrial and Power Systems.
- [44] J. D. Aspenes, R. P. Merritt, S. I. Akasofu, "Harmonic Generation in Transformers Related to DC Excitation and System Loading," IEEE Trans. on Power Apparatus and Systems, Vol. PAS-100, No. 4, April 1981.
- [45] V. D. Albertson, J. A. Van Bellen, "Electric and Magnetic Fields at the Earth's Surface Due to Auroral Currents," IEEE Trans. on Power Apparatus and Systems Vol. PAS-89, No. 4, April 1970.
- [46] C. E. Lin, J-B. Wei, C-L. Huang, C-J. Huang, "A New Model for Transformer Saturation Characteristics by Including Hysteresis Loops," IEEE Trans. on Magnetics, Vol. 25, No. 3, May 1989.
- [47] L. O. Chua, K. A. Stromsmoe, "Lumped-Circuit Models for Nonlinear Inductors Exhibiting Hysteresis Loops," IEEE Trans. on Circuit Theory, Vol. CT-17, No. 4, November 1970.
- [48] "Effects of Geomagnetic Disturbances on Electric Power Transmission Systems," EPRI Report EL-7333, Research Project 2115-24, August 1991.
- [49] Ansoft Corporation, « ANSOFT », University Technology Development Center, 4516 Henry Street, Pittsburgh, PA 15213, (412)683-4846, January, 1989.

- [50] M. V. K. Chari, P. P. Silvester, eds., *Finite Elements in Electrical and Magnetic Field Problems* (John Wiley & Sons, New York, 1980).
- [51] G. T. Heydt, *Electric Power Quality* (Purdue University, 1991)
- [52] L. F. Blume, G. Camilli, A Boyajian, *Transformer Engineering*, (John Wiley & Sons, Inc., New York, 1938)
- [53] W. Pasco, E. T. Norton, S. L. Nilsson, "High Voltage Direct Current Converter Transformer Magnetics" EPRI Report EL-4340, Research Project 1424-3, December 1985.

VITAE

Ms. Shu Lu (陸抒 in Chinese) was born in Guangzhou, the biggest city in southern China, in December 1962. She received her B.S. degree with honor majoring in semiconductor physics and devices in South China Institute of Technology in 1984. She worked for three and half years as a R&D engineer in South China Computer Company since then. In January 1988, she came to United State and started her graduate study at Radford University. Half year later, she transferred to the Bradley Department of Electrical Engineering at Virginia Tech and studied in the areas of electromagnetics and electronic device modeling under the guidance of Dr. Aicha Elshabini-Riad and Dr. Sedki Riad. After receiving her M.S. degree in Electrical Engineering in 1990, she continued her Ph.D. program under the guidance of Dr. Yilu Liu at the same department. Her research interests are in Power Engineering, specially in power device modeling, and Power Electronics. She have published five technical papers as a first author in major journals and many others in conference proceedings. She is an IEEE student member. She is also a member of the honor societies Phi Kappa Phi and Eta Kappa Nu.

Ms. Shu Lu has a wonderful husband, Dr. Jianqing He, who is very understanding and very patient. She is also the mother of a beautiful and lovely daughter, Victoria, who is going to be seventeen months old. While she is trying to be successful in her professional career, she has been a good wife and a good mother as well.



Shu Lu